Flow and Heat Transfer Analysis of MHD Upper-Convected Maxwell Fluid over a Sheet with Non-Fourier's Heat Law

by

Sajid Shah

A thesis submitted in partial fulfillment for the
degree of Doctor of Philosophy

in the

2020

Flow and Heat Transfer Analysis of MHD Upper-Convected Maxwell Fluid over a Sheet with Non-Fourier's Heat Law

By

Sajid Shah

(PA-133006)

Dr. Mingchao Cai

Morgan State University, Baltimore, Maryland, USA

(Foreign Evaluator 1)

Dr. Abderrahim Quazzi

Technische Universitat Dortmund, Germany

(Foreign Evaluator 2)

Dr. Shafqat Hussain

(Thesis Supervisor)

Dr. Muhammad Sagheer

(Head, Department of Mathematics)

Dr. Muhammad Abdul Qadir

(Dean, Faculty of Computing)

DEPARTMENT OF MATHEMATICS

CAPITAL UNIVERSITY OF SCIENCE AND TECHNOLOGY

ISLAMABAD

2020

Dedicated to

My respected parents and teachers

who are always be a source of inspiration and encouragement for me

My caring and supporting wife and children

who have always given me care and love

CERTIFICATE OF APPROVAL

This is to certify that the research work presented in the thesis, entitled **"Flow and Heat Transfer Analysis of MHD Upper-Convected Maxwell Fluid over a Sheet with non-Fourier's Heat Law"** was conducted under the supervision of **Dr. Shafqat Hussain**. No part of this thesis has been submitted anywhere else for any other degree. This thesis is submitted to the **Department of Mathematics, Capital University of Science and Technology** in partial fulfillment of the requirements for the degree of Doctor in Philosophy in the field of **Mathematics**. The open defence of the thesis was conducted on **December 23, 2019**.

Student Name :   Mr. Sajid Shah (PA133006)

The Examining Committee unanimously agrees to award PhD degree in the mentioned field.

Examination Committee :

(a)   External Examiner 1:   Prof. Dr. Muhammad Ashraf
                            Professor
                            BZU, Multan

(b)   External Examiner 2:   Prof. Dr. Siraj ul Haq
                            Professor
                            GIKI, Topi, Swabi

(c)   Internal Examiner :   Dr. Abdul Rehman Kashif
                            Associate Professor
                            CUST, Islamabad

Supervisor Name :   Dr. Shafqat Hussain
                            Associate Professor
                            CUST, Islamabad

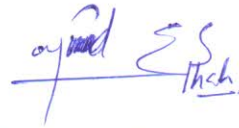**Name of HoD :**   Prof. Dr. Muhammad Sagheer
                            Professor
                            CUST, Islamabad

Name of Dean :   Prof. Dr. Muhammad Abdul Qadir
                            Professor
                            CUST, Islamabad

AUTHOR'S DECLARATION

I, **Mr. Sajid Shah (Registration No. PA-133006)**, hereby state that my PhD thesis titled, '**Flow and Heat Transfer Analysis of MHD Upper-Convected Maxwell Fluid over a Sheet with non-Fourier's Heat Law**' is my own work and has not been submitted previously by me for taking any degree from Capital University of Science and Technology, Islamabad or anywhere else in the country/ world.

At any time, if my statement is found to be incorrect even after my graduation, the University has the right to withdraw my PhD Degree.

(Mr. Sajid Shah)

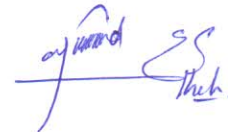Dated: December, 2019   Registration No : PA133006

PLAGIARISM UNDERTAKING

I solemnly declare that research work presented in the thesis titled "**Flow and Heat Transfer Analysis of MHD Upper-Convected Maxwell Fluid over a Sheet with non-Fourier's Heat Law**" is solely my research work with no significant contribution from any other person. Small contribution/ help wherever taken has been duly acknowledged and that complete thesis has been written by me.

I understand the zero tolerance policy of the HEC and Capital University of Science and Technology towards plagiarism. Therefore, I as an author of the above titled thesis declare that no portion of my thesis has been plagiarized and any material used as reference is properly referred/ cited.

I undertake that if I am found guilty of any formal plagiarism in the above titled thesis even after award of PhD Degree, the University reserves the right to withdraw/ revoke my PhD degree and that HEC and the University have the right to publish my name on the HEC/ University Website on which names of students are placed who submitted plagiarized thesis.

(Mr. Sajid Shah)

Dated: December, 2019   Registration No : PA133006

List of Publications

It is certified that following publication(s) have been made out of the research work that has been carried out for this thesis:-

1. **S. Shah**, S. Hussain, and M. Sagheer, "MHD effects and heat transfer for the UCM fluid along with Joule heating and thermal radiation using Cattaneo-Christov heat flux model," *AIP Advances*, vol. 6, pp. 085103, 2016.

2. **S. Shah**, S. Hussain, and M. Sagheer, "Thermal stratification effects on mixed convective Maxwell fluid flow with variable thermal conductivity and homogeneous/heterogeneous reactions," *Journal of the Brazilian Society of Mechanical Sciences and Engineering*, vol. 40, pp. 452, 2018.

Sajid Shah

(PA-133006)

Acknowledgements

All who embark on a quest desire recognition and recommendation once they have attained what they set out to accomplish. But the alacrity to acknowledge those who paved their road to glory is a greater virtue and I must exercise this virtue because many are the people who contributed in making me, 'me'.

First and foremost, I thank the Almighty Allah, the Creator, whose bounties we cannot reckon and whose grandeur we cannot gauge. He transformed a boy from the humble settings of Attock and gave him the resilience and intellectual talent to rise as high as he did. Indeed He taught me 'What I knew not'. I bow to Him. This task could not have achieved fructification without the beckoning light of the benefactor of all mankind; our Holy Prophet Hazrat Muhammad (May the peace and blessings of Allah always be upon him). His teachings have taught me to be dignified in glory, exercise restraint in rejoicing and be humble in victory.

I acknowledge, wholeheartedly, the contributions of my honorable teachers. They lit my path with the light of enlightenment. They showed, not only the beauty that is knowledge but also triggered in me the desire to quest for it. One such personality is Dr. Shafqat Hussain who mentored me through the lengths and breadths of this project. To him my debt is immense and so is my gratitude.

Next, I thank Prof. Muhammad Sagheer (Head of The Department of Mathematics, Faculty of Basic Sciences, CUST) for affording me all opportunities and guidance in my Ph.D research work. I extend my gratitude to Prof. Rashid Ali for his continuous support. The other members of The Mathematics Department at CUST also deserve my thanks particularly; Prof. Abdul Rehman Kashif and Prof. Muhammad Afzal for their support and camaraderie.

I am highly grateful to my wonderful friend Tazeem Ahmed Khan for always being there for me. Sincere thanks is, also, due to my colleagues at Government Postgraduate College Asghar Mall, Rawalpindi. I thank Prof. Masood Hussain, Prof. Muhammad Safdar, Prof. Musarrat Khan, Prof. Jaffer Raza, Prof. Asif Shah, Prof. Nadeem Safdar, Prof. Ameer Asim, Dr. Muhammad Bilal, Dr. Khalid

Mahmood, Dr. Yasir Mahmood, Prof. Sajid Hussain, Prof. Farooq Aslam, Prof. Muhammad Nasir, Prof. Tariq Nawaz, Prof. Abdul Wahab, Prof. Zohaib Aarfi and Prof. Imran Haider.

Finally, my family. How can I thank my parents and for what? For the sleepless nights I gave them, for clearing my path from the thorns of life and a lot more. Anyway this is as opportune a moments as any for me to say 'thank you' to both of them. Similar emotions I express towards my siblings and wife. Their presence in my life is a continuous source of comfort.

And finally a word of advice for all those who are about to embark on an odyssey similar to mine. I say 'Ladies and gentlemen, the path towards academic excellence is ridden with frustrations, impediments and constant trials'. My advice is not to let these factors faze you, because the rewards are great and worth striving for. Perseverance is the name of the game.

Abstract

This thesis intends to establish numerical solutions to certain boundary layer flows of upper-convected Maxwell (UCM) fluid caused by moving or stretching surfaces under the influence of a magnetic field. To investigate heat transfer characteristics, a recently modified heat conduction model known as Cattaneo-Christov heat flux model (CCHFM) is implemented instead of the convectional heat flux model (Fourier's law). The influence of heat transfer in many industrial and engineering processes is significant since the process involves the rate of heat transfer. An extensive work on the boundary layer flow and heat transfer of non-Newtonian fluids has been considered over linear/non-linear stretching surfaces. We have analyzed the various flow-configurations including the flow of UCM fluid over a constantly moving surface with magnetohydrodynamic (MHD) effects. Intensive and extensive scrutiny has also been conducted regarding the MHD mixed convective UCM fluid flow over a non-linear stretching surface near a stagnation point. We, then, also broadened our research to explore the effects of variable thermal conductivity in a thermally stratified medium due to non-linear stretching surface. In addition, the impact of thermal radiation with heat generation/absorption in a porous medium was included in the research. Finally the non-linear velocity-slip effects over an inclined stretching surface in a porous medium was thoroughly observed and researched upon. The application of a new model has brought to light some amazingly new results regarding the flow behavior of UCM fluid under different physical effects. The significant effect of relaxation characteristics of UCM fluid on thermal transmission is observed. The mathematical formulation of these problems leads to partial differential equations (PDEs) which are first converted into ordinary differential equations (ODEs) via suitable similarity transformations and then solved numerically through two different techniques known as the shooting with Runge-Kutta scheme of order four and the MATLAB built-in solver bvp4c. The solutions under the impacts of different physical governing parameters are illustrated by means of graphs and tables. The culmination of the research was the comparison between this work with the Newtonian fluids as special cases.

Contents

List of Figures

List of Tables

Abbreviations

BCs	Boundary conditions
BVP	Boundary value problem
CCHFM	Cattaneo-Christov heat flux model
IVP	Initial value problem
MC	Maxwell-Cattaneo
MHD	Magneto-hydrodynamics
ODEs	Ordinary differential equations
PDEs	Partial differential equations
RK4	Runge-Kutta 4th order method
UCM	Upper-convected Maxwell

Symbols

A	stretching ratio parameter
B_0	strength of uniform magnetic field
c, d	positive constants
C	nanoparticle volume fraction
C_w	nanoparticle fraction at wall
C_∞	ambient concentration
C_f	coefficient of skin-friction
C_p	specific heat
C_r	chemical reaction parameter
D_T	coefficient of thermal diffusion
D_B	coefficient of Brownian diffusion
f'	non-dimensional velocity
g	acceleration due to gravity
k	thermal conductivity of fluid
k_∞	thermal conductivity of ambient fluid
k_*	absorption coefficient
K_c	chemical reaction rate
K	homogeneous reaction parameter
Ks	heterogeneous reaction parameter
K_p	porosity parameter
Δ	velocity slip length
M	magnetic parameter
Nu_x	local Nusselt number

N_b Brownian motion parameter

N_t thermophoresis parameter

P_r Prandtl number

q_r radiative heat flux

q_w wall heat flux

R velocity slip parameter

R_d radiation parameter

Re_x local Reynolds number

S thermal stratification parameter

S_c Schmidt number

T temperature of fluid

T_w wall temperature

T_∞ ambient temperature

U_w surface stretching velocity

U_e free stream velocity

u velocity x-component

v velocity y-component

x horizontal coordinate

y vertical coordinate

α_w sheet thickness parameter

α thermal diffusivity of the fluid

β visco-elastic/Maxwell parameter

β_T thermal expansion coefficient

β_C concentration expansion coefficient

Γ_e thermal relaxation parameter

Γ_c mass flux relaxation parameter

σ electrical conductivity

σ^* Stefan-Boltzmann constant

δ thermal conductivity parameter

λ_t thermal buoyancy/mixed convection parameter

λ_c concentration buoyancy parameter

λ_s heat source/sink parameter

Λ fluid relaxation time

Λ_h relaxation time of the heat flux

Λ_m relaxation time of mass flux

θ dimensionless temperature

ϕ dimensionless concentration

ψ stream function

μ fluid dynamic viscosity

ν fluid kinematic viscosity

ρ_f density of base fluid

ρ_p density of nanoparticles fluid

ρ density of fluid

η dimensionless variable

Ω inclined sheet angle

Chapter 1

Background

The study of the boundary-layer flow and heat transfer of the visco-elastic fluids (e.g. Jeffery, Oldroyd-B, Maxwell etc.) caused by moving or stretching surfaces has remarkable engineering and industrial applications such as cooling of electronic chips or metallic sheets [1], polymer or metal extrusion [2], wire drawing [3], petroleum production [4], etc. The "Boundary-Layer Theory" stands out as a quintessentially significant notion, providing a marked impetus towards research in the discipline of fluid mechanics. From the onset of the last century, the "Boundary-Layer Theory" evolved extremely rapidly, primarily, because of the multitude of applications that emanate from it [5]. The calculations of the friction drag of bodies in a flow such as the body of an airplane, a turbine blade, a ship or airfoil etc., is cardinal to the applications of the boundary-layer theory. This theory acts as a kind of an excess between it being a simple theory and practical applied aspects. It is indeed a glaring reality that the most significant progress in the discipline of fluid mechanics has occurred when theoretical ideas are supported by fundamental experimentations. The boundary-layer flow anlysis, triggered by stretching surfaces, is an important mechanism. It is present in various manufacturing processes such as metal extrusion, polymer extrusion, wire drawing, stretching of artificial fibers, aerodynamics and extrusion of plastic sheets are few examples of flow caused by the stretching surfaces. Thermal properties of the fluid near the surface is a matter of clever control. For this purpose the Fourier's law

1

has been abandoned for the more practicable Cattaneo-Christov heat flux model (CCHFM). Many recent researchers have opted for this model to examine the heat transfer mechanism [6–12]. The last decade has seen a number of research articles, related to the problems of the visco-elastic fluids over stretching surfaces using CCHFM.

The analysis of transfer of heat for two-dimensional ($2D$) boundary-layer fluid flow with regards to stretching surface has become a seriously debatable topic hence invoking a keen interest amongst the modern researchers. The interest has risen, primarily, owing to the vast of applications of such investigations in the manufacturing industry e.g. processes, of extrusion and sheet-manufacturing, air coolers, coating and paper production, drying technology [13] etc. A milestone investigation in this regard was initiated by Sakiadis [14] who researched a $2D$ flow assuming the velocity of the stretching sheet as constant. He established a relation between a boundary-layer thickness and skin-friction for both laminar and turbulent boundary-layers. This work was further explored for the heat transfer analysis by Erickson *et al.* [15]. Erickson's research was based on the assumption that uniformly stretched-velocity is of practical use in the extrusion of polymer sheets. Crane [16] was the first who examined the flow of incompressible fluids. He imposed the condition of a constant temperature and stretching sheet. Crane's idea was further explored in different directions by many researchers [17–20]. In practical situations, the stretching of the sheet in many processes like plastic production is not necessarily linear. Due to this fact, many researchers opted to analyze different fluid flow problems over non-linear stretching surfaces. Cortell [21] studied the transfer of heat for flow by imposing the condition of non-linear stretching and different temperature of the sheet. The noted effect of non-linear parameter related to the stretching sheet was significant. The transfer of heat and flow of the visco-elastic fluid with viscous dissipation under the non-linearity of the stretching sheet was taken up by Nandeppanavar *et al.* [22]. The result was that the rate of transfer of heat can be controlled by selecting some appropriate parametric values for the visco-elasticity, the Eckert and the Prandtl numbers. The effect of non-li-

near thermal radiation with suction/injection tendencies and taking the magnetic field into account due to non-linearity of the stretching sheet was investigated by Laxmi and Shankar [23]. Khan *et al.* [24] addressed the phenomena of transfer of heat and mass of Maxwell fluid flow caused by a non-linearity of the stretching surface with homogeneous/hetrogeneous reactions and internal heat absorption/generation source. Recently, Elbashbeshy *et al.* [25] evaluated the transfer of heat and flow with heat generation effects for Maxwell fluid over a stretching surface of variable thickness. A decrement in the distributions of velocity and temperature was discovered with the ascending values of elasticity parameter. In the above stated studies, the heat transfer characteristics are investigated through the convectional heat conduction model named as Fourier's law.

The study of heat transfer characteristics of the boundary-layer fluid flows has numerous applications in engineering and industrial processes. It includes extrusion processes, cooling of electronic devices, fuel cells, heat propagation in tissues, hybrid power generators, high capacity cooling and energy systems, photosynthesis and many others [26]. The difference in temperature between two different kinds of bodies leads to the heat transfer mechanism which plays an important role in castings of metals, cooling of nuclear reactors, crystal growth, drug targeting and heat conduction in tissues [27] etc. About 200 years back, Fourier [28] pioneered the phenomena of heat transfer in order to analyze its characteristics. According to him, a temperature field has a parabolic behavior of energy equation. One of the drawbacks of Fourier heat conduction model is that initial disturbance is instantaneously felt by the material under investigation due to the parabolic nature of energy equation. To overcome this restriction, Cattaneo [29] later on, modified the Fourier's law for effective heat transfer enhancement by considering the relaxation time which causes the transfer of heat with finite speed. Practically, different fluid possesses require different relaxation times, so, Christov [30] further developed this work by proposing a material derivative for Cattaneo's law, named as CCHFM in which the derivative with respect to time is omitted and Oldroyd's upper-convected derivative is used instead. The equation with respect to CCHFM is of a hyperbolic

type [31–33]. The modified model has been widely employed in many developments to construct energy equation and discusses the flow and heat transfer behavior of various non-Newtonian fluids. Han *et al.* [34] and Hayat *et al.* [35] examined the heat transfer behavior of visco-elastic fluids pasted through a stretched sheet using CCHFM. The thermo diffusion properties of peristalsis flow in view of CCHFM was researched by Tanveer *et al.* [36]. The flow of UCM fluid in the region close to the surface deploying CCHFM with radiation effects and magnetic field through a porous sheet was explored by Shahid *et al.* [37]. They examined the effects of pronounce parameters like the modified Deborah number, stretching ratio parameter and magnetic parameter etc., on the profiles of the velocity, temperature and concentration. Sarkar and Kundu [38] discussed the flow of UCM nanofluid through the CCHFM past a stretching sheet of variable thickness. A marked reduction in temperature distribution is observed for comparatively larger relaxation parameter. Using the CCHFM, Hayat *et al.* [39] studied the stagnation-point flow over a non-linear stretched surface with temperature dependent variable thermal conductivity. The influence of variable thermal conductivity by utilizing the CCHFM through Darcy-Forchheimer porous medium was addressed by Meraj *et al.* [40]. A decline in the velocity and associated boundary-layer thickness was observed for the ascending values of Darcy-Forchheimer parameter. Mustafa's [41] research on the UCM fluid over a stretching sheet led him to the conclusion that the thermal relaxation time and the thickness of the thermal boundary layer have an inverse impact on each other. These conclusions were drawn using CCHFM. The numerical solutions of Sakiadis flow for UCM fluid by implementing the CCHFM were obtained by Mushtaq *et al.* [42]. Hayat *et al.* [43] explored the thermally stratified stagnation-point flow of a second grade fluid with the CCHFM. Reddy *et al.* [44] analyzed the flow of MHD micropolar fluid through the CCHFM past a convectively heated vertical stretching sheet with viscous dissipation. Recently, Awais *et al.* [45] investigated the hydro-magnetic flow over a surface of variable thickness under the impacts of the CCHFM and internal heat generation/absorption. A marked reduction in the temperature profile is noted for the ascending values of thermal relaxation parameter. Very little work is available in literature regarding

the flow and heat transfer characteristics of visco-elastic fluids in view of the modified Fourier's heat conduction law which is proposed by Cattaneo and Christov.

The study of flow and heat transfer of non-Newtonian fluids which are electrically conducting allied with a magnetic field has wide-ranging applications in numerous fields like pharmaceutical, hydrometallurgical industry etc. This has generated a keen interest among the modern day researchers. Few examples regarding non-Newtonian fluids are blood, crude oil, paint thinners, slurries, emulsions etc. These fluids, because of their complex characteristics are not capable of formulating a single constitutive relationship. Due to this reason, non-Newtonian fluids behave quite differently in comparison to the Newtonian fluids. Accordingly, many models of non-Newtonian fluids are available in literature. But most of the models amongst these are related to differential-type fluids such as fluids of grade two. In differential-type fluids, the stress components in terms of velocity components can easily be expressed, while this does not hold in general for the rate-type fluids e.g. in Maxwell, Jeffrey, Burgers or Oldroyd-B fluids. So, the rate-type fluid flows particularly in two-dimensional cases are limited. The flow and heat transfer analysis of unsteady Oldryod-B nanofluid past a stretching sheet is narrated by Faiz et al. [46]. They considered the zero nanoparticle flux at the boundary and solved the momentum, heat and mass equations by utilizing spectral relaxation method. Able et al. [47] took up the flow of UCM fluid over a stretching sheet in the presence of a magnetic field. It was observed that the velocity distributions show a decreasing trend due to an increase in the magnetic and Maxwell parameters. Abel et al. [48] investigated the thermal radiation and buoyancy force effects in magnetohydrodynamics visco-elastic fluid flow over a continually moving stretching surface. Sarpakaya [49] was the pioneer in the study of non-Newtonian fluid flows when the magnetic field is present. Chen [50] calculated the analytical solution of MHD visco-elastic fluid flow for heat transfer analysis with thermal radiation and internal heat source. Akbar et al. [51] investigated the MHD effects on the Eyring-Powell fluid flow over a stretching sheet and found that the larger value of the Eyring-Powell fluid and the magnetic parameters resist the flow. Mabood et

al. [52] investigated the MHD nanofluid flow over a non-linear stretching sheet and concluded that the larger values of the magnetic parameter cause an increment in skin friction co-efficient. However, an opposite trend is seen for the Nusselt and Sherwood numbers. Hayat *et al.* [53] presented the solution in the series form for MHD flow of an UCM fluid with the help of the homotopy analysis method. Wang and Hayat [54] discussed the two-dimensional boundary-layer flow of Maxwell fluid over a permeable infinite plate. A considerable work on the flow of MHD non-Newtonian fluid can be found in literature [55–57].

The stagnation-point flow over a stretching sheet emerged as a popular subject of research over the years due to its wide-range industrial and engineering applications. Many investigators have shown keen interest in the boundary-layer flows near the stagnation-point. Submarines over oil-ship tips, aircraft and rocket are some examples of the stagnation-point flows. After the pioneering work by Heimenz [58], many researchers have investigated the problems regarding the stagnation-point flow with different geometrical aspects taking different fluid models into account. Rashidi and Freidoonimehr [59] analyzed the entropy generation in the MHD boundary-layer flow close to the stagnation-point with heat transfer. They observed that the rate of entropy generation can be reduced by increasing the Brinkman number or decreasing the Prandtl or Reynolds numbers. The unsteady boundary-layer flow of a third grade fluid through a porous stretching/shrinking surface close to stagnation-point was explored by Naganthran *et al.* [60]. Srinivasulu *et al.* [61] discussed the Casson nanofluid flow near a stagnation-point by considering the magnetic field and viscous dissipation effects. It is noted that the velocity and the momentum boundary-layer thickness diminishes for higher values of the Casson parameter. The simultaneous effects of MHD and thermal radiation on the nanofluid flow near a stagnation-point over a permeable vertical shrinking/stretching sheet was investigated by Kandasamy *et al.* [62]. It was concluded that both the velocity and temperature profiles are significantly increased for the up-going values of the magnetic parameter and the thermal radiation parameter respectively. Recently, Tlili *et al.* [63] performed the entropy analysis for MHD

stagnation-point nanofluid flow under the influence of thermal radiation. An enhancement in the entropy generation rate is found for the increasing values of the Brownian motion parameter and the Brinkman number. A few recent contributions regarding the stagnation-point flows for different non-Newtonian fluid models can be seen in [64–68].

An investigation of the slip flow of non-Newtonian fluids has attracted many researchers due to its wide range of applications in the engineering and industrial sectors in the recent years. The assumption of no-slip velocity condition is not appropriate for the case of micro/nano-scale and low pressure flows [69]. Bhattacharyya *et al.* [70] stated that the assumptions of no-slip conditions are not applicable for all types of fluid flows. The slip condition may be imposed under certain circumstances. Zhu *et al.* [71], for the first time, quantitatively argued that the high surface-roughness produces a no-slip boundary condition. The consideration of the boundary slip condition in the case of non-Newtonian fluid flows has more significant impact than that the case of Newtonian fluid flows. Navier [72] originally proposed the slip boundary condition which linearly relates the shear rate and the velocity slip at the wall. A vast variety of problems in fluid mechanics has been solved with the Navier slip condition [73–76]. Melting polymer is an example of physical interest which requires the velocity slip at the wall. Furthermore, slip flows are also experienced through the polished artificial heart valves and internal cavities. The effect of partial velocity slip in the visco-elastic fluid flows due to the stretching of sheet was explored by Ariel *et al.* [77], Anand [78] and Megahed [79]. Li *et al.* [80] scrutinized the MHD effects on the UCM fluid taking the slip boundary condition with an improved version of the heat conduction model. According to them, the heat transfer rate is reduced for the ascending values of the slip parameter whereas it is enhanced for the augmentation in relaxation parameter. The boundary-layer flow analysis of the Williamson fluid on an upper horizontal surface of a paraboloid of revolution induced by buoyancy and partial slip was investigated by Abegunrin and Animasaun [81]. An enhancement in the horizontal and vertical velocities was noticed for the increasing values of thermal

buoyancy parameter in the presence of partial slip and thermal jump. Moreover, a prominent increment in the local skin-friction with thermal buoyancy parameter in the absence of partial slip and thermal jump was examined. Haritha *et al.* [82] explored the Navier slip effects on an unsteady Maxwell fluid flow along with the magnetic field and the convective boundary conditions. They concluded that the velocity profile was declined for an increment in the slip parameter whereas an opposite trend is witnessed in the temperature and the concentration fields. Non-linear slip boundary conditions can also be imposed on the fluid flows as discussed in [83]. Turkyilmazoglu [84] examined the slip effects on the MHD flow for two types of visco-elastic fluids past a stretching sheet. Kumar *et al.* [85] addressed the unsteady stagnation-point flow of nanofluid under the influence of velocity slip over an exponentially stretching surface. Recently, the MHD flow of nanofluid under the second-order velocity slip condition in the presence of nanoparticle migration is explored by Zhu *et al.* [86]. Mahdy and Chamkha [87] analyzed the slip flow of Maxwell fluid over an unsteady vertical stretching/shrinking surface under the impact of chemical reaction and magnetic field. It was pointed out that an enhancement in the magnetic and slip parameters shows a decreasing trend in the velocity while an opposite behavior was witnessed for the concentration distribution.

Many researchers analyzed the behavior of non-Newtonian fluid flows in the presence of a magnetic field using the CCHFM. The study of heat transfer characteristics in the MHD boundary-layer flows has innumerable applications like MHD generators, thermal therapy for the treatment of cancer, the cooling of nuclear reactors, sensors, geothermal energy extraction, magnetic drug targeting, plasma studies, design of heat exchangers, the use of non-metallic inclusion for the molten metals purification, astrophysics and many more [88]. Researchers have focused primarily, on the varying behavior of the non-Newtonian fluids when subjected to the influence of the magnetic field. The heat transfer rate which is an important factor on which the quality of the product depends, can be controlled effectively by MHD system in the electrically conducting fluids [89]. Furthermore, MHD

flow can exhibit particular characteristics in thermal conductivity. The metals in liquid form with the small Prandtl number of order $0.01 - 0.1$ such as Bismuth which has Prandtl number equal to 0.01 and mercury with Prandtl number equal to 0.023 etc., are utilized generally as coolants due to possessing large thermal conductivity [90]. Besides the flow due to horizontal stretching sheet, the influence of mixed convection because of buoyancy force cannot be neglected for the vertical sheet. There has been an increasing trend to study the problems of MHD flows with mixed convection and heat transfer properties over a stretching sheet. The MHD mixed convective flow past a permeable vertical plate in the presence of velocity and thermal slip was investigated by Mukhopadhyay and Mandal [91]. Recently, Sharada and Shankar [92] examined the MHD mixed convection Casson fluid flow along with Joule heating and convective boundary conditions over vertically stretched surface. They found that the magnetic parameter and Casson fluid parameter yield reduction in the velocity field. Few more studies regarding the flow on MHD can be consulted therein [93, 94]. The scientists and engineers are engaged to investigate the boundary-layer analysis of the rate-type fluid (UCM fluid) flows in the presence of a magnetic field.

1.1 Objectives of the Present Study

Sequel to all the existing reports, the aim of the present study is to theoretically investigate the UCM fluid flow under the influence of different physical parameters involved in the non-dimensional governing equations in laminar flow and heat transfer with CCHFM which is a generalized version of Fourier's heat flux model when the magnetic field is present. The objectives of this theoretical research are:

- To calculate the heat transfer rate of the visco-elastic fluids (UCM) over a linear/non-linear stretching sheet.

- The effects of the relaxation parameters on the skin-friction and heat transfer rate in various flow situations.

- The impacts of the applied magnetic field, porous medium, non-linear velocity slip and convective heat transfer on physical quantities involved in a particular problem.

Different chapters are constructed to present the material easily understandable for the readers. Chapter 2, is devoted to give some preliminaries and explains some basic concepts regarding the fundamentals of fluid motion and solution techniques.

In Chapter 3, attention has been focused to examines the MHD flow of UCM fluid with Joule heating and thermal radiation effects. The novel idea of heat flux recently developed by Cattaneo and Christov is considered. The aim is to inspect the involved flow governing parameters on the non-dimensional velocity and temperature distributions. To obtain the non-dimensional ODEs, suitable similarity transformations are invoked and numerical solutions of converted ODEs are archived through the shooting technique. The contents of this chapter are published in **"AIP Advances"**, 6, (2016); 085103.

In Chapter 4, the numerical results of MHD flow in the area close to the surface of UCM fluid via a porous medium over a surface caused by a non-linear stretching by deploying the updated Fourier's heat conduction model is investigated. The non-linear slip condition of velocity is imposed and investigated. This article aims at examining the impacts of noteworthy parameters such as the velocity slip, The Deborah number, the stretching ratio and the magnetic field parameters on the flow and heat transfer by making use of graphs and tables. Using similarity transformations, the system of coupled flow governing equations which are in the form of PDEs is converted into a system of non-linear ODEs. The shooting technique has been put to attain the numerical solutions of the velocity and temperature profiles. The contents of this chapter are accepted in **"Open Physics"**.

In Chapter 5, the MHD mixed convective UCM fluid flow over a vertical stretching sheet with variable thickness close to a stagnation-point is explored numerically.

The variable thermal conductivity has been assumed for the analysis of heat transfer characteristics. Furthermore, homogeneous-heterogeneous chemical reactions and thermal stratification have also been considered. Both the assisting and the opposing flows are discussed through tables and graphs. The ODEs are obtained via suitable similarity transformations. The numerical solutions of the non-dimensional velocity, temperature and concentration profiles are obtained by employing the shooting method and examined for different physical parameters such as the thermal stratification, the thermal relaxation, the mixed convection, the thermal conductivity, the stretching ratio, the homogeneous and heterogeneous reaction parameters. The contents of this chapter are published in **"Journal of the Brazilian Society of Mechanical Sciences and Engineering"**, $40, (2018); 452$.

In Chapter 6, a systematic study is ascertained for the boundary-layer slip flow of an UCM nanofluid flow induced by an inclined stretching surface in the presence of porous medium and a magnetic field. The Cattaneo-Christov double diffusion model of heat and mass transfer is incorporated in the modeling process. The relaxation framework visco-elastic system is formulated for UCM nanofluid to determine both heat and mass transfer by the CCHFM. The effects of the thermophoresis, the Brownian motion and the heat generation under the influence of chemical reaction have also been scrutinized. For a definitive confirmation of the boundary-layer approximations, it is assumed that the ratio between the forces of inertia and those of viscosity are high enough. Similarity transformations are put to use in order to acquire a dimensionless form of governing equations. These dimensionless equations have been cracked, numerically, with the shooting method. Using graphs and tables, the influence of physical parameters on the distributions of dimension free velocity, temperature and concentration are made conspicuous. The graphical presentation of the results of skin-friction, Nusselt and Sherwood numbers have also been delineated. The contents of this chapter are submitted in **"Applied Mathematics and computations"**.

Chapter 7, particularly deals with the numerical solution of an UCM nanofluid flow in the presence of a magnetic field over an inclined stretching sheet. A special consideration has been given to the effects of non-linear velocity slip, thermal radiation and heat generation. The modified Fourier and Fick's laws are incorporated in the modeling process. This model has the tendency to describe the characteristics of relaxation time for both the heat and fluid flow. The mass transfer phenomenon is investigated under the effects of the chemical reaction, the Brownian motion and the thermophoresis. By making use of some appropriate similarity transformations, the governing equations are stripped off, of their dimensionless existence and then solved through the shooting technique numerically. This research also brings into the spotlight such crucial physical parameters as are inevitable for describing the flow and heat transfer behavior. This has been done through graphs and tables with as much precision and exactitude as is possible. The results of skin-friction, Nusselt and Sherwood numbers are also calculated and presented in graphical form. The contents of this chapter are revised in **"Applied Mathematics and Information Sciences"**.

Chapter 8, is finally prepared to reveal the concluding remarks of the study.

Chapter 2

Priliminaries

This chapter envisages some cardinal concepts that this thesis deal with. Certain elementary equations, concerning the governing of fluid flows are discussed. Attempts have been made to describe and decipher the temperature equation in the light of CCHFM. To make matters even clear for the reader, the numerical technique employed for the solution of the governing equations has also been included.

2.1 Some Basic Governing Laws [95]

The most influential and effective equations in the area of fluid dynamics are specifically the ones dealing with the laws of conservation of mass, momentum and energy. These laws examine the momentum and thermodynamical properties of both compressible as well as incompressible viscous fluids. The present study confines its focus, exclusively, to the incompressible fluids. "The conservation law of linear momentum is also known as Newton's second law of motion and the law of conservation of energy is also known as the first law of thermodynamics. The above mentioned governing laws are stated for incompressible viscous fluids only which are read as:

$$\nabla \cdot \mathbf{v} = 0, \quad \text{(Law of conservation of mass)} \tag{2.1}$$

$$\rho \frac{D\mathbf{v}}{Dt} = \nabla \cdot \tau_{\mathbf{c}} + \mathbf{J} \times \mathbf{B} + \mathbf{R}, \text{ (Law of conservation of momentum)} \tag{2.2}$$

$$\rho C_p \frac{DT}{Dt} = \Phi_v + k\nabla^2 T, \text{ (Law of conservation of energy)} \tag{2.3}$$

where the total derivative is equal to the sum of local and convective derivatives i.e.,

$$\frac{D}{Dt} = \frac{\partial}{\partial t} + \mathbf{v} \cdot \nabla, \tag{2.4}$$

and $\mathbf{v}$ denotes the velocity vector of the fluid, T the fluid temperature, ρ the fluid density, p the pressure, $\mathbf{J}$ the current density, $\mathbf{B} = \mathbf{B_0} + \mathbf{b_0}$ the magnetic flux, $\mathbf{B_0}$ the applied magnetic field and $\mathbf{b_0}$ the induced magnetic field, $\mathbf{R}$ the Darcy's resistance, C_p the specific heat, k the thermal conductivity of the fluid which is assumed to be constant and Φ_v the viscous dissipation.

In addition when the magnetic field is present, four more laws are considered in addition to (2.1)-(2.3) [96]:

$$\nabla \cdot \mathbf{E} = \frac{\rho_c}{\epsilon_p}, \quad \text{(Gauss's Law)} \tag{2.5}$$

$$\nabla \times \mathbf{E} = -\frac{\partial \mathbf{B}}{\partial t}, \quad \text{(Faraday's Law)} \tag{2.6}$$

$$\nabla \times \mathbf{B} = \mu_0 \mathbf{J} + \mu_0 \epsilon_p \frac{\partial \mathbf{E}}{\partial t}, \quad \text{(Ampere's Law with Maxwell's correction)} \tag{2.7}$$

$$\nabla \cdot \mathbf{B} = 0, \quad \text{(Gauss's Law for magnetism)} \tag{2.8}$$

where $\mathbf{J} = \sigma(\mathbf{v} \times \mathbf{B} + \mathbf{E})$. Here ϵ_p is the permittivity of free space, μ_0 the magnetic permeability, σ the fluid electrical conductivity, $\mathbf{E}$ the electric field and $\mathbf{B}$ the magnetic field.

The momentum Eq. (2.2) for UCM fluid model is

$$\rho \mathbf{a} = \rho \frac{D\mathbf{v}}{Dt} = \nabla \cdot \tau_{\mathbf{c}} + \mathbf{J} \times \mathbf{B} + \mathbf{R}, \tag{2.9}$$

where $\mathbf{a}$ is the acceleration vector and $\tau_{\mathbf{c}}$ the Cauchy stress tensor for UCM fluid given by

$$\tau_{\mathbf{c}} = -p\mathbf{I} + \mathbf{S}, \tag{2.10}$$

The extra stress tensor $\mathbf{S}$ is defined as

$$\mathbf{S} + \Lambda \frac{D\mathbf{S}}{Dt} = \mu \mathbf{A_1}, \tag{2.11}$$

where Λ denotes the relaxation time and $\mathbf{A_1}$ the first Rivlin-Ericksen tensor defined as

$$\mathbf{A_1} = L + L^t, \quad L = \nabla \mathbf{v}. \tag{2.12}$$

The following equations are used for the two-rank tensor $\mathbf{S}$, a vector $\mathbf{b}$ and a scalar function ψ, respectively.

$$\frac{D\mathbf{S}}{Dt} = \frac{\partial \mathbf{S}}{\partial t} + (\mathbf{v} \cdot \nabla) \mathbf{S} - L\,\mathbf{S} - \mathbf{S}\,L^t, \tag{2.13}$$

$$\frac{D\mathbf{b}}{Dt} = \frac{\partial \mathbf{b}}{\partial t} + (\mathbf{v} \cdot \nabla) \mathbf{b} - L\,\mathbf{b}, \tag{2.14}$$

$$\frac{D\psi}{Dt} = \frac{\partial \psi}{\partial t} + (\mathbf{v} \cdot \nabla) \psi. \tag{2.15}$$

Using Eq. (2.10), the equation of motion takes the form:

$$\rho\,\mathbf{a} = -\nabla\,p + \nabla \cdot \mathbf{S} + \mathbf{J} \times \mathbf{B} + \mathbf{R}. \tag{2.16}$$

The electromagnetic body force ignoring induced magnetic field takes the form:

$$\mathbf{J} \times \mathbf{B} = \sigma((\mathbf{v} \times \mathbf{B_0}) \times \mathbf{B_0}) \tag{2.17}$$

$$= \sigma[(\mathbf{v} \cdot \mathbf{B_0})\mathbf{B_0} - \mathbf{v}(\mathbf{B_0} \cdot \mathbf{B_0})] \tag{2.18}$$

$$= -\sigma \mathbf{B_0^2}\mathbf{v}. \tag{2.19}$$

To eliminate $\mathbf{S}$ from Eqs. (2.11) and (2.16), applying the operator $(1 + \Lambda \frac{D}{Dt})$ onto Eq. (2.16), we have

$$\left. \begin{aligned} \rho\left(\mathbf{a} + \Lambda\frac{D\mathbf{a}}{Dt}\right) = &-\left(1 + \Lambda\frac{D}{Dt}\right)\nabla\,p + \left(1 + \Lambda\frac{D}{Dt}\right)\nabla \cdot \mathbf{S} \\ &+ \left(1 + \Lambda\frac{D}{Dt}\right)\mathbf{R} + \left(1 + \Lambda\frac{D}{Dt}\right)(\mathbf{J} \times \mathbf{B}), \end{aligned} \right\} \tag{2.20}$$

Eq. (2.20) in view the result $(D/Dt)(\nabla\cdot) = \nabla \cdot (D/Dt)$ given by Harris [97] is

$$\rho \left(\mathbf{a} + \Lambda \frac{D\mathbf{a}}{Dt} \right) = - \left(1 + \Lambda \frac{D}{Dt} \right) \nabla p + \nabla \cdot \left(1 + \Lambda \frac{D}{Dt} \right) \mathbf{S}$$
$$+ \left(1 + \Lambda \frac{D}{Dt} \right) \mathbf{R} + \left(1 + \Lambda \frac{D}{Dt} \right) (\mathbf{J} \times \mathbf{B}), \tag{2.21}$$

or

$$\rho \left(\mathbf{a} + \Lambda \frac{D\mathbf{a}}{Dt} \right) = - \left(1 + \Lambda \frac{D}{Dt} \right) \nabla p + \mu \nabla \cdot \mathbf{A_1}$$
$$+ \left(1 + \Lambda \frac{D}{Dt} \right) \mathbf{R} + \left(1 + \Lambda \frac{D}{Dt} \right) (\mathbf{J} \times \mathbf{B}). \tag{2.22}$$

According to Tan and Masuoka [98], Darcy's resistance in an Oldroyd-B fluid satisfes the following expression:

$$\left(1 + \Lambda \frac{D}{Dt} \right) \mathbf{R} = - \frac{\nu}{\epsilon_0} \left(1 + \Lambda_r \frac{D}{Dt} \right) \mathbf{v} \tag{2.23}$$

where Λ_r is the retardation time and ϵ_0 is the permeability of the porous medium. For Maxwell fluid $\Lambda_r = 0$ and hence

$$\left(1 + \Lambda \frac{D}{Dt} \right) \mathbf{R} = - \frac{\nu}{\epsilon_0} \mathbf{v} \tag{2.24}$$

For two-dimensional flow having the velocity $\mathbf{v} = [u(x, y), v(x, y), 0]$ and using Eq. (2.12), we have

$$L = \begin{pmatrix} \frac{\partial u}{\partial x} & \frac{\partial u}{\partial y} \\ \frac{\partial v}{\partial x} & \frac{\partial v}{\partial y} \end{pmatrix}, \quad L^t = \begin{pmatrix} \frac{\partial u}{\partial x} & \frac{\partial v}{\partial x} \\ \frac{\partial u}{\partial y} & \frac{\partial v}{\partial y} \end{pmatrix}, \tag{2.25}$$

The first Rivlin-Ericksen tensor is given by

$$\mathbf{A_1} = \begin{pmatrix} 2\frac{\partial u}{\partial x} & \frac{\partial u}{\partial y} + \frac{\partial v}{\partial x} \\ \frac{\partial v}{\partial x} + \frac{\partial u}{\partial y} & 2\frac{\partial v}{\partial y} \end{pmatrix}, \tag{2.26}$$

Using Eq. (2.14), for steady case, we have

$$\frac{D\mathbf{a}}{Dt} = (\mathbf{v} \cdot \nabla) \mathbf{a} - L\mathbf{a}, \tag{2.27}$$

along with

$$\mathbf{a} = \left[u\frac{\partial u}{\partial x} + v\frac{\partial u}{\partial y}, u\frac{\partial v}{\partial x} + v\frac{\partial v}{\partial y}, 0 \right]. \tag{2.28}$$

Making use of Eqs. (2.25), (2.27) and (2.28), we have

$$\frac{D\mathbf{a}}{Dt} = \left[u^2\frac{\partial^2 u}{\partial x^2} + 2uv\frac{\partial^2 u}{\partial x \partial y} + v^2\frac{\partial^2 u}{\partial y^2}, u^2\frac{\partial^2 v}{\partial x^2} + 2uv\frac{\partial^2 v}{\partial x \partial y} + v^2\frac{\partial^2 v}{\partial y^2}, 0 \right], \tag{2.29}$$

$$\nabla \cdot \mathbf{A_1} = \left[\frac{\partial^2 u}{\partial x^2} + \frac{\partial^2 u}{\partial y^2}, \frac{\partial^2 v}{\partial x^2} + \frac{\partial^2 v}{\partial y^2}, 0 \right]. \tag{2.30}$$

Thus for two-dimensional flow having velocity $\mathbf{v} = [u(x,y), v(x,y), 0]$, the governing equations in the component form, are

$$\left. \begin{aligned} \rho \left[u\frac{\partial u}{\partial x} + v\frac{\partial u}{\partial y} + \Lambda \left(u^2\frac{\partial^2 u}{\partial x^2} + v^2\frac{\partial^2 u}{\partial y^2} + 2uv\frac{\partial^2 u}{\partial x \partial y} \right) \right] + \left(1 + \Lambda\frac{D}{Dt} \right) \frac{\partial p}{\partial x} \\ = \mu \left(\frac{\partial^2 u}{\partial x^2} + \frac{\partial^2 u}{\partial y^2} \right) - \sigma B_0^2 u - \sigma B_0^2 \Lambda v\frac{\partial u}{\partial y} - \frac{\nu}{\epsilon_0}u, \end{aligned} \right\} \tag{2.31}$$

$$\left. \begin{aligned} \rho \left[u\frac{\partial v}{\partial x} + v\frac{\partial v}{\partial y} + \Lambda \left(u^2\frac{\partial^2 v}{\partial x^2} + v^2\frac{\partial^2 v}{\partial y^2} + 2uv\frac{\partial^2 v}{\partial x \partial y} \right) \right] + \left(1 + \Lambda\frac{D}{Dt} \right) \frac{\partial p}{\partial y} \\ = \mu \left(\frac{\partial^2 v}{\partial x^2} + \frac{\partial^2 v}{\partial y^2} \right). \end{aligned} \right\} \tag{2.32}$$

Using the boundary-layer approximations [5]:

$$u = \mathcal{O}(1), \quad v = \mathcal{O}(\delta), \quad x = \mathcal{O}(1), \quad y = \mathcal{O}(\delta), \tag{2.33}$$

the above equations may be written as:

$$\left. \begin{aligned} u\frac{\partial u}{\partial x} + v\frac{\partial u}{\partial y} + \Lambda \left(u^2\frac{\partial^2 u}{\partial x^2} + v^2\frac{\partial^2 u}{\partial y^2} + 2uv\frac{\partial^2 u}{\partial x \partial y} \right) + \frac{1}{\rho} \left(1 + \Lambda\frac{D}{Dt} \right) \frac{\partial p}{\partial x} \\ = \nu\frac{\partial^2 u}{\partial y^2} - \frac{\sigma B_0^2}{\rho} \left(u + \Lambda v\frac{\partial u}{\partial y} \right) - \frac{\nu}{\epsilon_0}u. \end{aligned} \right\} \tag{2.34}$$

In the free stream $u = U_e = 0$, Eq. (2.34) reduces to

$$0 = U_e\frac{\partial U_e}{\partial x} + \Lambda U_e^2\frac{\partial^2 U_e}{\partial x^2} + \frac{\nu}{\epsilon_0}U_e = -\frac{1}{\rho} \left(1 + \Lambda\frac{D}{Dt} \right) \frac{\partial p}{\partial x} \tag{2.35}$$

Eliminating $-\left(1 + \Lambda\frac{D}{Dt} \right) \frac{\partial p}{\partial x}$ from Eq. (2.34), we obtain the flow equation as:

$$u\frac{\partial u}{\partial x} + v\frac{\partial u}{\partial y} + \Lambda\left(u^2\frac{\partial^2 u}{\partial x^2} + v^2\frac{\partial^2 u}{\partial y^2} + 2uv\frac{\partial^2 u}{\partial x\partial y}\right) + \frac{\sigma B_0^2}{\rho}\left(u + \Lambda v\frac{\partial u}{\partial y}\right) \left.\right\}$$
$$= \nu\frac{\partial^2 u}{\partial y^2} - \frac{\nu}{\epsilon_0}u, \qquad (2.36)$$

where (u, v) are the velocities along (x, y) directions respectively."

2.2 Slip Boundary Condition

In fluid dynamics, it is a well-known fact at macroscopic level that the condition at a solid wall boundary for a viscous fluid is of no-slip nature i.e. the velocity of the fluid coincides with the velocity of the solid boundary. However, in many practical situations, the fluid may slip on the surface of a solid. In general, the dependence of slip on the shear stress on the wall is assumed which may be stated as:

$$u - U_w = \Delta\frac{\partial u}{\partial m}, \qquad (2.37)$$

where Δ denotes the slip length and m the coordinate perpendicular to the wall.

2.3 Boundary-Layer Equations

One of the most significant contributions to science of fluid motion was presented by L. Prandtl. He analyzed the diversity of ways in which viscosity does influence the high Raynolds number flows. Prandtl also enunciated how the Navier-Stokes equations can reduced simple so that they ought come out with solutions that may be close to approximations under this limiting case. Coming to the simplifications that stem from the Navier-Stokes equations particularly in the matter of small friction forces, we use a physically illustrative technique. To make thinks more comprehensible, we take the case of a two-dimensional flow of an incompressible viscous fluid. "The continuity and momentum equations in the absence of body forces are written as [5]:

$$\frac{\partial u}{\partial x} + \frac{\partial v}{\partial y} = 0, \tag{2.38}$$

$$\frac{\partial u}{\partial t} + u\frac{\partial u}{\partial x} + v\frac{\partial u}{\partial y} = -\frac{1}{\rho}\frac{\partial p}{\partial x} + \nu\left(\frac{\partial^2 u}{\partial x^2} + \frac{\partial^2 u}{\partial y^2}\right), \tag{2.39}$$

$$\frac{\partial v}{\partial t} + u\frac{\partial v}{\partial x} + v\frac{\partial v}{\partial y} = -\frac{1}{\rho}\frac{\partial p}{\partial y} + \nu\left(\frac{\partial^2 v}{\partial x^2} + \frac{\partial^2 v}{\partial y^2}\right), \tag{2.40}$$

where $\nu = \frac{\mu}{\rho}$ is the kinematic viscosity. In order to non-dimensionalize the Eqs. (2.38)-(2.40), the following transformations are introduced

$$t^* = \frac{tU_r}{L}, \; x^* = \frac{x}{L}, \; y^* = \frac{y}{L}, \; u^* = \frac{u}{U_r}, \; v^* = \frac{v}{U_r}, \; p^* = \frac{p}{\rho U_r^2}, \tag{2.41}$$

where U_r is the reference velocity and L is the characteristic length of surface in x-direction. The utilization of transformations (2.41) in Eqs. (2.38)-(2.40) results in the following system:

$$\frac{\partial u^*}{\partial x^*} + \frac{\partial v^*}{\partial y^*} = 0, \tag{2.42}$$

$$\frac{\partial u^*}{\partial t^*} + u^*\frac{\partial u^*}{\partial x^*} + v^*\frac{\partial u^*}{\partial y^*} = -\frac{\partial p^*}{\partial x^*} + \frac{1}{Re}\left(\frac{\partial^2 u^*}{\partial x^{*2}} + \frac{\partial^2 u^*}{\partial y^{*2}}\right), \tag{2.43}$$

$$\frac{\partial v^*}{\partial t^*} + u^*\frac{\partial v^*}{\partial x^*} + v^*\frac{\partial v^*}{\partial y^*} = -\frac{\partial p^*}{\partial y^*} + \frac{1}{Re}\left(\frac{\partial^2 v^*}{\partial x^{*2}} + \frac{\partial^2 v^*}{\partial y^{*2}}\right), \tag{2.44}$$

where $Re = \frac{U_r L}{\nu}$ is the Reynolds number.

For momentum boundary-layer approximation, the order of magnitude analysis of Eqs. (2.42)-(2.44) is done as described in [5]. The order of magnitude of length x^* and velocity u^* is taken to be one, i.e. $x^* = \mathcal{O}(1)$, $u^* = \mathcal{O}(1)$ and the length y^* and velocity v^* have order of magnitude of the boundary-layer thickness $\mathcal{O}(\delta^*)$.

Moreover, it is considered that the local accelerations (i.e, $\frac{\partial u^*}{\partial t^*}$) have the same order of magnitude as the convective acceleration (i.e. $u^* \frac{\partial u^*}{\partial x^*}$) and the factor $\frac{1}{Re}$ has order of magnitude $\mathcal{O}(\delta^{*2})$. Also $\frac{\partial p^*}{\partial x^*} = \mathcal{O}(1)$ and $\frac{\partial p^*}{\partial y^*} = \mathcal{O}(\frac{1}{\delta^*})$. The continuity equation has the same order of magnitude. Then

$$
\begin{array}{ccccccccc}
\dfrac{\partial u^*}{\partial t^*} & + & u^*\dfrac{\partial u^*}{\partial x^*} & + & v^*\dfrac{\partial u^*}{\partial y^*} & = & -\dfrac{\partial p^*}{\partial x^*} & + & \dfrac{1}{Re} & \left(\dfrac{\partial^2 u^*}{\partial x^{*2}} + \dfrac{\partial^2 u^*}{\partial y^{*2}}\right) \\
\downarrow & & \downarrow & & \downarrow & & & & \downarrow & \downarrow \qquad\qquad \downarrow \\
1 & & 1.1 & & \delta^*\cdot\dfrac{1}{\delta^*} & & & & \delta^{*2} & 1 \qquad\quad \dfrac{1}{\delta^{*2}}
\end{array}
\tag{2.45}
$$

$$
\begin{array}{ccccccccc}
\dfrac{\partial v^*}{\partial t^*} & + & u^*\dfrac{\partial v^*}{\partial x^*} & + & v^*\dfrac{\partial v^*}{\partial y^*} & = & -\dfrac{\partial p^*}{\partial y^*} & + & \dfrac{1}{Re} & \left(\dfrac{\partial^2 v^*}{\partial x^{*2}} + \dfrac{\partial^2 v^*}{\partial y^{*2}}\right) \\
\downarrow & & \downarrow & & \downarrow & & & & \downarrow & \downarrow \qquad\qquad \downarrow \\
\delta^* & & 1.\delta^* & & \delta^*.1 & & & & \delta^{*2} & \delta^* \qquad\quad \dfrac{1}{\delta^*}
\end{array}
\tag{2.46}
$$

Ignoring the terms of δ^* and δ^{*2}, we have

$$
\frac{\partial u^*}{\partial t^*} + u^*\frac{\partial u^*}{\partial x^*} + v^*\frac{\partial u^*}{\partial y^*} = -\frac{\partial p^*}{\partial x^*} + \frac{1}{Re}\frac{\partial^2 u^*}{\partial y^{*2}},
\tag{2.47}
$$

$$
\frac{\partial p^*}{\partial y^*} = 0.
\tag{2.48}
$$

The two-dimensional energy equation reads as:

$$
\frac{\partial T}{\partial t} + u\frac{\partial T}{\partial x} + v\frac{\partial T}{\partial y} = \frac{k}{\rho C_p}\left(\frac{\partial^2 T}{\partial x^2} + \frac{\partial^2 T}{\partial y^2}\right),
\tag{2.49}
$$

The above equation can be normalized by using (2.41) and by introducing the dimensionless temperature

$$
T^* = \frac{T - T_\infty}{T_w - T_\infty},
\tag{2.50}
$$

as:

$$
\frac{\partial T^*}{\partial t^*} + u^*\frac{\partial T^*}{\partial x^*} + v^*\frac{\partial T^*}{\partial y^*} = \frac{1}{P_r Re}\left(\frac{\partial^2 T^*}{\partial x^{*2}} + \frac{\partial^2 T^*}{\partial y^{*2}}\right),
\tag{2.51}
$$

where $P_r = \frac{\mu C_p}{k}$ is the Prandtl number. $T = \mathcal{O}(1)$, $y = \mathcal{O}(\delta^*)$ and $P_r Re = \mathcal{O}(\frac{1}{\delta^{*2}})$.

It is also observed that $\frac{\partial^2 T^*}{\partial x^{*2}} << \frac{\partial^2 T^*}{\partial y^{*2}}$. On this basis, we have

$$
\begin{array}{ccccccc}
\frac{\partial T^*}{\partial t^*} & + & u^*\frac{\partial T^*}{\partial x^*} & + & v^*\frac{\partial T^*}{\partial y^*} & = & \frac{1}{P_r Re} & \left(\frac{\partial^2 T^*}{\partial x^{*2}} & + & \frac{\partial^2 T^*}{\partial y^{*2}}\right) \\
\downarrow & & \downarrow & & \downarrow & & \downarrow & \downarrow & & \downarrow \\
1 & & 1.1 & & \delta^* \cdot \frac{1}{\delta^*} & & \delta^{*2} & 1 & & \frac{1}{\delta^{*2}}
\end{array}
\tag{2.52}
$$

Under these assumptions, the thermal boundary-layer equation is given as:

$$
\frac{\partial T^*}{\partial t^*} + u^*\frac{\partial T^*}{\partial x^*} + v^*\frac{\partial T^*}{\partial y^*} = \frac{1}{P_r Re}\frac{\partial^2 T^*}{\partial y^{*2}}.
\tag{2.53}
$$

"

2.4 Heat Transfer

As a branch of engineering "heat transfer" focusses on the transfer of thermal energy from one medium to another or within a medium caused by the variation in temperature. This movement transpires in either of the three elementary forms [99] namely *conduction, convection, and radiation.* "The transfer of heat within a medium due to diffusion process is called conduction heat transfer. Fourier's law states that the heat flow is proportional to the temperature gradient. The proportionality parameter is known as the thermal conductivity. Note that for heat conduction to occur there must be temperature differences between neighboring points.

Convection heat transfer is the energy transport affected by the motion of a fluid. The convection heat transfer between two dissimilar media is governed by Newton's law of cooling. It states that the heat flow is proportional to the difference of the temperatures between the two media. The proportionality parameter is called the convection heat transfer coefficient. For heat convection to occur there must be a fluid or another medium that can transport energy to and from the primary medium.

Radiation is a mechanism that is different from two transport processes we discussed so far, namely, (1) energy transport by conduction that is proportional to the negative of the temperature gradient and (2) energy transport by convection that is proportional to the difference in temperatures of the body and the moving fluid in contact with the body. Thermal radiation is an electromagnetic mechanism, which allows energy transport with the speed of light through regions of space that are devoid of any matter. Radiant energy exchange between surfaces or between a region and its surroundings is described by the Stefan-Boltzmann law, which states that the radiant energy transmitted is proportional to the difference of the fourth power of the temperatures of the surfaces. The proportionality parameter is known as the Stefan-Boltzmann parameter."

2.4.1 Fourier's Heat Conduction Law

In the classical continuum mechanics, "the thermal flux vector $\mathbf{q}$ obeys the Fourier's heat conduction law [30] namely

$$\mathbf{q} = -k\nabla T, \tag{2.54}$$

where k is the thermal conductivity and T the temperature of the fluid. The negative sign in Eq. (2.54) indicates that heat flows downhill on the temperature scale. The balance of energy requires that $(e = C_p T)$

$$\rho C_p \frac{DT}{Dt} = \Phi_v - \nabla \cdot \mathbf{q} + \rho r_h, \qquad \frac{D}{Dt} = \frac{\partial}{\partial t} + \mathbf{v} \cdot \nabla \tag{2.55}$$

which, in view of Eq. (2.54), becomes

$$\rho C_p \frac{DT}{Dt} = \Phi_v + k\nabla^2 T + \rho r_h, \tag{2.56}$$

where r_h is the internal heat generation per unit volume, ρ the density and C_p the specific heat of the material (assumed to be independent of time t). For a fluid medium, Eq. (2.56) becomes

$$\rho C_p \left(\frac{\partial T}{\partial t} + \mathbf{v} \cdot \nabla T \right) = \Phi_v + k \nabla^2 T + \rho r_h, \tag{2.57}$$

where $\mathbf{v}$ is the velocity field and Φ_v the viscous dissipation function.

The Eq. (2.54), also known as Fick's law in the context of mass diffusion, is one of the basic constitutive relations in the physical sciences. Unfortunately, Fourier's law predicts that thermal signals propagate with infinite speed, a drawback which appears to have first been noted by Nernst in 1917 (see Ref. [100]). Such behavior, which is most apparent under low temperature and/or high heat-flux conditions ([101, 102]), clearly violates causality.

The balance law for the internal (heat) energy can, in the absence of all thermal sources or sinks and neglecting internal dissipation, be expressed in terms of T as (see Ref. [103]):

$$\rho C_p \frac{DT}{Dt} + \nabla \cdot \mathbf{q} = 0, \tag{2.58}$$

where C_p, the specific heat at constant pressure, is a constant. Here, $\mathbf{v}$ is the velocity vector of the material point, t is time, ρ is the mass density and we note that the equation of continuity,

$$\frac{\partial \rho}{\partial t} + \nabla \cdot (\rho \mathbf{v}) = 0, \tag{2.59}$$

was employed in obtaining Eq. (2.58) from the balance equation for the internal energy. In addition,

$$\frac{D}{Dt} = \frac{\partial}{\partial t} + \mathbf{v} \cdot \nabla, \tag{2.60}$$

which denotes the material derivative, acknowledges the fact that the time rate of change of a material quantity at a certain geometrical point is the result of two processes: A change in the geometrical point, i.e., the partial time derivative and a change due to the fact that a different quantity is transported from the neighboring points to the point under consideration. When combined with Eq. (2.58), the conservation of energy law, Eq. (2.54), yields the heat transport equation

$$T_t + \mathbf{v} \cdot \nabla T - \alpha \nabla^2 T = 0, \tag{2.61}$$

where $\alpha = \frac{k}{\rho C_p}$ is the thermal diffusivity. Like the much better known heat (or diffusion) equation, which Eq. (2.61) reduces to when $\mathbf{v} = 0$, the latter is also a PDE of the parabolic type. Consequently, it is predicted that a thermal disturbance at any point in a material body will be felt instantly, but unequally, at all other points of the body. From this, it is obvious that Fourier's law does not fully describe the diffusion process."

2.4.2 Heat Transport Equation under the MC Law [30]

"To correct this unrealistic feature, which is known as the paradox of heat conduction, various modifications of the Fourier's law have been proposed over the years, not all of which have been successful (see [104]). Of these, the best known is the MC law ([100, 101, 104–106]),

$$(1 + \Lambda_h \partial_t)\mathbf{q} = -k\nabla T, \qquad (2.62)$$

where ∂_t denotes $\frac{\partial}{\partial t}$. Here, the thermal relaxation constant $\Lambda_h > 0$ represents the time lag required to establish steady heat conduction in a volume element once a temperature gradient has been imposed across it [101]. This generalization of the Fourier's law accounts for the finite speed of heat conduction by adding a term proportional to the time derivative of the flux vector, known as the thermal inertia term, to the left-hand side of Eq. (2.54). It should be mentioned that the value of Λ_h has been experimentally determined for a number of materials [107–109].

Let us begin by observing that $\mathbf{q}$ can be eliminated from Eq. (2.58) using Eq. (2.62). Consequently, the heat transport equation arising from the MC law is found to be

$$\Lambda_h(T_{tt} + (\mathbf{v} \cdot \nabla T)_t) + T_t + \mathbf{v} \cdot \nabla T = \Lambda_h c^2 \nabla^2 T, \qquad (2.63)$$

where $c = \sqrt{\frac{k}{\Lambda_h}}$ and again no thermal sources or sinks are present.

To simplify our analysis, we introduce the following non-dimensional variables: $x' = x/l$, $t' = t/\Lambda_h$, $T' = T/T_0$ and $\mathbf{v}' = \mathbf{v}/c$, where $l = \sqrt{k\Lambda_h}$ and $T_0(>$

0), respectively, denote a characteristic length and temperature. On making the indicated replacements, Eq. (2.63) is reduced to the dimensionless form

$$T_{tt} + (\mathbf{v} \cdot \nabla T)_t + T_t + \mathbf{v} \cdot \nabla T = \nabla^2 T, \tag{2.64}$$

where all primes have been omitted for convenience."

2.4.3 MC Law in Material Framework

"The MC law in the material framework [30], in general $3D$ case, is

$$\mathbf{q} + \Lambda_h(\partial_t + \mathbf{v} \cdot \nabla)\mathbf{q} = -k\nabla T. \tag{2.65}$$

This reveals that in case of more than one dimension, the material MC law is seriously coupled with the Eq. (2.58). The reason being that it cannot be solved with respect to $\mathbf{q}$. So, the Eqs. (2.58), (2.59) and (2.65) form a coupled system."

2.4.4 MC Law with Upper-Convected Oldroyd Derivative

"The objective time derivative of a vector density has the form (see details [30])

$$\frac{D\mathbf{A}}{Dt} = \frac{\partial \mathbf{A}}{\partial t} + \mathbf{v} \cdot \nabla\mathbf{A} - \mathbf{A} \cdot \nabla\mathbf{v} + (\nabla \cdot \mathbf{v})\mathbf{A}. \tag{2.66}$$

Following the established terminology ([73]), we can call Eq. (2.66) 'the upper convected' material derivative (objective rate) of vector $\mathbf{A}$.

The partial time derivative is replaced in the MC law with the upper-convected Oldroyd derivative, which is a frame indifferent objective rate. Since for a scalar T, the invariant time derivative is simply the total (material, susbtantial, convective, etc.) derivative, then the material invariant form of the balance law for the internal energy reads

$$\rho C_p \left(\frac{\partial T}{\partial t} + \mathbf{v} \cdot \nabla T \right) = -\nabla \cdot \mathbf{q}. \tag{2.67}$$

Now in addition to Eq. (2.58), we have the frame-indifferent generalization of the Fourier's law with relaxation of the heat flux, namely

$$\Lambda_h \left[\frac{\partial \mathbf{q}}{\partial t} + \mathbf{v} \cdot \nabla \mathbf{q} - \mathbf{q} \cdot \nabla \mathbf{v} + (\nabla \cdot \mathbf{v})\mathbf{q} \right] + \mathbf{q} = -\alpha \nabla T, \qquad (2.68)$$

where we recall that Λ_h is the relaxation time of heat flux and α stands for the thermal conductivity. We call Eq. (2.68) the frame-indifferent MC model of heat conduction. This model is a straightforward generalization of the model from Christov and Jordan [110], which is based on the material derivative. That model was shown to be irreducible, in the sense that the flux cannot be eliminated (i.e., a single equation for the temperature field cannot be derived, see [110]). Hence, it is important to interrogate the new model for reducibility."

2.4.5 A Single Temperature Equation in View of CCHFM

The Christov [30] research focuses, seriously, on the consequences that emerge when and if we take the upper-convected derivative instead of the more material derivative. It has tried to clarify that "the flux vector $\mathbf{q}$ can be removed between the two Eqs. (2.58) and (2.68) if we follow the crux of a similar derivation for the displacement current as explored in another article by Christov [111]. As Christov [30] has worked out:

$$\nabla \cdot \left[\frac{\partial \mathbf{q}}{\partial t} + \mathbf{v} \cdot \nabla \mathbf{q} - \mathbf{q} \cdot \nabla \mathbf{v} + (\nabla \cdot \mathbf{v})\mathbf{q} \right] = (\nabla \cdot \mathbf{q})_t + \nabla \cdot [(\nabla \cdot \mathbf{q})\mathbf{v}] \qquad (2.69)$$

This derivation gives the liberty to derive from Eq. (2.68) the below mentioned equation

$$\Lambda_h \left[(\nabla \cdot \mathbf{q})_t + \nabla \cdot [(\nabla \cdot \mathbf{q})\mathbf{v}] \right] + \nabla \cdot \mathbf{q} = -\nabla \cdot (\alpha \nabla T). \qquad (2.70)$$

It further enables us to alternate Eq. (2.58) in Eq. (2.70) and render a single equation, more plausible equation for the temperature field, as:

$$\Lambda_h[T_{tt} + 2\mathbf{v} \cdot \nabla T_t + \mathbf{v}_t \cdot \nabla T + (T_t + \mathbf{v} \cdot \nabla T)(\nabla \cdot \mathbf{v}) + \mathbf{v} \cdot \nabla(\mathbf{v} \cdot \nabla T)]$$

$$+ T_t + \mathbf{v} \cdot \nabla T = \nabla \cdot (\alpha \nabla T), \quad \alpha = \frac{k}{\rho C_p} \tag{2.71}$$

where α becomes the coefficient of heat diffusion."

The conclusion in Eq. (2.71) is very significant. It reveals, very clearly, that once an accurate invariant time derivative is put to use for the relaxation term in the MC law, it can lead to a solitary equation for the temperature distribution.

2.5   Shooting Method

There are several approaches to solve BVPs. The basic flow governing equations are in PDEs. These PDEs are converted to ODEs via similarity transformations. To solve our ODEs, we employ the numerical technique i.e., the non-linear shooting technique with RK4 method for various physical parameters. In the shooting method, we consider the BVP as an IVP and try to determine the value $y(a_0)$ which results in $y(b_0) = b_0$. For the details of the shooting procedure, we are considering the following example [112]

"Consider the BVP for the second order differential equation of the form

$$y'' = f(x, y, y'), \quad a_0 \leq x \leq b_0, \; y(a_0) = \alpha_0 \; \text{ and } \; y(b_0) = \beta_0, \tag{2.72}$$

where $f(x, y, y')$ is linear in y and y', the shooting method solves a system of two initial value problems and the solution $y(x)$ of the boundary value problem (2.72) is of the form

$$y(x) = y_1(x) + \frac{\beta_0 - y_1(b_0)}{y_2(b_0)} y_2(x) \tag{2.73}$$

where $y_1(x)$ and $y_2(x)$ are solutions of two initial value problems, respectively. Now we consider the cases where $f(x, y, y')$ is not linear in y and y'. Assume a given boundary value problem has a unique solution $y(x)$. We will approximate the solution $y(x)$ by solving a sequence of initial value problems

$$y'' = f(x, y, y'), \quad a_0 \leq x \leq b_0, \; y(a_0) = \alpha_0 \; \text{ and } \; y'(a_0) = s_k, \tag{2.74}$$

where s_k are real numbers. Let $y(x, s_k)$ be solution of the initial value problem (2.74). We want to have a sequence $\{s_k\}$ so that

$$\lim_{k \to \infty} y(x, s_k) = y(x) \tag{2.75}$$

One of choices for s_0 is

$$s_0 = y'(a_0) \approx \frac{y(b_0) - y(a_0)}{b_0 - a_0} = \frac{\beta_0 - \alpha_0}{b_0 - a_0}, \tag{2.76}$$

How to choose s_k for $k \geq 1$? Choose s such that

$$y(b_0, s) - \beta_0 = 0 \tag{2.77}$$

that is s is a solution of the equation. Observe that the equation $y(b_0, s) - \beta_0 = 0$ is a non-linear equation in one variable. We have studied numerical methods: Bisection method, Newton method, secant method and fixed-point method for non-linear equations of the form $g(s) = 0$. For given s_0, the Newton method computes s_k for $k \geq 1$ as follows:

$$s_k = s_{k-1} - \frac{g(s_{k-1})}{g'(s_{k-1})} \tag{2.78}$$

These methods can be used here to solve the non-linear Eq. (2.77). Use Newton's method to approximate the solution of $y(b_0, s) - \beta_0 = 0$.

$$s_k = s_{k-1} - \frac{y(b_0, s_{k-1}) - \beta_0}{\frac{dy(b_0, s_{k-1})}{ds}} \tag{2.79}$$

Again, $y(b_0, s_{k-1}) - \beta_0$ is the last element in the array y. Since we do not know $y(x)$ explicitly, how can we determine $\frac{dy(b_0, s_{k-1})}{ds}$?

Let $y(x, s)$ be the solution of the initial value problem (2.74). Then from (2.74), we have

$$y''(x, s) = f(x, y(x.s), y'(x, s)), \quad a_0 \leqslant x \leqslant b_0, \; y(a_0, s) = \alpha_0, \; y'(a_0, s) = s. \tag{2.80}$$

By differentiating both sides of (2.80) with respect to s, we have

$$\frac{\partial y''(x,s)}{\partial s} = \frac{\partial f(x, y(x.s), y'(x,s))}{\partial s}$$
$$= f_x x_s + f_y \frac{\partial y(x.s)}{\partial s} + f_{y'} \frac{\partial y'(x.s)}{\partial s}$$

Since x and s are independent, $x_s = 0$. Hence,

$$\frac{\partial y''(x,s)}{\partial s} = f_y \frac{\partial y(x.s)}{\partial s} + f_{y'} \frac{\partial y'(x.s)}{\partial s} \qquad (2.81)$$

for $a_0 \leqslant x \leqslant b_0$. The initial conditions are

$$\frac{\partial y(a_0.s)}{\partial s} = \frac{d}{ds}[\alpha_0] = 0, \quad \frac{\partial y'(a_0.s)}{\partial s} = \frac{d}{ds}[s] = 1, \qquad (2.82)$$

Define $z(x,s) = \frac{\partial y(x.s)}{\partial s}$. Since

$$\frac{\partial^3 y(x.s)}{\partial x^2 \partial s} = \frac{\partial}{\partial s}\left[\frac{\partial^2 y(x.s)}{\partial x^2}\right] = \frac{\partial}{\partial s}[y''(x.s)], \qquad (2.83)$$

we denote

$$z''(x,s) = \frac{\partial}{\partial s}[y''(x.s)]. \qquad (2.84)$$

Then the initial value problem (2.80) becomes the initial value problem

$$z''(x,s) = f_y z(x,s) + f_{y'} z'(x,s), \ a_0 \leqslant x \leqslant b_0, \ z(a_0, s) = 0, \ z'(a_0, s) = 1. \quad (2.85)$$

We can update s_k through

$$s_k = s_{k-1} - \frac{y(b_0, s_{k-1}) - \beta_0}{z(b_0, s_{k-1})}. \qquad (2.86)$$

and using the information from $z(x,s)$."

For more understanding of the solution methodology, Fig. 2.1 is also presented.
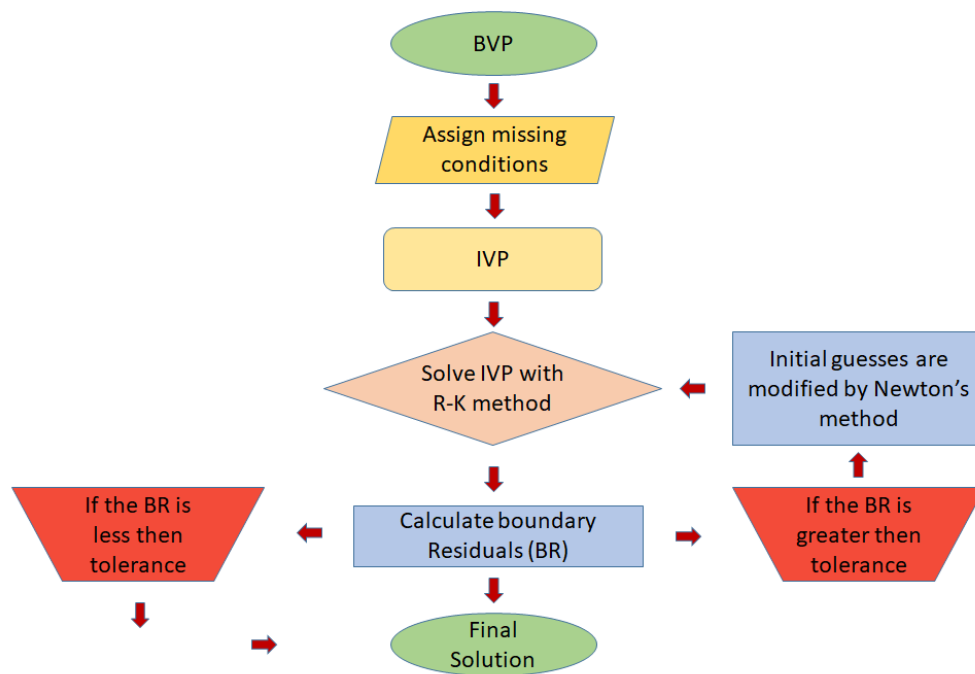
Fig. 2.1: Flow chart of shooting method.

2.6 Some Pronounced Dimensionless Numbers/-Parameters

The quantities which are expressed without any physical dimensions/units are termed as non-dimensional numbers. These numbers are either ratios of the physical quantities or have no units. They are important in order to investigate the flow and heat transport properties. The differential equations are numerically scaled through these numbers and the solution can be achieved in compact form. Some non-dimensional numbers, involved in the thesis are stated as [113]:

2.6.1 Reynolds Number

"The Reynolds number Re is named on the English engineer and physicist Osborne Reynolds and is expressed as the ratio of the fluid inertia force to that of molecular

friction (viscosity). Mathematically, it is defined as

$$Re = \frac{wL}{\nu},$$

(2.87)

where w is flow velocity, L the characteristic length and ν the kinematic viscosity. It characterizes the hydrodynamic conditions for viscous fluid flow. It determines the character of the flow (laminar, turbulent and transient flows). With low values of the Re number, the viscous friction muffles the originating dynamic influence of the flow relatively quickly and intensively, due to which the streamlines and elementary fluid volumes cannot be deformed substantially and the flow remains laminar. With large Re numbers, the dynamic flow effect cannot be equalized by viscous friction and the flow stability is lost, which is manifested by swirls and turbulence in the fluid.

2.6.2 Skin-Friction Coefficient

It is expressed as the dynamic friction resistance originating in viscous fluid flow around a fixed wall. Mathematically,

$$C_f = \frac{\tau_w}{\rho U_w^2},$$

(2.88)

where

$$\tau_w = \mu \left(\frac{\partial u}{\partial y} \right)_{y=0},$$

(2.89)

and μ is the fluid viscosity.

2.6.3 Nusselt Number

A non-dimensional quantity known as the Nusselt number after the named of a German engineer Ernst Kraft Wilhelm Nusselt, is the ratio of the total heat transfer in a system to the heat transfer by conduction. It characterizes the heat transfer by convection between a fluid and the environment close to it or, alterna-

tively, the connection between the heat transfer intensity and the temperature field in a flow boundary-layer. It is defined as

$$Nu = \frac{xq_w}{k\Delta T},\tag{2.90}$$

where x is the distance of the flow from the surface edge, q_w the rate of heat transfer at the surface, k the thermal conductivity of the fluid and ΔT the difference of the fluid and ambient fluid temperature. Moreover,

$$q_w = -k\left(\frac{\partial T}{\partial y}\right)_{y=0}.\tag{2.91}$$

2.6.4   Prandtl Number

The Prandtl number is a number which expresses the relation between the heat conduction and the fluid viscosity. The ratio of kinematic viscosity to the thermal diffusivity is termed as the Prandtl number and is written in mathematical form as:

$$P_r = \frac{\nu}{\alpha},\tag{2.92}$$

where ν is the kinematic viscosity and α the thermal diffusivity of the fluid. It characterizes the physical properties of a fluid with convective and diffusive heat transfers. It describes, for example, the phenomena connected with the energy transfer in a boundary-layer.

2.6.5   Magnetic Parameter

The magnetic parameter M is the ratio of the electromagnetic force to the viscous force. It was first introduced by Hartmann performing an experiment on the magnetohydrodynamic viscous channel flow. Mathematically,

$$M = B_0 L\sqrt{\frac{\sigma}{\mu}},\tag{2.93}$$

where B_0 is the strength of magnetic field, L the characteristic length, σ the electrical conductance and μ the dynamic viscosity. It characterizes the magnetic field influence on the flow of viscous and electrically conducting fluid. With small M values, the motion proceeds as if no magnetic field were acting. With great M values, the viscosity forces act only on a thin layer of the electrically conducting fluid (ionized gas) which adheres closely to a by-passed wall surface. In other cases, the motion resistance does depend on the viscosity and is determined completely by electromagnetic volume forces which are acting on the fluid.

2.6.6 Darcy Law

Darcy's law was enunciated by Henry Philibert Gaspard Darcy. The flow of a fluid through a porous medium is described by the Darcy's law. It states that the volumetric flux (Darcy velocity) is proportional to the pressure gradient.

$$\mathbf{v} = \frac{K_p}{\mu}\nabla P, \tag{2.94}$$

where $\mathbf{v}$ is the volumetric flux, K_p the permeability parameter, μ the dynamic viscosity and ∇P the pressure gradient."

2.7 Matlab Built-in Function Bvp4c

A bvp4c is a Matlab programme to formulate, solve and plot the solutions of a system of non-linear BVP in a finite domain. It is a finite difference code which follows collocation method. A system of algebraic equations after implementing collocation conditions, Esfandiari [114] is solved by dividing the domain of the problem into sub-intervals. Moreover, bvp4c calculates the error residual of estimated solution at each sub-interval unless the tolerance criteria is achieved. The prologues to bvp4c, bvpset, bvpinit, bvpget and bvpval provide some information not discussed here and details are found in [115]. "To solve the problem with bvp4c, you must provide functions that evaluate the differential equations and the

residual in the boundary conditions. These functions must return column vectors. With components of y corresponding to the original variables, these functions can be coded in Matlab (for details see [116]).

The guess is supplied to bvp4c in the form of a structure. However, it must contain two fields that must be called x and y. A guess for a mesh that reveals the behavior of the solution is provided as the vector $solinit.x$. A guess for the solution at these mesh points is provided as the array $solinit.y$, with each column $solinit.y(:, i)$ approximating the solution at the point $solinit.x(i)$. It is not difficult to form a guess structure, but a helper function $bvpinit$ makes it easy in the most common circumstances. It creates the structure when given the mesh and a guess for the solution in the form of a constant vector or the name of a function for evaluating the guess. For example, the structure is created for a mesh of five equally spaced points in $[0, 1]$ and a constant guess for the solution by

$$solinit = bvpinit(linspace(0, 1, 5), [111 - 100.91]); \qquad (2.95)$$

This constant guess for the solution is good enough for bvp4c to solve the BVP. The guess structure is then formed with $bvpint$ by

$$solinit = bvpinit(linspace(0, 1, 5), @ex1init); \qquad (2.96)$$

The BVP has now been defined by means of functions for evaluating the differential equations and the boundary conditions and a structure providing a guess for the solution. When default values are used, that is all you need to solve the problem with bvp4c:

$$sol = bvp4c(@ex1ode, @ex1bc, solinit); \qquad (2.97)$$

The output of bvp4c is a structure called here sol. The mesh determined by the code is returned as sol.x and the numerical solution approximated at these mesh points is returned as $sol.y$. As with the guess, $sol.y(:, i)$ approximates the solution at the point $sol.x(i)$."

Chapter 3

MHD Effects on UCM Fluid along with Joule Heating Using CCHFM

3.1 Introduction

In this chapter, we examine MHD flow of UCM fluid alongside the effects of Joule heating and thermal radiation. The novel idea of heat flux recently developed by Cattaneo and Christov is considered to analyze the heat transfer characteristics. By making use of some appropriate similarity transformations, the governing equations are stripped off, of their dimensionless existence and then solved through the shooting technique numerically. This research also brings into the spotlight such crucial physical parameters as are inevitable for describing the flow and heat transfer behavior. This has been done through graphs and tables with as much precision and exactitude as is possible. A comparison with published results is also made and found in an excellent agreement. This study follows a definite format. Section 3.2 deals with the problem pertaining to configuration. Section 3.3 concerns itself with the information regarding the formulation of governing equations, the numerical approach and validation of the code. The resultant numerical and

graphical conclusions stand elaborated in section 3.4. Section 3.5 is the sum and product, annunciating the more significant findings of the entire research of the chapter.

3.2 Mathematical Formulation of the Problem

Consider the steady, laminar, incompressible 2-D MHD flow of UCM fluid induced due to a plate moving with the velocity U coinciding with the plane $y = 0$ (Fig. 3.1). Supposedly, the plate must possess a constant temperature T_w. The ambient fluid temperature is considered as T_∞. The CCHFM has been used as the standard in this regard [30]. A magnetic field B_0 is implemented perpendicular to the $x-$direction. The assumption at work here is that the magnitude of the induced magnetic field is almost non-existent. The assumption extends further that the external electric field is also zero [117]. In view of the boundary-layer approximations [118] and the above imposed assumptions, the set of coupled non-linear equations for mass, momentum and heat transfer taking the effects of Joule heating and radiation for MHD incompressible flow of UCM fluid with zero pressure gradient and viscous dissipation can be formulated as follow [117–120]:

$$\frac{\partial u}{\partial x} + \frac{\partial v}{\partial y} = 0, \tag{3.1}$$

$$u\frac{\partial u}{\partial x} + v\frac{\partial u}{\partial y} + \Lambda\left(u^2\frac{\partial^2 u}{\partial x^2} + v^2\frac{\partial^2 u}{\partial y^2} + 2uv\frac{\partial^2 u}{\partial x\partial y}\right) = \nu\frac{\partial^2 u}{\partial^2 y} - \frac{\sigma B_0^2}{\rho}\left(u + \Lambda v\frac{\partial u}{\partial y}\right), \tag{3.2}$$

$$\rho C_p\left(u\frac{\partial T}{\partial x} + v\frac{\partial T}{\partial y}\right) = -\nabla \cdot \mathbf{q} + \sigma B_0^2 u^2 - \frac{\partial q_r}{\partial y}, \tag{3.3}$$

where the u and v are the velocity coordinates in the plane. The relaxation time of fluid is symbolized by Λ and heat flux by $\mathbf{q}$. As discussed by Christov[30], we have the following relation

$$\mathbf{q} + \Lambda_h\left(\frac{\partial \mathbf{q}}{\partial t} + \mathbf{v} \cdot \nabla\mathbf{q} - \mathbf{q} \cdot \nabla\mathbf{v} + (\nabla \cdot \mathbf{v})\mathbf{q}\right) = -k\nabla T, \tag{3.4}$$
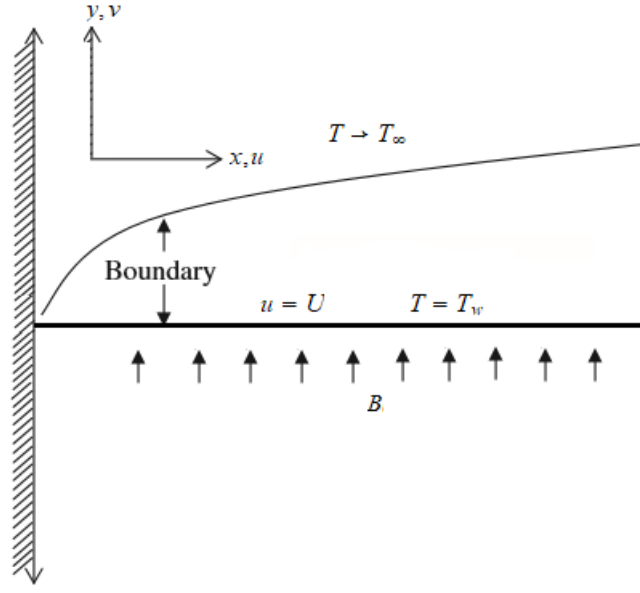
Fig. 3.1: Schematic of physical model

where Λ_h stands for relaxation time for heat flux of the fluid. Elimination of **q** from Eqs. (3.3) and (3.4), gives the following equation ([30])

$$u\frac{\partial T}{\partial x} + v\frac{\partial T}{\partial y} = \alpha\frac{\partial^2 T}{\partial y^2} + \frac{\sigma B_0^2}{\rho C_p}u^2 - \frac{1}{\rho C_p}\frac{\partial q_r}{\partial y} - \Lambda_h\,\Omega_h, \qquad (3.5)$$

where

$$\Omega_h = \left(u\frac{\partial u}{\partial x} + v\frac{\partial u}{\partial y}\right)\frac{\partial T}{\partial x} + \left(u\frac{\partial v}{\partial x} + v\frac{\partial v}{\partial y}\right)\frac{\partial T}{\partial y} + u^2\frac{\partial^2 T}{\partial x^2} + v^2\frac{\partial^2 T}{\partial y^2} + 2uv\frac{\partial^2 T}{\partial x\partial y}.$$

Working on the prognosis that the model for radiative heat flux q_r by Rosseland, as holds true. An attempt has been made to incorporate the Rosseland approximation model [121]:

$$q_r = -\frac{4\sigma^*}{3k^*}\frac{\partial T^4}{\partial y}, \qquad (3.6)$$

with

$$T^4 \cong 4T_\infty^3 T - 3T_\infty^4, \qquad (3.7)$$

ignoring the smaller terms, we have

$$\frac{\partial q_r}{\partial y} = -\frac{16 T_\infty^3 \sigma^*}{3 k^*} \frac{\partial^2 T}{\partial y^2}. \tag{3.8}$$

To keep the research confined with the administering boundaries, the associated BCs of the governing PDEs are

$$\begin{aligned}
u &= U, \quad v = 0, \quad T = T_w, \quad \text{at} \quad y = 0, \\
u &\to 0, \quad T \to T_\infty, \quad \text{as} \quad y \to \infty.
\end{aligned} \tag{3.9}$$

The modelled equations are made dimensionless by variables:

$$\eta = \sqrt{\frac{U}{\nu x}} y, \; u = U f'(\eta), \; \theta(\eta) = \frac{T - T_\infty}{T_w - T_\infty}, \; v = -\frac{1}{2} \sqrt{\frac{U \nu}{x}} (f - \eta f'). \tag{3.10}$$

The resultant ODEs are

$$f''' + \frac{1}{2} f f'' - \frac{\beta}{2} \left(\eta f'^2 f'' + 2 f f' f'' + f^2 f''' \right) - M(f' - \beta(f - \eta f') f'') = 0, \tag{3.11}$$

$$\frac{1}{P_r} \left(1 + \frac{4}{3} R_d \right) \theta'' + \frac{1}{2} f \theta' - \frac{\Gamma_e}{2} \left(3 f f' \theta' + f^2 \theta'' \right) + M E_c f'^2 = 0. \tag{3.12}$$

The BCs after the transformation get the following form:

$$\left. \begin{aligned}
f'(0) &= 1, \quad f(0) = 0, \quad \theta(0) = 1, \\
f'(\eta) &= 0, \quad \theta(\eta) = 0 \quad \text{as} \quad \eta \to \infty.
\end{aligned} \right\} \tag{3.13}$$

The various dimension free parameters in Eqs. (3.11) − (3.12) are depicted as

$$\left. \begin{aligned}
\beta &= \frac{\Lambda U}{2x}, \quad M = \frac{\sigma B_0^2 x}{\rho U}, \quad P_r = \frac{\nu}{\alpha} = \frac{\mu C_p}{k}, \\
R_d &= \frac{4 \sigma^* T_\infty^3}{k k^*}, \quad E_c = \frac{U^2}{C_p (T_w - T_\infty)}, \Gamma_e = \frac{\Lambda_h U}{2x}.
\end{aligned} \right\} \tag{3.14}$$

The important quantities of physical interest are stated as:

$$C_f = \frac{\left[\mu \frac{\partial u}{\partial y} - \Lambda \left(v^2 \frac{\partial u}{\partial y} + 2uv \frac{\partial u}{\partial x} \right) \right]_{y=0}}{\rho U^2}, \quad Nu_x = \frac{x q_w}{k (T_w - T_\infty)}, \tag{3.15}$$

where q_w is given by

$$q_w = - \left[\left(k + \frac{16\sigma^* T_\infty^3}{3k^*} \right) \frac{\partial T}{\partial y} \right]_{y=0}. \tag{3.16}$$

Making the above relations (3.15) dimensionless as:

$$Nu_x Re_x^{-\frac{1}{2}} \left(\frac{3}{3+4R_d} \right) = -\theta'(0), \quad C_f Re_x^{\frac{1}{2}} = f''(0), \tag{3.17}$$

3.3 Solution Methodology

Using the shooting technique [112], the ODEs $(3.11) - (3.12)$ with BCs given in (3.13) have been cracked numerically. This has been done for several values of the physical parameters involved in $(3.11) - (3.12)$. We are considering a finite domain as $[0, \ \eta_{max}]$ instead of $[0, \ \infty)$. We symbolize f by y_1 and θ by y_4 for converting the BVP $(3.11)-(3.13)$ to the following IVP consisting of 5 ODEs of order 1

$$
\left.
\begin{aligned}
y_1' &= y_2, & y_1(0) &= 0 \\
y_2' &= y_3, & y_2(0) &= 1 \\
y_3' &= \frac{1}{2 - \beta y_1^2}(\beta(\eta y_2^2 y_3 + 2y_1 y_2 y_3) - y_1 y_3 + 2M(y_2 - \beta(y_1 - \eta y_2)y_3)), & y_3(0) &= s_1 \\
y_4' &= y_5, & y_4(0) &= 1 \\
y_5' &= \frac{3P_r}{6 + 8R_d - 3P_r \Gamma_e y_1^2}(3\Gamma_e y_1 y_2 y_5 - y_1 y_5 - 2M\, E_c\, y_2^2). & y_5(0) &= s_2
\end{aligned}
\right\}
$$
$$\tag{3.18}$$

With s_1 and s_2 as our primary choices we put into practise the $RK4$ technique hoping to solve the above stated IVP. We then apply the Newton method with the intention of refining the values of s_1 and s_2. This will be done until to achieve the following criteria in which $\varepsilon > 0$.

$$\max\{|y_2(\eta_{max}) - 0|, |y_4(\eta_{max})) - 0|\} < \varepsilon,$$

All numerical outcomes, in this chapter, have been acquired by using $\varepsilon = 10^{-6}$. In order to rectify the MATLAB code, the acquired results have been compared

P_r	[122]	[123]	$-\theta'(0)$ shooting	bvp4c	$\eta_{\max}$
0.6	0.313519	0.31352	0.313525362805899	0.313520841971729	50
5.5	1.216049	1.21605	1.216049558288886	1.216049504356529	18
7.0	1.387033	1.38703	1.387033263096086	1.387033209335388	18
10	1.680293	1.68029	1.680293270509232	1.680293226787643	18
50	3.890918	3.89091	3.890917682778074	3.890917690311104	17
100	5.544663	5.54464	5.544662963116551	5.544662700196411	16

Table 3.1: Data comparing the numerical results of $-\theta'(0)$ with Cortell [122] and Mustafa *et al.* [123].

with those of Cortell [122] and Mustafa *et al.* [123] in Table 3.1. The results tally very significantly. Furthermore, the value of $-f''(0) = 0.443748380473711$ at $\eta_{max} = 20$ for $\beta = \Gamma_e = M = E_c = R_d = 0$ and $P_r = 1$ and the value of $-\theta'(0) = 0.406598929930808$ at $\eta_{max} = 20$ for $\beta = M = E_c = R_d = 0$ and $P_r = 1, \Gamma_e = 0.25$ are also agrees with the results computed by Mushtaq *et al.* [42].

3.4 Results and Discussion

Using the shooting method, a detailed discussion on the numerical solutions is presented here. The variation in velocity and temperature profiles are displayed graphically and the effects on the profiles for various parametric values of M, R_d, β, E_c and P_r will be discussed in detail. The impact of physical parameters on $-f''(0)$ and $-(1+\frac{4}{3}R_d)\theta'(0)$ have been acquired, tabulated and the product stands displayed in Tables 3.2 and 3.3. Table 3.2 clearly exhibits that $-f''(0)$ reduces for the rising values of β but ascends for M respectively. Furthermore, Table 3.3 clarifies that increasing P_r and R_d simultaneously enhances $-(1+\frac{4}{3}R_d)\theta'(0)$ while a contrary trend is marked when M, Γ_e, β and E_c are increased. In order to visualize various physical parameter's impact on f' (velocity field) and θ (temperature field), Figs. 3.2-3.9 are plotted. In all these computations, we have considered $P_r = 0.72, \Gamma_e = 0.5, \beta = 0.5, M = 0.1, E_c = 0.1, R_d = 0.23$. Fig. 3.2 discloses the variation in f' against the distinct values of M. This graphical representation

β	M	$-f''(0)$	
		shooting	bvp4c
0.5	0.1	0.490991419224158	0.490991438965521
0.2		0.519067226689762	0.519067249339577
0.5		0.490991419224158	0.490991438965521
0.7		0.471755768609328	0.471755776168386
	0.3	0.663320245611277	0.663320270941078
	0.5	0.803877920879802	0.803877945568001
	0.7	0.924666023380632	0.924666056335969

Table 3.2: Numerical values of $-f''(0)$ for $E_c = 0.1$, $\Gamma_e = 0.5$, $P_r = 0.72$, $R_d = 0.23$.

shows that rise in M, decreases the velocity profile f'. It happens because the Lorentz force which reduces the horizontal flow is increased by increasing M. The temperature profile against M is plotted in Fig. 3.3. It can be seen that the effect of M on f' and θ is opposite. It can be observed from Fig. 3.4 that for the larger values of E_c, θ is increased. Fig. 3.5 shows the effect of R_d on θ. Here θ increases whenever the value of R_d increases. Through Fig. 3.6, θ decreases when thermal relaxation parameter (Deborah number) Γ_e which is the ratio of relaxation time and the deformation process time, increases. Physically, the increasing Γ_e implies decrease in time of deformation process which resultantly reduce the temperature of the fluid. The effect of β on f' is delineated in Fig. 3.7. As we approach closer to the plate, we noticed a marked increase in f', this is due to larger β. Conversely, it decreases while increasing β for the remaining part of the boundary-later. At lesser distances from the plate, the profiles reduce to a status of free stream condition. This happens when β is increased. Hence, may conclude that by raising the values of β the boundary-layer thickness reduces. On tackling the comparatively larger values of β, the fluid took longer to gain equilibrium in reaction to the force exerted, thus leading to a much lower penetration depth for f'. Fig. 3.8 shows that θ increases for higher β. Fig. 3.9 portrays the behavior of θ for diverse values of P_r. It stands noted that as the values of P_r rise, the temperature falls. Once there is a rise in P_r, a marked reduction in the thermal boundary-layer is noted. In other words, higher P_r results lower thermal diffusivity. Hence concluded that higher P_r lowers diffusivity, thereby increases variation in the thermal characteristics.

P_r	Γ_e	β	M	E_c	R_d	$-(1+\frac{4}{3}R_d)\theta'(0)$	
						shooting	bvp4c
0.72	0.5	0.5	0.1	0.1	0.23	0.317119737234546	0.317119742965519
0.3						0.168302703191519	0.168302704393970
0.5						0.244098720490035	0.244098723546805
0.7						0.310982806705002	0.310982812171561
	0.2					0.337473330636536	0.337473332913591
	0.3					0.330808587893319	0.330808591095289
	0.4					0.324027578437144	0.324027582793393
		0.2				0.320483460280900	0.320483475280035
		0.5				0.317119737234546	0.317119742965519
		0.7				0.314128257038426	0.314128256182742
			0.3			0.285263791545578	0.285263799205478
			0.5			0.259280252215455	0.259280252570489
			0.7			0.237888220212451	0.237888226052013
				0.5		0.297454121258977	0.297454122748427
				0.9		0.277788504545703	0.277788502531121
				1.2		0.263039287454585	0.263039287368283
					0.3	0.323817004114587	0.323817004654815
					0.7	0.354008960045772	0.354008960434816
					1.8	0.414378863698563	0.414378862681644

Table 3.3: Numerical values of $-(1 + \frac{4}{3}R_d)\theta'(0)$ for different values of P_r, M, E_c, R_d, Γ_e, β.
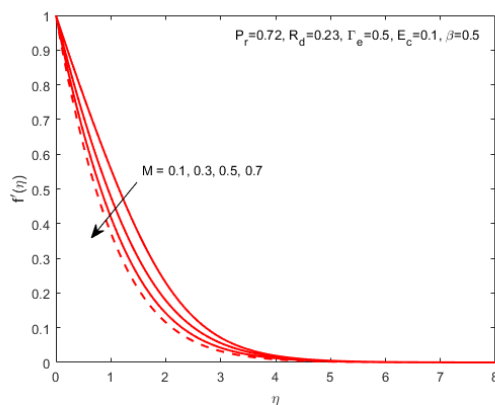
Fig. 3.2: Impact of M on f'.
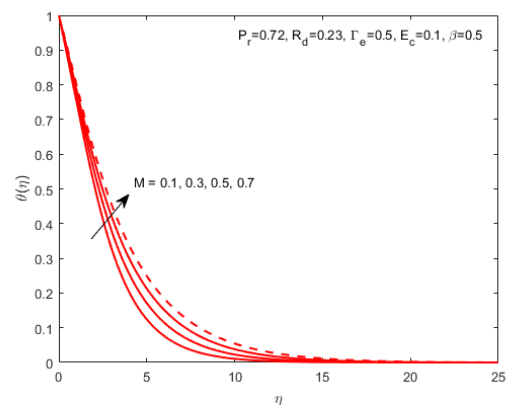
Fig. 3.3: Impact of M on θ.
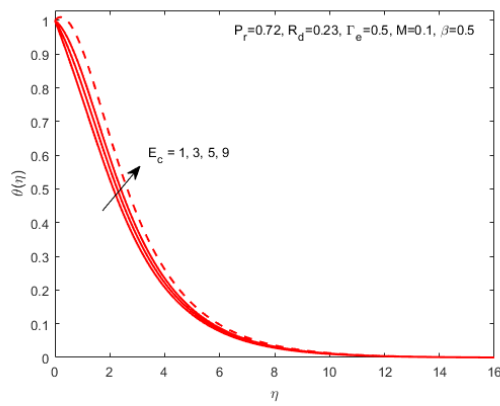
Fig. 3.4: Impact of E_c on θ.
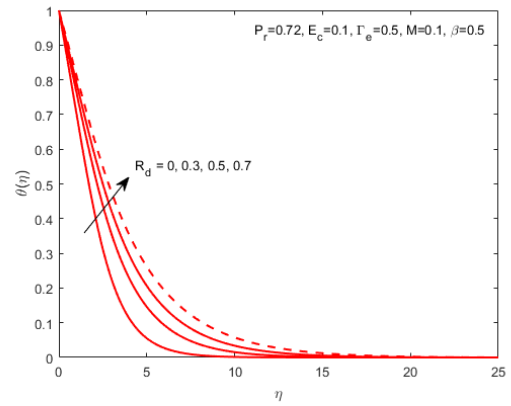
Fig. 3.5: Impact of R_d on θ.
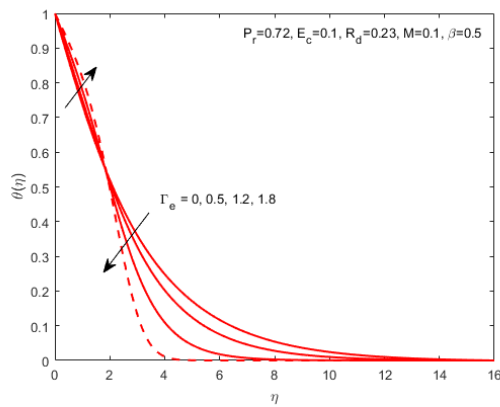
Fig. 3.6: Impact of Γ_e on θ.
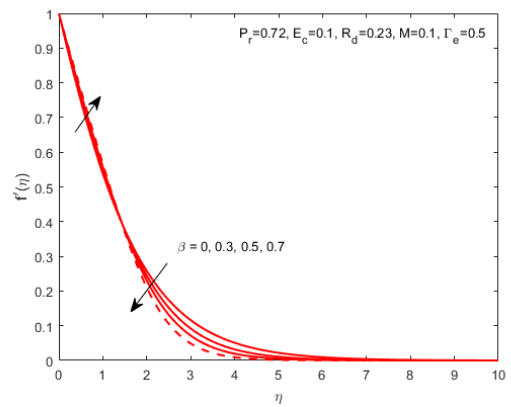
Fig. 3.7: Impact of β on f'.
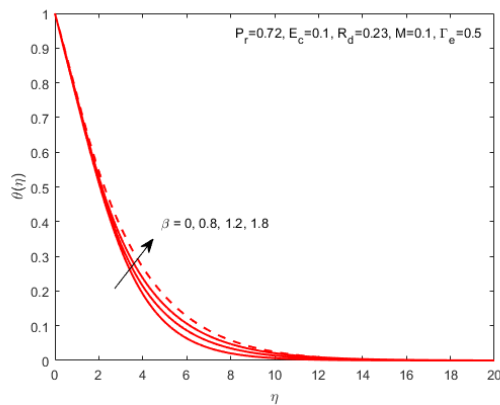
Fig. 3.8: Impact of β on θ.
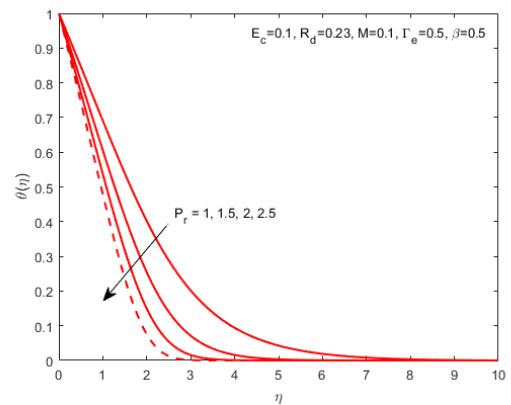
Fig. 3.9: Impact of P_r on θ.

3.5   Final Remarks

This chapter addresses the issue of MHD flow of UCM fluid in the region close to boundary of a surface taking the effects of Joule heating and radiation. The novel idea of heat flux recently developed by Cattaneo and Christov is considered to analyze the heat transfer characteristics. By making use of some appropriate similarity transformations, the governing equations are stripped off, of their dimensionless existence and then solved numerically. The bvp4c is the method against which the results have been compared. This research also brings into the spotlight such crucial physical parameters as are inevitable for describing the flow and heat transfer behavior. The obtained numerical results agree closely with the previous published results. The main points are as follows:

- With an increase in β, the velocity profile f' in the flow direction is decreased whereas the temperature θ rises.

- Once the parametric values of M are raised, θ also rises simultaneously and f' decreases.

- An increase in R_d and E_c also raises θ.

- The higher values of P_r decreases θ.

Chapter 4

MHD Boundary-Layer Flow of UCM Fluid through a Porous Medium with CCHFM

4.1   Introduction

This chapter discusses the numerical results of MHD flow in the area close to the surface of UCM fluid via a porous medium over a surface caused by a non-linear stretching by deploying the updated Fourier's heat conduction model. A non-linear slip condition is imposed and investigated. This article aims at examining the impacts of noteworthy parameters on the heat transfer and flow of fluid by making use of graphs and tables. Through a similarity transformation, the system of coupled flow governing equations which are in the form of PDEs is converted into ODEs. The shooting technique has been put to attain the numerical solutions of the velocity and temperature profiles. The velocity profile falls down for larger β whereas an accretion in θ is witnessed. Moreover, an enhancement in f' is found for larger A whereas a decrement in θ is noticed. Moreover, θ is observed to decay more rapidly for non-linearity of the stretching sheet. This study follows a definite format. Section 4.2 deals with the problem pertaining to configuration. Section 4.3

45

concerns itself with the information regarding the formulation of governing equations, the numerical approach and validation of the code. The resultant numerical and graphical conclusions stand elaborated in section 4.4. Section 4.5 is the sum and product, annunciating the more significant findings of the entire research of the chapter.

4.2   Mathematical Formulation of the Problem

Here, an incompressible, steady, laminar and 2-D flow of UCM fluid generated by a stretching sheet has been considered. The velocity slip effects are also taken into account. As shown in Fig. 4.1, the velocity of moving sheet is $U_w(x) = s_0 x^n$ where n is the velocity power index (non-linearity parameter) which has a great significance in the present problem. A non-Fourier's heat conduction model named as CCHFM is employed to describe the heat transfer characteristics. A non-uniform magnetic field $B(x)$ is applied perpendicular to $x-$direction. Variable permeability is also assumed. The approximations in analysis of boundary-layer flow are assumed for the modeled problem as discussed by Renardy [118]. The system of equations, in the presence of the pressure gradient, has been formulated as follows [124]:

$$\frac{\partial v}{\partial y} + \frac{\partial u}{\partial x} = 0, \tag{4.1}$$

$$u\frac{\partial u}{\partial x} + v\frac{\partial u}{\partial y} + \Lambda\left(u^2\frac{\partial^2 u}{\partial x^2} + v^2\frac{\partial^2 u}{\partial y^2} + 2vu\frac{\partial^2 u}{\partial x \partial y}\right) = \nu\frac{\partial^2 u}{\partial^2 y} + g\beta_T(T - T_\infty)$$

$$+ U_e\frac{\partial U_e}{\partial x} + \Lambda U_e^2\frac{\partial^2 U_e}{\partial x^2} - \frac{\sigma B^2(x)}{\rho}\left(u - U_e + \Lambda v\frac{\partial u}{\partial y}\right) - \frac{\nu}{\epsilon(x)}(u - U_e), \tag{4.2}$$

$$\rho C_p\left(u\frac{\partial T}{\partial x} + v\frac{\partial T}{\partial y}\right) + \nabla \cdot \mathbf{q} = 0, \tag{4.3}$$

The fluid relaxation time is symbolized by Λ and $\mathbf{q}$ represents the heat flux [124] stated as:

$$\Lambda_h\left(\frac{\partial \mathbf{q}}{\partial t} + (\nabla \cdot \mathbf{v})\mathbf{q} + \mathbf{v} \cdot \nabla\mathbf{q} - \mathbf{q} \cdot \nabla\mathbf{v}\right) + \mathbf{q} = -k\nabla T, \tag{4.4}$$

where the heat flux relaxation time of the fluid is denoted by Λ_h and $\mathbf{v}$ is velocity vector.
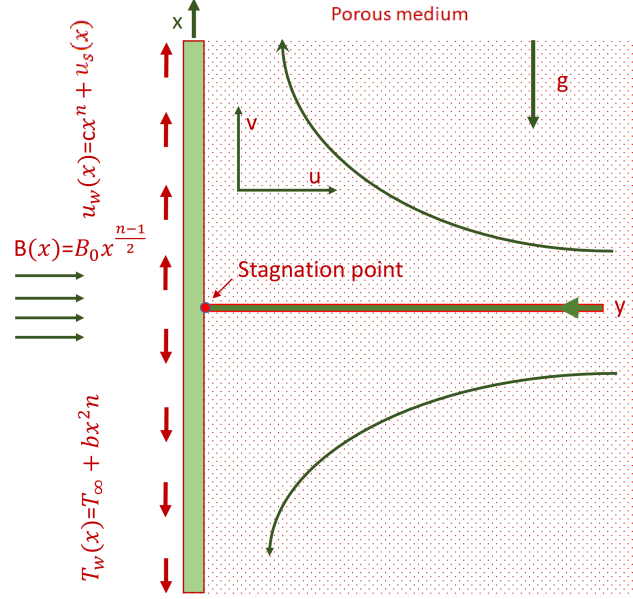
Fig. 4.1: Schematic of physical model

The following equation is obtained by eliminating $\mathbf{q}$ from Eqs. (4.3) and (4.4):

$$u\frac{\partial T}{\partial x} + v\frac{\partial T}{\partial y} - \alpha\frac{\partial^2 T}{\partial y^2} + \Lambda_h\Omega_h = 0, \quad \text{where} \tag{4.5}$$

$$\Omega_h = 2uv\frac{\partial^2 T}{\partial x \partial y} + u^2\frac{\partial^2 T}{\partial x^2} + v^2\frac{\partial^2 T}{\partial y^2} + \left(u\frac{\partial u}{\partial x} + v\frac{\partial u}{\partial y}\right)\frac{\partial T}{\partial x} + \left(u\frac{\partial v}{\partial x} + v\frac{\partial v}{\partial y}\right)\frac{\partial T}{\partial y}.$$

The corresponding BCs with velocity slip [124] are recounted as:

$$\left.\begin{array}{l} u = U_w(x) + U_s(x) = s_0 x^n + \Delta\dfrac{\partial u}{\partial y} - \Lambda\left(u\dfrac{\partial u}{\partial x} - ns_0 x^{n-1}u + v\dfrac{\partial u}{\partial y}\right), \\[2mm] v = 0, \;\; T = T_w = T_\infty + b^{**}x^{2n} \;\; \text{at} \;\; y = 0, \\[2mm] u = U_e(x) = d_0 x^n, \; T \to T_\infty \;\; \text{as} \;\; y \to \infty, \end{array}\right\} \tag{4.6}$$

where $\Delta = \Delta_0 x^{\frac{1-n}{2}}$ is the velocity slip length [125].

The modeled equations which are in the form of PDEs, are made dimensionless using variables [126]:

$$\left.\begin{aligned}
\eta &= \sqrt{\frac{s_0}{\nu}}\, x^{\frac{n-1}{2}}\, y, \quad u = s_0 x^n f'(\eta), \\
v &= -\frac{(n+1)\sqrt{s_0\nu}}{2x^{(1-n)/2}}\left(f + \frac{n-1}{n+1}\eta f'\right), \ \theta(\eta) = \frac{T - T_\infty}{T_w - T_\infty}.
\end{aligned}\right\} \tag{4.7}$$

To obtain the similarity solutions, the functional forms of the magnetic field and the variable permeability [126–128] are taken as:

$$B(x) = B_0 x^{(n-1)/2}, \quad \epsilon(x) = \epsilon_0 x^{1-n}. \tag{4.8}$$

The resultant ODEs are

$$\left.\begin{aligned}
&\left(1 - \frac{(n+1)^2}{4}\beta f'^2\right)f''' + \frac{n+1}{2}ff'' + n(n-1)\beta A^3 - K_p(f' - A) \\
&+ nA^2 - \beta\left(n(n-1)f'^3 - \frac{n^2-1}{4}\eta f'^2 f'' - \frac{(n+1)(3n-1)}{2}ff'f''\right) \\
&+ \lambda_t\theta - nf'^2 - M\left(f' - A - \frac{n+1}{2}\beta ff'' - \frac{n-1}{2}\eta\beta f'f''\right) = 0,
\end{aligned}\right\} \tag{4.9}$$

$$\left.\begin{aligned}
&\left(\frac{1}{P_r} - \frac{(n+1)^2}{4}\Gamma_e f^2\right)\theta'' + \frac{n+1}{2}f\theta' - 2nf'\theta \\
&- \Gamma_e\left(2n(3n-1)\theta f'^2 + \frac{(3-9n)(n+1)}{4}ff'\theta' - n(n+1)\theta ff''\right) = 0.
\end{aligned}\right\} \tag{4.10}$$

Using the variables introduced in (4.7), the BCs given in (4.6) get the following form:

$$\left.\begin{aligned}
&f'(0) = 1 + n\beta[f'(0) - f'^2(0)] + Rf''(0), \ f(0) = 0, \ \theta(0) = 1, \\
&f'(\eta) = A, \ \theta(\eta) = 0 \text{ as } \eta \to \infty.
\end{aligned}\right\} \tag{4.11}$$

The parameters appearing in Eqs. $(4.9) - (4.11)$ in the dimensionless form are defined as:

$$\left.\begin{aligned}
K_p &= \frac{\nu}{s_0\epsilon_0}, \quad M = \frac{\sigma B_0^2}{\rho s_0}, \quad A = \frac{d_0}{s_0}, \quad P_r = \frac{\nu}{\alpha} = \frac{\mu C_p}{k}, \quad R = \Delta\sqrt{\frac{s_0}{\nu}}, \\
\lambda_t &= \frac{g\beta_T(T_w - T_\infty)x}{U_w^2}, \quad \beta = \Lambda s_0 x^{n-1}, \quad \Gamma_e = \Lambda_h s_0 x^{n-1}, \quad Re_x = \frac{xU_w}{\nu}.
\end{aligned}\right\} \tag{4.12}$$

The important quantities of physical interest are elucidated as:

$$C_f = \frac{\tau_w}{\rho U_w^2(x)}, \quad Nu_x = \frac{xq_w}{k(T_w - T_\infty)},$$

where τ_w and q_w are formulated as fellows:

$$\tau_w = \left[\mu\frac{\partial u}{\partial y} - \Lambda\left(v^2\frac{\partial u}{\partial y} + 2uv\frac{\partial u}{\partial x}\right)\right]_{y=0}, \quad q_w = -k\left(\frac{\partial T}{\partial y}\right)_{y=0}.$$

After non-dimensioning on account of (4.7), we establish the following relations:

$$C_f Re_x^{1/2} = f''(0), \quad Nu_x Re_x^{-1/2} = -\theta'(0).$$

4.3   Solution Methodology

The ODEs $(4.9)-(4.10)$ along with BCs stated in (4.11) has been explored numerically via shooting technique. After performing successive iterations, the bounded domain $[0, \eta_{max}]$ has been considered instead of $[0, \infty)$ for an appropriate value of η_{max}, the value after which the solution converges asymptotically. The variable f is denoted by y_1 and θ by y_4. The BVP $(4.9)-(4.11)$ in new variables is converted into an IVP:

$$\left.\begin{aligned}
y_1' &= y_2,\\
y_2' &= y_3,\\
y_3' &= \frac{4}{4-\beta(n+1)^2 y_1^2}\left[\begin{array}{c} ny_2^2 + M(y_2-A) - \lambda_t y_4 - \frac{n+1}{2}y_1 y_3 - nA^2 \\ +\beta n(n-1)y_2^3 - \beta\frac{n^2-1}{4}\eta y_2^2 y_3 - \beta\frac{(n+1)(3n-1)}{2}y_1 y_2 y_3 \\ -n(n-1)\beta A^3 - \frac{n+1}{2}M\beta y_1 y_3 - \frac{n-1}{2}\eta M\beta y_2 y_3 \\ +K_p(y_2-A)\end{array}\right],\\
y_4' &= y_5,\\
y_5' &= \frac{4P_r}{4-\Gamma_e P_r(n+1)^2 y_1^2}\left[\begin{array}{c} 2ny_2 y_4 - \frac{n+1}{2}y_1 y_5 + 2n(3n-1)\Gamma_e y_2^2 y_4 \\ +\frac{(3-9n)(n+1)}{4}\Gamma_e y_1 y_2 y_5 - n(n+1)\Gamma_e y_1 y_3 y_4\end{array}\right],
\end{aligned}\right\}$$

$$(4.13)$$

Table 4.1: Data comparing the numerical results of $-f''(0)$ for distinct values of A when $M = \lambda_t = K_p = \Gamma_e = R = 0, n = 1$ (linear stretching) and $\beta = 0$ (Newtonian case).

A	Mahapatra and Gupta [131]	Ishak *et al.* [132]	Abbas *et al.* [133]	Present results
0.10	0.9694	0.9694	0.9694	0.96943
0.20	0.9181	0.9181	0.9181	0.91810
0.50	0.6673	0.6673	0.6673	0.66732
2.00	-2.0175	-2.0175	-2.0175	-2.01749
3.00	-4.7293	-4.7294	-4.7293	-4.72928

under the conditions:

$$\left.\begin{array}{l} y_1(0) = 0, \ y_2(0) = s_1, \ y_3(0) = (s_1 - \beta(s_1 - s_1^2) - 1)/R, \\ y_4(0) = 1, \ y_5(0) = s_2. \end{array}\right\} \tag{4.14}$$

The above IVP is solved by employing RK4 method for some initial choice of s_1 and s_2. To modify our primary choices s_1 and s_2, the Newton method is used until the following criteria is met

$$\max\{|y_2(\eta_{max}) - A|, |y_4(\eta_{max})) - 0|\} < \varepsilon, \tag{4.15}$$

where $\varepsilon > 0$, in particular ε has been taken as 10^{-6} throughout this article.

To validate our MAT-LAB code, we reproduced the results of $f''(0)$ for the problems discussed by Ishak *et al.* [129] and Grubka and Bobba [130]. To archive the accuracy of the results bvp4c is also invoked. Results presented in Tables 4.1-4.3 are found in an excellent agreement.

4.4 Results and Discussion

Tables 4.4 and 4.5 are prepared for the numerical results of $-f''(0)$ and $-\theta'(0)$ to ascertain the impacts of various physical parameters. From Table 4.4, we are able to look at the nature of $f''(0)$ for distinct values of A, λ_t, R, β, n, M, K_p, P_r and Γ_e. It is analyzed that the magnitude of $f''(0)$ subsides for the parameters A, λ_t

Table 4.2: Data comparing the numerical results of $-f''(0)$ for different values of A when $M = \lambda_t = K_p = \Gamma_e = R = 0, n = 1$ (linear stretching) and $\beta = 0$ (Newtonian case).

A	Mahapatra and Gupta [131]	Nazar *et al.* [134]	Sajid *et al.* [135]	Hayat *et al.* [136]	Present results shooting	bvp4c
0.01	-	0.9980	0.9981	0.9963	0.999198	0.998149
0.02	-	0.9958	0.9958	0.9930	0.996774	0.995875
0.05	-	0.9876	0.9876	0.9830	0.988181	0.987616
0.10	0.9694	0.9694	0.9694	0.9603	0.969656	0.969395
0.20	0.9181	0.9181	0.9181	0.9080	0.918165	0.918108
0.50	0.6673	0.6673	0.6673	0.6605	0.667686	0.667264
1.00	-	0.0000	0.0000	0.0000	0.000000	0.0000000
2.00	-2.0175	-2.0175	-2.0175	-2.0181	-2.017503	-2.0175028

Table 4.3: Data comparing the numerical results of $-f''(0)$ for different values of A when $M = \lambda_t = K_p = \Gamma_e = R = 0, n = 1$ (linear stretching) and $\beta = 0.2$ (non-Newtonian case).

A	Sajid *et al.* [135]	Present results bvp4c	shooting
0.01	1.0499	1.049960	1.049960
0.02	1.0476	1.047683	1.047683
0.05	1.0393	1.039350	1.039350
0.10	1.0207	1.024857	1.020812
0.20	0.9681	0.969684	0.968239
0.50	0.7078	0.710409	0.719704
1.00	0.0000	0.000000	0.000018
2.00	-2.2225	-2.216987	-2.226116

and R but increases for the parameters β, n, M, K_p, P_r and Γ_e. From Table 4.5, the increasing values of β, M, K_p and R are found to abate $-\theta'(0)$ but $n, \lambda_t, Pr, \Gamma_e$ and A have an opposite effect. The tabular results are observed to be consistent with the graphical representation.

To ascertain effects of physical parameters involved in the non-dimensional system of ODEs, on f' (velocity field) and θ (temperature field), Figs. (4.2)-(4.11) are plotted. The values of the parameters while computing the results are fixed throughout this study as $\Gamma_e = 0.1, n = 2, M = 1.0, K_p = 0.1, P_r = 1, \lambda_t = 0.3, \beta = 0.1, A = 0.1$ and $R = 0.2$ unless otherwise mentioned. The effects of A on

Table 4.4: Data comparing the numerical results of $-f''(0)$ for different values of $A, M, P_r, \lambda_t, K_p, \beta, \Gamma_e, R$ and n at $\eta_{max} = 6$.

A	M	P_r	R	n	β	K_p	λ_t	Γ_e	shooting	bvp4c
0.1	1.0	1.0	0.2	2.0	0.1	0.1	0.3	0.1	1.154779	1.154779
0.2									1.074652	1.074652
0.3									0.979465	0.979465
	1.0								1.154779	1.154779
	3.0								1.404526	1.404526
	5.0								1.587876	1.587876
		1.0							1.154779	1.154779
		1.5							1.163638	1.163638
		2.0							1.169495	1.169495
			0.2						1.154779	1.154779
			1.0						0.540539	0.540539
			2.0						0.326850	0.326850
				1.0					0.948286	0.948286
				1.5					1.056427	1.056427
				2.0					1.154779	1.154779
					0.1				1.154779	1.154779
					0.2				1.237978	1.237978
					0.3				1.318382	1.318382
						1.0			1.272718	1.272718
						3.0			1.480405	1.480405
						5.0			1.640569	1.640569
							0.1		1.195403	1.195403
							0.3		1.154779	1.154779
							0.5		1.115442	1.115442
								0.1	1.154779	1.154779
								0.2	1.159286	1.159286
								0.3	1.163127	1.163127

f' and θ are displaced in Fig. 4.2. Fig. 4.2(a) highlights that the elevated values of A enhance f'. Fig. 4.2(b) evinces that θ is decreased for an enhancement in A. Fig. 4.2(b) further elaborates that once $A < 1$, the boundary-layer structure stands inverted. This phenomenon occurs because of the fact that when $A < 1$, the stretching velocity of a surface supersedes the external stream velocity. It can also be seen from Fig. 4.2 that for the linearly stretching sheet, A slightly affects f' but the same prominently affects θ for the non-linear case. Further, it is witnessed that the decrement in θ is more rapid when the stretching of sheet is non-linear. Through Fig. 4.3, the effect of β on f' and θ is made evident. A fall-off

Table 4.5: Data comparing the numerical results of $-\theta'(0)$ for different values of $A, M, P_r, \lambda_t, K_p, \beta, \Gamma_e, R$ and n at $\eta_{max} = 6$.

A	M	P_r	R	n	β	K_p	λ_t	Γ_e	shooting	bvp4c
0.1	1.0	1.0	0.2	2.0	0.1	0.1	0.3	0.1	1.914552	1.914552
0.2									2.000818	2.000818
0.3									2.089760	2.089760
	1.0								1.914552	1.914552
	3.0								1.731090	1.731090
	5.0								1.602707	1.602707
		1.0							1.914552	1.914552
		1.5							2.430084	2.430084
		2.0							2.868991	2.868991
			0.2						1.914552	1.914552
			1.0						1.477228	1.477228
			2.0						1.298307	1.298307
				1.0					1.272193	1.272193
				1.5					1.605673	1.605673
				2.0					1.914552	1.914552
					0.1				1.914552	1.914552
					0.2				1.910105	1.910105
					0.3				1.903126	1.903126
						1.0			1.828580	1.828580
						3.0			1.680846	1.680846
						5.0			1.571849	1.571849
							0.1		1.883908	1.883908
							0.3		1.914552	1.914552
							0.5		1.943192	1.943192
								0.1	1.914552	1.914552
								0.2	2.191412	2.191412
								0.3	2.450220	2.450220

in f' is noted for the augmentation in β as depicted in Fig. 4.3(a). Physically, the fluid becomes at rest when the shear stress is removed. The escalating values of β generate a resisting force in the flow between the adjacent layers that's why f' and momentum boundary-layer thickness are declined. But for θ the trend is opposite for β as observed from Fig. 4.3(b). Fig. 4.4(a) depicts the impact of P_r on θ, which reflects that θ is receded for the raise in P_r. This occurrence transpires because the thermal diffusion of a fluid is low for comparatively bigger values of P_r in comparison to the viscous fluid. Consequently, its the thermal boundary-layer thickness and coefficient of heat transfer are reduced. In Fig. 4.4(b), the decreas-

ing behavior of θ can be witnessed for increasing Γ_e. Physically, for the larger values of Γ_e, the particles of the material in order to transfer their heat to the neighbouring particle require more time. In other words, the material exhibits a non-conducting behavior for the ascending values of Γ_e and hence this leads to a reduction in θ. Moreover, it can be noticed that the temperature boundary-layer becomes thinner for the larger values of Γ_e. In Fig. 4.5, for different values of λ_t, f' and θ are plotted. The comparison measurement between the free stream flow or inertia of external force and buoyancy's effect on the heat and fluid flow by the parameter λ_t is represented Mahdy [137] in which the computed results convince to accept that when the values of λ_t increase, f' is increased but the behavior is quite opposite in θ. The reason behind this phenomenon is the increment in the Grashof number. An increment in the value of Grashof number accelerates the buoyancy force with respect to the viscous forces. The impact on f' and θ of M is delineated in Fig. 4.6. The perpendicular magnetic field to the fluid flow generates a force called the Lorentz force. This force resists fluid motion. As a result, this resistive force opposes the transport phenomenon which contributes to a reduction in the momentum boundary-layer thickness and a lowering in f'. Moreover, an opposite trend is observed in θ when M is increased. Fig. 4.7 is presented for different values of n. A decrement in f' and θ occurs, as n is enhanced. An enhancement in the momentum boundary-layer thickness is noted for larger n. This is because a rise in the non-linearity enhances the wall friction with the fluid at $\eta = 0$ and hence the boundary-layer thickness is increased as noticed in Fig. 4.7(a). A similar effect of n on θ has been seen in Fig. 4.7(b). Fig. 4.8 is sketched to recount the influence of R on f' and θ. It is observed from Fig. 4.8(a) that an increase in R reduces f'. Factually speaking, the actual occurrence of the slip phenomenon renders the flow velocity near the stretching wall unequal to the stretching velocity of the wall. A rise in the slip velocity causes a decrement in the fluid velocity. An opposite and obvious trend is noticed in θ in Fig. 4.8(b). The variation in f' and θ is presented in Fig. 4.9 with respect to different values of K_p. A decline in f' is seen for an increment in K_p while θ is observed to increase for K_p. It is expected because the presence of porous medium represents flow resistance

mechanism. Moreover, it is seen that the down-fall in f' is more prominent in non-linear stretching case. Fig. 4.10 is sketched to examine the impact of β, R and K_p on $f''(0)$. The magnitude of $f''(0)$ is found to increase for the increasing values of β and K_p as depicted in Fig. 4.10(a) but an opposite behavior for R is noted from Fig. 4.10(b). Fig. 4.11 is portrayed to see the variation in $f''(0)$ against β for both the linear and non-linear stretching case. A prominent increasing trend in the magnitude of $f''(0)$ is noticed for the ascending β for the non-linear case. The variation in $-\theta'(0)$ exhibits a decreasing behavior for higher β as reflected in Fig. 4.11(b). However, this reduction is prominent for non-linear stretching case.
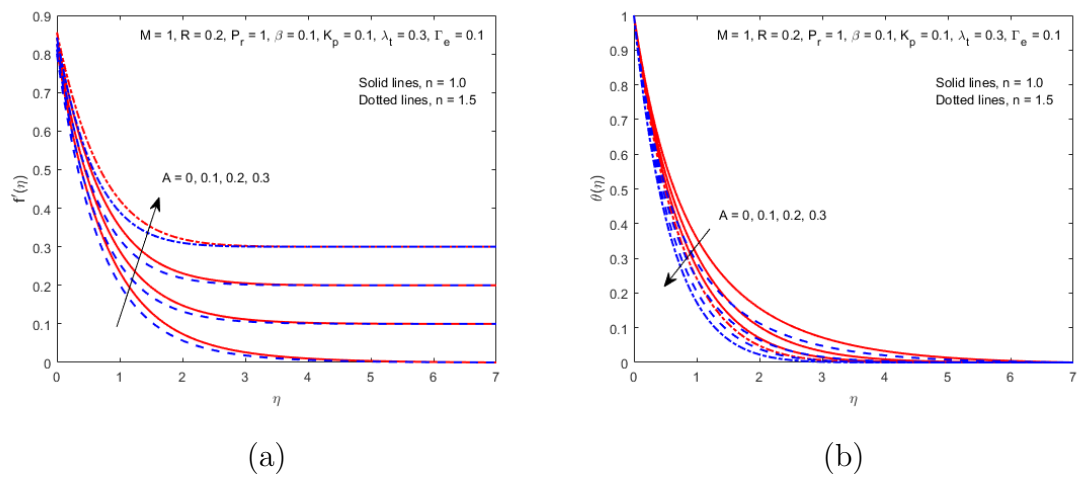
Fig. 4.2: Impact of A on (a) $f'(\eta)$, (b) $\theta(\eta)$.
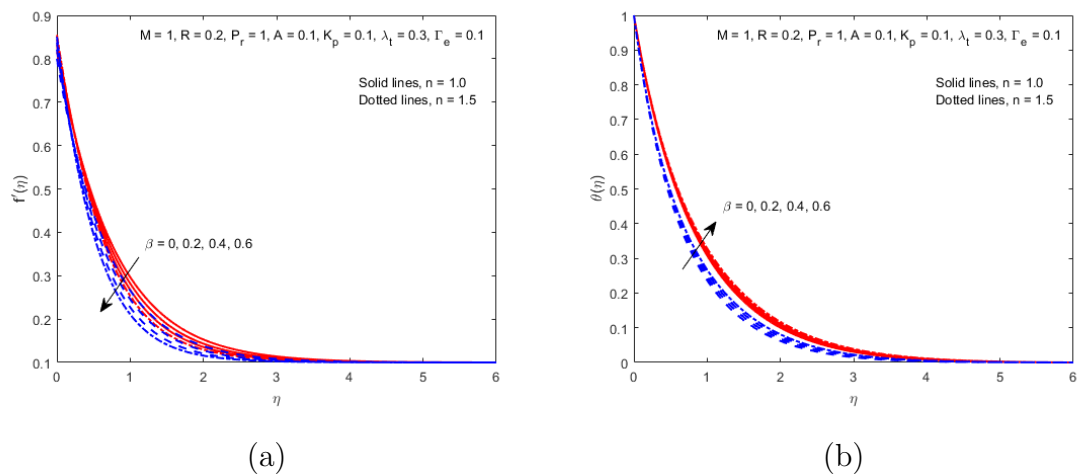
Fig. 4.3: Impact of β on (a) $f'(\eta)$, (b) $\theta(\eta)$.
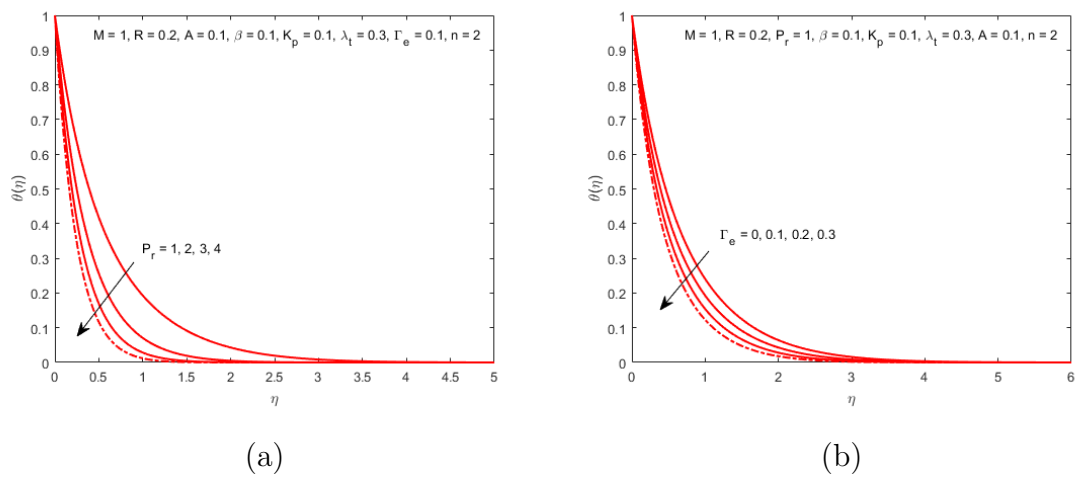
Fig. 4.4: Impact of (a) P_r and (b) Γ_e on $\theta(\eta)$.
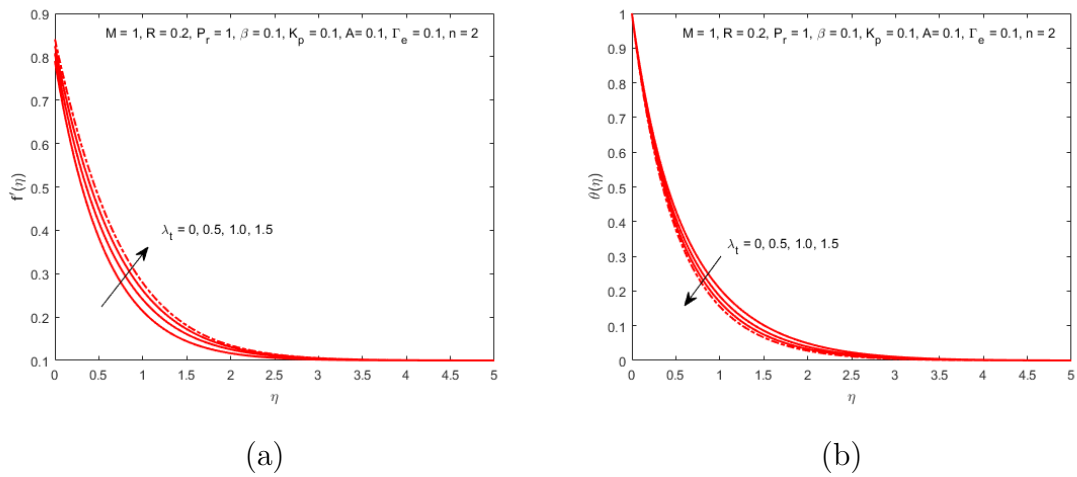
Fig. 4.5: Impact of λ_t on (a) $f'(\eta)$, (b) $\theta(\eta)$.
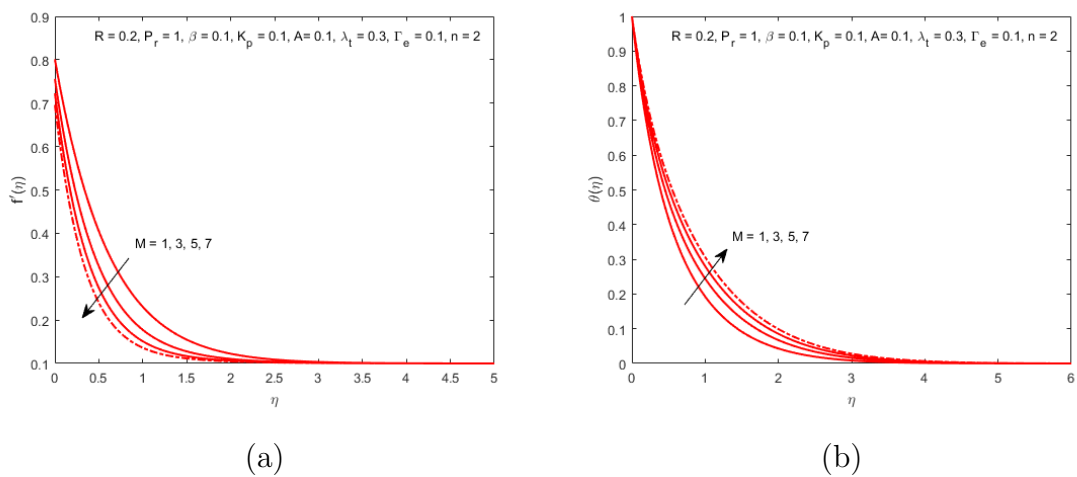
Fig. 4.6: Impact of M on (a) $f'(\eta)$, (b) $\theta(\eta)$.
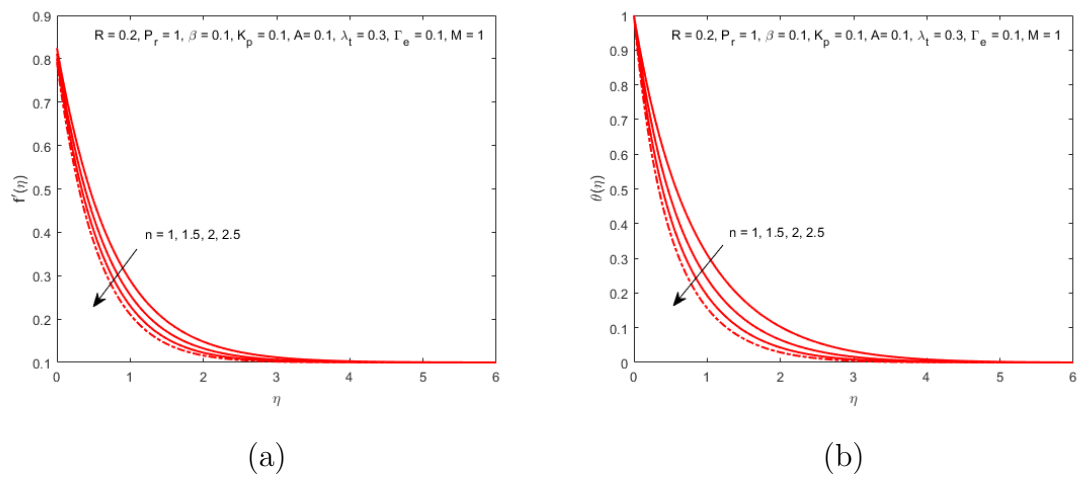
Fig. 4.7: Impact of n on (a) $f'(\eta)$, (b) $\theta(\eta)$.
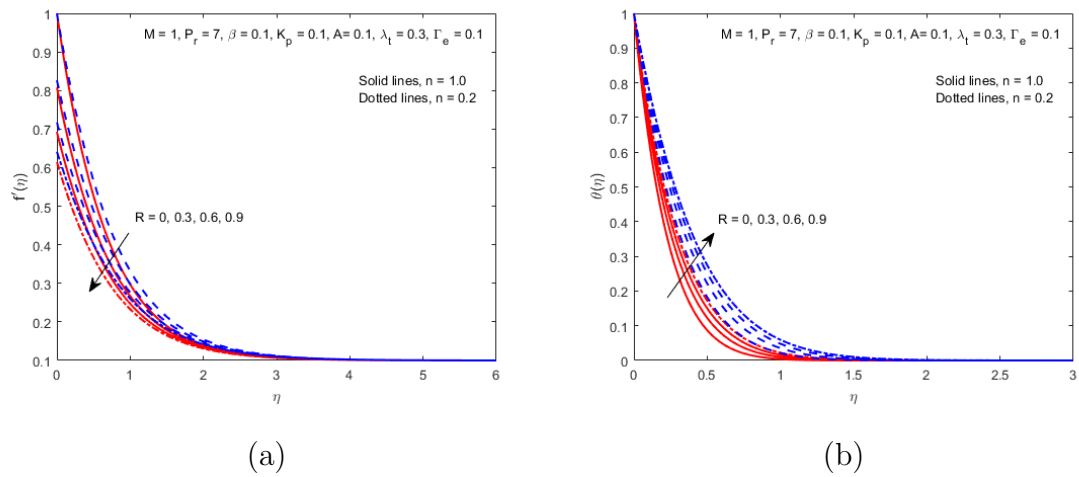
Fig. 4.8: Impact of R on (a) $f'(\eta)$, (b) $\theta(\eta)$.
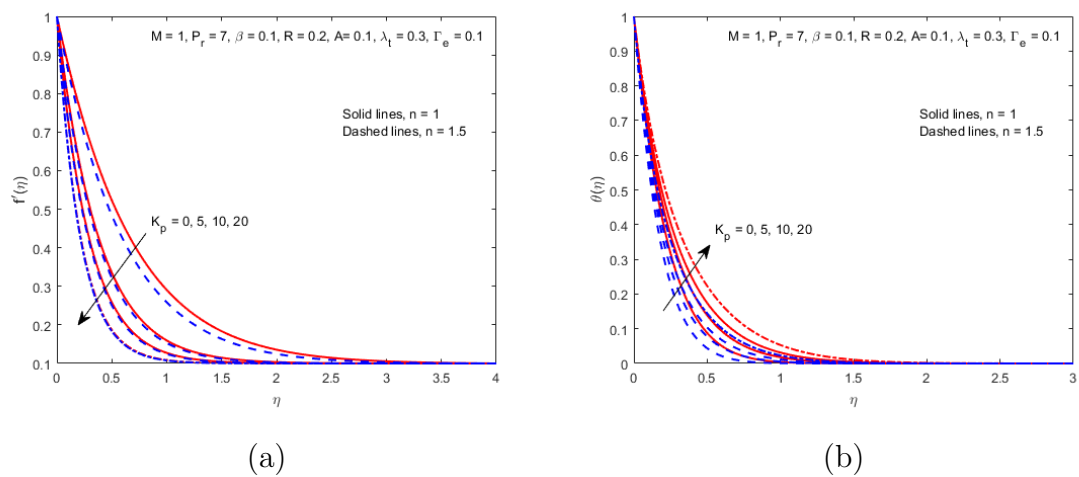
Fig. 4.9: Impact of K_p on (a) $f'(\eta)$ (b) $\theta(\eta)$.
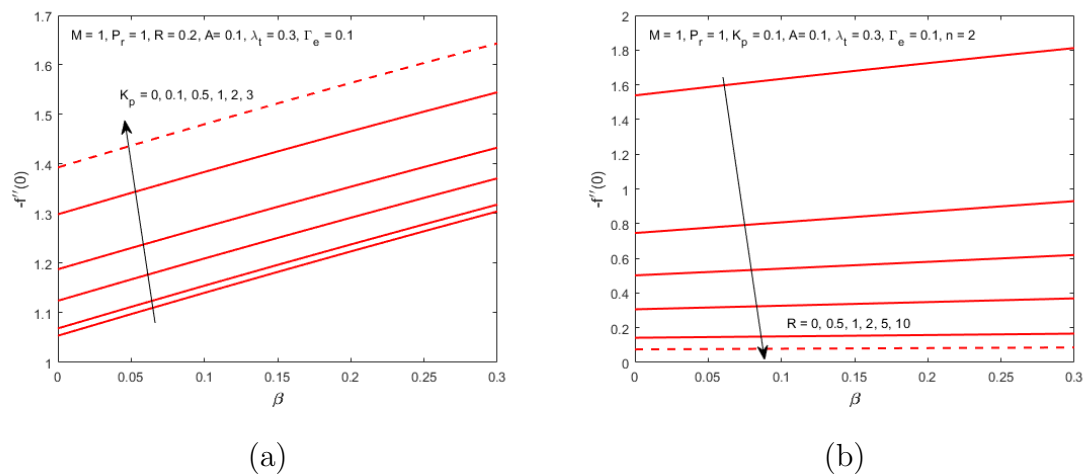
Fig. 4.10: Impact of (a) K_p, (b) R on $-f''(0)$.
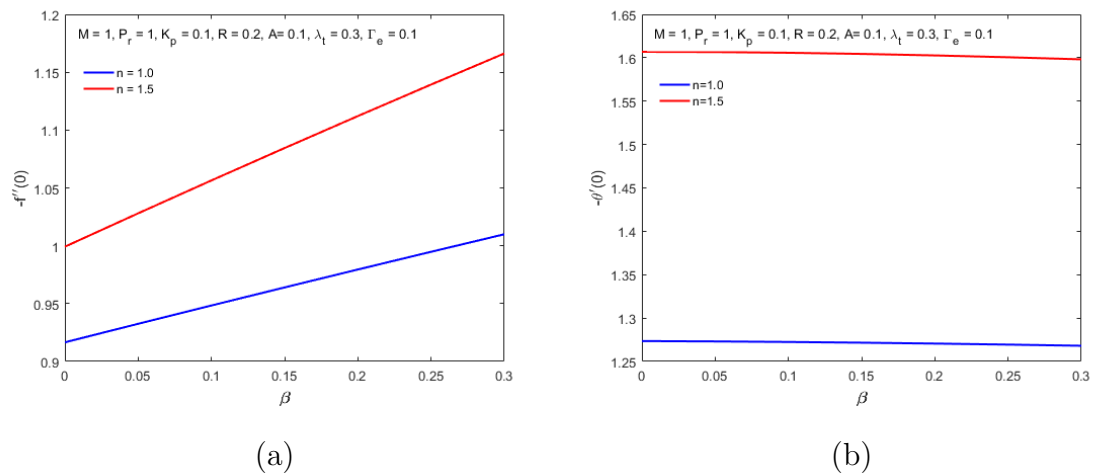
Fig. 4.11: Impact of (a) β on $-f''(0)$, (b) β on $-\theta'(0)$ for both linear and non-linear stretching case.

4.5   Final Remarks

This chapter discusses the numerical results of MHD flow in the area close to the surface of UCM fluid via a porous medium over a surface caused by a non-linear stretching by deploying the updated Fourier's heat conduction model. A non-linear slip condition is imposed and investigated. This article aims at examining the impacts of noteworthy parameters on the heat transfer and flow of fluid by making use of graphs and tables. The shooting technique has been put to attain the numerical solutions of the velocity and temperature profiles. The main points

are summarized as follows:

- For the higher β, a more prominent increment in the values of $-f''(0)$ for the case of non-linear stretching sheet is noticed as compared to the linear stretching sheet.

- It stands tested and affirmed that once the values of β is raised, f' plummets whereas an accretion in θ is witnessed.

- The parameter M significantly reduces the fluid transport whereas an increment in M causes θ to rise.

- Observantly, θ displays a downward trend for the up-going values of Γ_e.

- An enhancement in f' is found for the larger values of A whereas a decrement in θ is noticed. Moreover, θ is observed to decay more rapidly in case of non-linear stretching.

- A rise in K_p reduces f' more promptly for non-linear stretching case.

- An increase in θ is noticed with the ascending values of R.

- An augmentation in P_r leads to decrease in θ.

Chapter 5

MHD Effects on UCM Fluid Flow with Variable Thermal Conductivity and CCHFM

5.1   Introduction

In this chapter, MHD mixed convective UCM fluid flow with variable thickness close to a stagnation-point is explored numerically. Heat transfer characteristics are analyzed assuming thermal conductivity of variable nature. Furthermore, homogeneous-heterogeneous chemical reactions and thermal stratification have also been considered in the present study. Both the assisting and the opposing flows are discussed through tables and graphs. The ODEs are obtained via suitable similarity transformations. The numerical solutions of temperature, velocity and concentration profiles are obtained and examined for different physical parameters such as the thermal stratification, thermal relaxation, mixed convection, thermal conductivity, stretching ratio, homogeneous reaction and heterogeneous reaction parameters. The temperature upturns for the higher values of the Maxwell and thermal conductivity parameters. This study follows a definite format. Section 5.2 deals with the problem pertaining to configuration. Section 5.3 concerns itself with the information regarding the formulation of governing equations, the numerical approach and validation of the code. The resultant numerical and graphical

conclusions stand elaborated in section 5.4. Section 5.5 is the sum and product, annunciating the more significant findings of the entire research of the chapter.

5.2   Mathematical Formulation of the Problem

The problem of a laminar $2 - D$ flow of UCM fluid with homogeneous-heterogeneous reactions towards a non-linearly stretching surface of variable thickness is considered. Heat transfer characteristics are analysed with modified Fourier's heat conduction law and a magnetic field $B(x) = B_0(x + b_1)^{\frac{n-1}{2}}$ normal to the flow field. It is also assumed that influences the fluid's thermal conductivity. Coordinate system is displayed in Fig. 5.1.
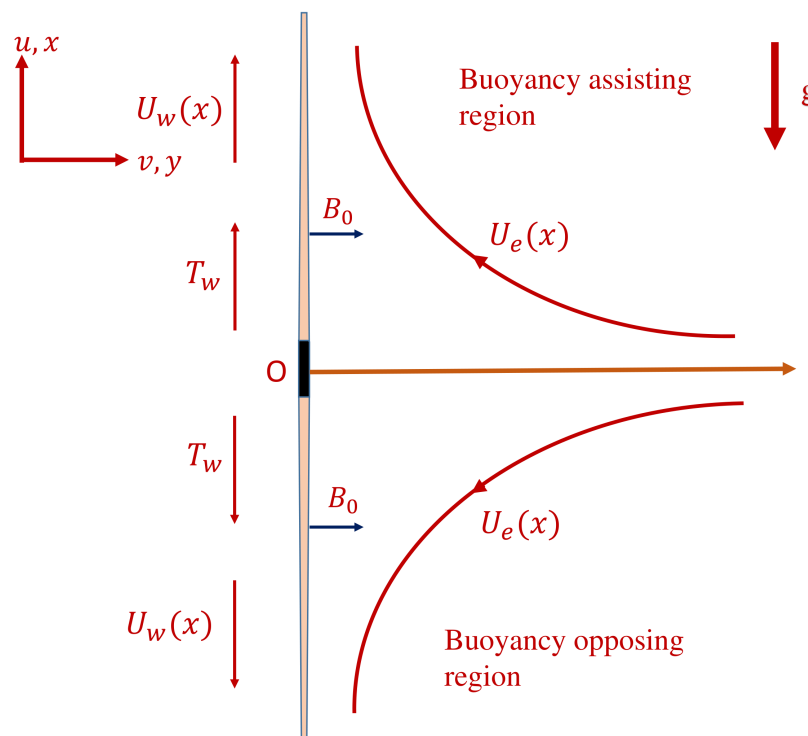
Fig. 5.1: Schematic physical model

Furthermore, the immediately adjacent layer of fluid is specified as $y = m_0(x + $

$b_1)^{\frac{1-n}{2}}$, where m_0 is positive constant. It is noticed that for $n = 1$ the thickness of the sheet will be uniform. Here $T_w = c(x + b_1) + T_0$ and $T_\infty = d(x + b_1) + T_0$ are the stratified surface and ambient temperature respectively. A homogeneous-heterogeneous model in the simplest form is chosen as below (see Bachok *et al.* [138]):

$$A^* + 2B^* \rightarrow 3B^*, \quad \text{rate} = k_1 ab^2. \tag{5.1}$$
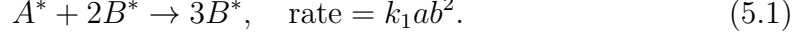
The first order isothermal relation is given by

$$A^* \rightarrow B^*, \quad \text{rate} = k_s a. \tag{5.2}$$
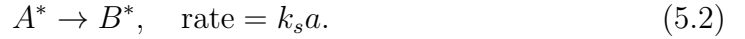
The constants a in the above relations denotes the concentration of the chemical specie A^* and constant b the chemical specie B^*. Moreover, k_1 and k_s denotes the constant rates. The constitutive equations of the Maxwell fluid model have been given below [124, 139].

$$\frac{\partial u}{\partial x} + \frac{\partial v}{\partial y} = 0, \tag{5.3}$$

$$u\frac{\partial u}{\partial x} + v\frac{\partial u}{\partial y} + \Lambda \left(u^2\frac{\partial^2 u}{\partial x^2} + v^2\frac{\partial^2 u}{\partial y^2} + 2uv\frac{\partial^2 u}{\partial x\partial y} \right) = -\frac{1}{\rho}\frac{\partial p}{\partial x} - \frac{\sigma B^2(x)}{\rho}\left(u + \Lambda v\frac{\partial u}{\partial y} \right)$$

$$+ g\beta_T(T - T_\infty) + \nu\frac{\partial^2 u}{\partial y^2}, \tag{5.4}$$

$$u\frac{\partial T}{\partial x} + v\frac{\partial T}{\partial y} = \frac{1}{\rho C_p}\frac{\partial}{\partial y}\left(k(T)\frac{\partial T}{\partial y} \right),$$

$$- \Lambda_h \left(u^2\frac{\partial^2 T}{\partial x^2} + v^2\frac{\partial^2 T}{\partial y^2} + 2uv\frac{\partial^2 T}{\partial x\partial y} + \left(u\frac{\partial u}{\partial x} + v\frac{\partial u}{\partial y} \right)\frac{\partial T}{\partial x} + \left(v\frac{\partial v}{\partial y} + u\frac{\partial v}{\partial x} \right)\frac{\partial T}{\partial y} \right), \tag{5.5}$$

$$u\frac{\partial a}{\partial x} + v\frac{\partial a}{\partial y} + k_1 ab^2 = D_{A^*}\frac{\partial^2 a}{\partial y^2}, \tag{5.6}$$

$$u\frac{\partial b}{\partial x} + v\frac{\partial b}{\partial y} - k_1 ab^2 = D_{B^*}\frac{\partial^2 b}{\partial y^2}, \tag{5.7}$$

where Λ is the visco-elasticity of UCM fluid, Λ_h the thermal relaxation time, $U_e(x)$ the free stream velocity, p the pressure, D_{A^*} diffusion of specie A^*, D_{B^*} diffusion of specie B^*, ρ the fluid density, T the temperature and k the fluid's thermal

conductivity. The associated BCs are

$$
\left.
\begin{aligned}
&u = U_w(x) = s_0(x + b_1)^n,\ v = 0,\ T = T_w = c(x + b_1) + T_0,\ D_{A^*}\frac{\partial a}{\partial y} = k_s a, \\
&D_{B^*}\frac{\partial b}{\partial y} = -k_s a \quad \text{at} \quad y = m_0(x + b_1)^{\frac{1-n}{2}}, \\
&U \longrightarrow U_e(x) = d_0(x + b_1)^n,\ T \longrightarrow T_\infty = d(x + b_1) + T_0,\ a \longrightarrow a_0,\ b \longrightarrow b_0 \\
&\text{when} \quad y \longrightarrow \infty,
\end{aligned}
\right\}
$$
(5.8)

where $U_w(x)$ is the stretching velocity and k_s is the mass transfer coefficient. In the free stream, Eq. (5.5), reduces to the following form:

$$
U_e\frac{\partial U_e}{\partial x} = -\frac{1}{\rho}\frac{\partial p}{\partial x} - \Lambda\, U_e^2\frac{\partial^2 U_e}{\partial x^2} - \frac{\sigma B^2(x)}{\rho}U_e,
$$
(5.9)

Eliminating the pressure term $\frac{\partial p}{\partial x}$ from Eqs. (5.4) and (5.9), we get

$$
\left.
\begin{aligned}
&v\frac{\partial u}{\partial y} + u\frac{\partial u}{\partial x} = \nu\frac{\partial^2 u}{\partial y^2} + U_e\frac{\partial U_e}{\partial x} + \Lambda U_e^2\frac{\partial^2 U_e}{\partial x^2} - \Lambda\left(u^2\frac{\partial^2 u}{\partial x^2} + v^2\frac{\partial^2 u}{\partial y^2} + 2uv\frac{\partial^2 u}{\partial x \partial y}\right) \\
&+ \frac{\sigma B^2(x)}{\rho}\left(U_e - u - \Lambda v\frac{\partial u}{\partial y}\right) + g\beta_T(T - T_\infty),
\end{aligned}
\right\}
$$
(5.10)

For liquid metals, the thermal conductivity $k(T)$ is found to vary in an approximately linear manner with temperature in the range 0^oF to 400^oF (see Kays [140]). Thus variable thermal conductivity is assumed (as in Arunachalam and Rajappa [141]) and defined as fellows

$$
k(T) = k_\infty\left[1 + \delta\left(\frac{T - T_\infty}{T_w - T_0}\right)\right],
$$
(5.11)

where k_∞ is the ambient fluid thermal conductivity, T_w the wall temperature

and δ is a comparatively small scalar parameter showing how the temperature influences the variable thermal conductivity, given as

$$
\delta = \frac{k_w - k_\infty}{k_\infty}.
$$
(5.12)

The transformations used [142] are

$$\left. \begin{aligned} \psi &= \sqrt{\frac{2}{n+1}} \nu s_0 (x+b_1)^{n+1} F(\eta), \quad \eta = \sqrt{\frac{n+1}{2} \frac{s_0}{\nu}} (x+b_1)^{n-1} y, \\ u &= s_0 (x+b_1)^n F'(\eta), \; v = -\sqrt{\frac{n+1}{2} \nu s_0 (x+b_1)^{n-1}} \left(F(\eta) + \eta \frac{n-1}{n+1} F'(\eta) \right), \\ \Theta(\eta) &= \frac{T-T_\infty}{T_w - T_0}, \quad G(\eta) = \frac{a}{a_0}, \quad H(\eta) = \frac{b}{a_0}, \end{aligned} \right\}$$

(5.13)

The continuity equation given in (5.3) is satisfied identically whereas Eqs. (5.4)to(5.7) take the following form:

$$\left. \begin{aligned} &F''' + FF'' - \frac{2n}{n+1} F'^2 + \frac{2n}{n+1} A^2 + 2\beta \frac{n(n-1)}{n+1} A^3 \\ &- \frac{2}{n+1} M(F' - A - \beta(\frac{n+1}{2} FF'' + \eta \frac{n-1}{2} F'F'')) + \frac{2}{n+1} \lambda_t \Theta \\ &+ \beta \left[(3n-1)FF'F'' - \frac{2n(n-1)}{n+1} F'^3 + \eta \frac{n-1}{2} F'^2 F'' - \frac{n+1}{2} F^2 F''' \right] = 0, \end{aligned} \right\}$$

(5.14)

$$\left. \begin{aligned} &\left((1+\delta\Theta)\Theta'' + \delta\Theta'^2 \right) + P_r F\Theta' + P_r \Gamma_e \left(\frac{n-3}{2} FF'\Theta' - \frac{n+1}{2} F^2\Theta'' \right) \\ &+ P_r(\Theta + S) \left(\Gamma_e FF'' - \frac{2n}{n+1} \Gamma_e F'^2 - \frac{2}{n+1} F' \right) = 0, \end{aligned} \right\}$$

(5.15)

$$G'' - \frac{2S_c K}{n+1} GH^2 + S_c FG' = 0,$$

(5.16)

$$H'' + \frac{2S_c K}{\epsilon_1(n+1)} GH^2 + \frac{S_c}{\epsilon_1} H'F = 0.$$

(5.17)

The related conditions at the boundary are

$$\left. \begin{aligned} &F(\alpha_w) = \alpha \frac{1-n}{1+n}, \quad F'(\alpha_w) = 1, \quad G'(\alpha_w) = \sqrt{\frac{2}{n+1}} \, Ks \, G(\alpha_w), \\ &\Theta(\alpha_w) = 1 - S, \quad H'(\alpha_w) = -\frac{1}{\epsilon_1} \sqrt{\frac{2}{n+1}} \, Ks \, G(\alpha_w), F'(\eta) = A, \\ &G(\eta) = 1, \quad \Theta(\eta) = 0, H(\eta) = 0, \text{ when } \eta \to \infty. \end{aligned} \right\}$$

(5.18)

The prime represents the differentiation with respect to η and $\eta = m_0 \sqrt{\frac{n+1}{2} \frac{s_0}{\nu}} = \alpha_w$ denotes the surface of the plate, the minimum value of η which accurately corresponds to the minimum value of y at $y = m_0 (x+b_1)^{\frac{1-n}{2}}$. In order to convert

the domain from $\eta \in [\alpha_w, \infty)$ to $\xi \in [0, \infty)$, the substitutions $F(\eta) = f(\eta - \alpha_w) = f(\xi)$, $\Theta(\eta) = \theta(\eta - \alpha_w) = \theta(\xi)$, $G(\eta) = g(\eta - \alpha_w) = g(\xi)$, and $H(\eta) = h(\eta - \alpha_w) = h(\xi)$, are adopted and the following governing equations are obtained

$$
\left.
\begin{aligned}
&f''' + f f'' - \frac{2n}{n+1} f'^2 + \frac{2n}{n+1} A^2 + \frac{2n(n-1)}{n+1} \beta A^3 \\
&- \frac{2}{n+1} M \left(f' - A - \beta \left(\frac{n+1}{2} f f'' + (\xi + \alpha_w) \frac{n-1}{2} f' f'' \right) \right) + \frac{2}{n+1} \lambda_t \theta \\
&+ \beta \left[\frac{n-1}{2} (\xi + \alpha_w) f'^2 f'' - \frac{2n(n-1)}{n+1} f'^3 + (3n-1) f f' f'' - \frac{n+1}{2} f^2 f''' \right] \\
&= 0,
\end{aligned}
\right\}
$$
(5.19)

$$
\left.
\begin{aligned}
&(1 + \delta\theta)\theta'' + \delta\theta'^2 + P_r(S + \theta) \left(\Gamma_e f f'' - \frac{2n}{n+1} \Gamma_e f'^2 - \frac{2}{n+1} f' \right) + P_r f \theta' \\
&+ P_r \Gamma_e \left(\frac{n-3}{2} f f' \theta' - \frac{n+1}{2} f^2 \theta'' \right) = 0,
\end{aligned}
\right\}
$$
(5.20)

$$
g'' - \frac{2 S_c K}{n+1} g h^2 + S_c f g' = 0,
$$
(5.21)

$$
h'' + \frac{2 S_c K}{\epsilon_1 (n+1)} h g^2 + \frac{S_c}{\epsilon_1} h' f = 0.
$$
(5.22)

The prime in Eqs. $(5.19) - (5.22)$ and thereafter means the differentiation with respect to ξ.

The corresponding BCs are

$$
\left.
\begin{aligned}
&f(0) = \alpha_w \frac{1-n}{1+n}, \ f'(0) = 1, \ \theta(0) = 1 - S, \ g'(0) = \sqrt{\frac{2}{n+1}} \, Ks \, g(0), \\
&h'(0) = -\frac{1}{\epsilon_1} \sqrt{\frac{2}{n+1}} \, Ks \, g(0), \ f'(\xi) = A, \ \theta(\xi) = 0, \ g(\xi) = 1, \\
&h(\xi) = 0, \ \text{when } \xi \to \infty.
\end{aligned}
\right\}
$$
(5.23)

The physical parameters involved in the transformed equations are as follow:

$$
\left.
\begin{aligned}
&S = \frac{d}{c}, \epsilon_1 = \frac{D_{B^*}}{D_{A^*}}, P_r = \frac{\mu C_p}{k}, Ks = \frac{k_s}{D_{A^*}} \sqrt{\frac{\nu(x + b_1)}{U_w}}, A = \frac{d_0}{s_0}, M = \frac{\sigma B_0^2}{\rho s_0}, \\
&\beta = \Lambda s_0 (x + b_1)^{n-1}, \Gamma_e = \Lambda_h s_0 (x + b_1)^{n-1}, S_c = \frac{\nu}{D_{A^*}}, K = \frac{k_1 a^2}{s_0 (x + b_1)^{n-1}}, \\
&\lambda_t = \frac{Gr_x}{Re_x^2}, \ Gr_x = \frac{g \beta_T (T_w - T_0)(x + b_1)^3}{\nu^2}, \ Re_x = \frac{(x + b_1) U_w(x)}{\nu}.
\end{aligned}
\right\}
$$
(5.24)

The diffusion coefficients D_{A^*} and D_{B^*} are considered of comparable size which leads to assume D_{A^*} be equal to D_{B^*} i.e. $\epsilon_1 = 1$, so

$$g(\xi) + h(\xi) = 1. \tag{5.25}$$

So Eqs. (5.21) and (5.22) are simplified to yield

$$g'' - \frac{2 S_c K}{n+1} g(1-g)^2 + S_c f g' = 0, \tag{5.26}$$

with boundary conditions

$$g'(0) = \sqrt{\frac{2}{n+1}} K s \, g(0), \quad g(\xi) \longrightarrow 1 \quad \text{as} \quad \xi \longrightarrow \infty. \tag{5.27}$$

5.3 Solution Methodology

The ODEs (5.19), (5.20) and (5.26) along with BCs stated in (5.23) and (5.27), is solved iteratively by an efficient numerical technique named as the shooting method [112] for several values of the involved pertinent parameters. The shooting method is more efficient as compared to the other computational techniques. For numerical solution, we replace the domain $[0, \infty)$ by $[0, \xi_{max}]$ for some suitable choice of ξ_{max}. We have observed an asymptotic convergence of the numerical solutions by increasing the value of ξ_{max}. The MATLAB bvp4c function is used for the verification of the shooting method results. We symbolized f by y_1, θ by y_4 and g by y_6 to convert the BVP into an IVP and set the stoping criteria as

$$\max \left\{ |y_2(\xi_{max}) - A|, |y_4(\xi_{max}) - 0|, |y_6(\xi_{max}) - 1| \right\} < \varepsilon_0. \tag{5.28}$$

To solve the system by the shooting technique, the initial guesses are required for the values missing at the starting points. The Newton method is implemented with the aim of refinement of the initial guesses which are subject to the tolerance ϵ_0 until the approximate solution of the problem is obtained. The numerical results throughout in this paper, are achieved with the tolerance $\epsilon_0 = 10^{-6}$.

To validate our MATLAB code, we very convincingly reproduced the results of $-\theta'(0)$ reported by Sadeghy *et al.* [143], and Vajravelu *et al.* [144] (see Table 5.1). Further, to envisage the impact of different physical parameters on $f''(0)$ in the absence of the convection parameter ($\lambda_t = 0$) and Maxwell parameter i.e., Newtonian fluid, $\beta = 0$, the results are obtained and presented in Tables 5.2. By comparing the numerical results of $f''(0)$ to the results reported by Mahapatra and Gupta [131], Ishak *et al.* [132] and Abbas *et al.* [133], the validity of the numerical scheme is achieved (Table 5.2).

Tables 5.3-5.4 are prepared to compare the values of $C_f Re_x^{1/2}$ and $Nu_x Re_x^{-1/2}$ with the results obtained by Abbas *et al.* [133] and Ishak *et al.* [132] in case of Newtonian fluid but $\lambda = 1$. It is worth noticing that the results are in a convincing agreement. From these tables, we can see that the magnitudes of $C_f Re_x^{1/2}$ and $Nu_x Re_x^{-1/2}$ decrease and increase respectively for higher P_r either in assisting or opposing flows as depicted in the graphic representations. Table 5.5 is presented to see the effects of Pr on $-f''(0)$ and $-\theta'(0)$ for assisting and opposing cases by using the method of slope linear regression through data points [145]. It is observed that a decrease in the magnitude of $f''(0)$ for assisting flow is -0.0007472 while for the opposing case, it is 0.0007560. From the same table, the increments in the magnitude of $-\theta'(0)$ for flows that is assisting and opposing are estimated as 0.086850 and 0.087069 respectively.

Table 5.1: Data comparing the numerical results of $f''(0)$ for distinct values of β allied with $P_r = 1$, $M = 0$, $\lambda_t = 0$, $\delta = 0$, $A = 0$, $\alpha_w = 0$, $\Gamma_e = 0$, $S = K = Ks = S_c = 0$ and $n = 1$.

	$\beta = 0.0$	$\beta = 0.2$	$\beta = 0.4$	$\beta = 0.6$	$\beta = 0.8$
Sadeghy *et al.* [143]	-1.0000	-1.0549	-1.10084	-1.0015016	-1.19872
Vajravelu *et al.* [144]	-1.0001743	-1.051975	-1.1019475	-1.1501625	-1.1967279
Present (shooting)	-1.0001725	-1.051973	-1.1019446	-1.1501585	-1.1967224
Present (bvp4c)	-1.0001726	-1.051973	-1.1019446	-1.1501584	-1.1967224

Table 5.2: Data comparing the numerical results of $f''(0)$ for distinct values of A when $\beta = 0$, $\lambda_t = 0$ and $P_r = 1, n = 1, M = \alpha_w = \Gamma_e = \delta = S = K = Ks = S_c = 0$ with those reported by Mahapatra and Gupta[131], Ishak *et al.* [132] and Abbas *et al.* [133].

				Present results	
A	[131]	[132]	[133]	shooting	bvp4c
0.10	-0.9694	-0.9694	-0.9694	-0.969395	-0.969395
0.20	-0.9181	-0.9181	-0.9181	-0.918108	-0.918108
0.50	-0.6673	-0.6673	-0.6673	-0.667264	-0.667264
2.00	2.0175	2.0175	2.0175	2.017503	2.017503
3.00	4.7293	4.7294	4.7293	4.729282	4.729282

Table 5.3: Data comparing the numerical results of $f''(0)$ and $-\theta'(0)$ for distinct values of P_r when $\lambda_t = 1$, $A = 1$ $n = 1, M = \alpha_w = \Gamma_e = \delta = S = K = Ks = S_c = 0$ and $\beta = 0$ (Newtonian case)

	Ishak *et al.* [132]		Abbas *et al.* [133]		Present	
	Buoyancy opposing flow		Buoyancy opposing flow		Buoyancy opposing flow	
P_r	$C_f \, Re_x^{\frac{1}{2}}$	$Nu_x \, Re_x^{-\frac{1}{2}}$	$C_f \, Re_x^{\frac{1}{2}}$	$Nu_x \, Re_x^{-\frac{1}{2}}$	$C_f \, Re_x^{\frac{1}{2}}$	$Nu_x \, Re_x^{-\frac{1}{2}}$
0.72	-0.3852	1.0293	-0.3852	1.0293	-0.385189	1.029251
6.8	-0.1833	3.2466	-0.1832	3.2466	-0.183232	3.246086
20	-0.1183	5.5924	-0.1183	5.5923	-0.118311	5.589598
40	-0.0876	7.9228	-0.0876	7.9227	-0.087581	7.914895
60	-0.0731	9.7126	-0.0731	9.7126	-0.073041	9.698182
80	-0.0643	11.2233	-0.0642	11.2235	-0.064078	11.201180
100	-0.0578	12.5565	-0.0579	12.5564	-0.057828	12.525150

Table 5.4: Data comparing the numerical results of $-f''(0)$ and $-\theta'(0)$ for distinct values of P_r when $\lambda_t = 1$, $A = 1$, $n = 1, M = \alpha_w = \Gamma_e = \delta = S = K = Ks = S_c = 0$ and $\beta = 0$ (Newtonian case)

| | Ishak *et al.* [132] | | Abbas *et al.* [133] | | Present | |
| | Buoyancy assisting flow | | Buoyancy assisting flow | | Buoyancy assisting flow | |
P_r	$C_f\,Re_x^{\frac{1}{2}}$	$Nu_x\,Re_x^{-\frac{1}{2}}$	$C_f\,Re_x^{\frac{1}{2}}$	$Nu_x\,Re_x^{-\frac{1}{2}}$	$C_f\,Re_x^{\frac{1}{2}}$	$Nu_x\,Re_x^{-\frac{1}{2}}$
0.72	0.3645	1.0931	0.3645	1.0931	0.364493	1.093108
6.8	0.1804	3.2902	0.1804	3.2902	0.180415	3.289574
20	0.1175	5.6230	0.1175	5.6230	0.117500	5.620131
40	0.0874	7.9464	0.0873	7.9463	0.087242	7.938306
60	0.0729	9.7327	0.0729	9.7327	0.072842	9.718013
80	0.0641	11.2414	0.0640	11.2413	0.063942	11.218741
100	0.0577	12.5725	0.0578	12.5726	0.057728	12.541100

Table 5.5: The quantitative analysis of $f''(0)$ and $-\theta'(0)$ for different values of P_r for both the assisting and opposing flows by the method of slope linear regression through the data points [145].

| | $C_f Re_x^{1/2}$ | | $Nu_x Re_x^{-1/2}$ | |
P_r	Assisting flow	Opposing flow	Assisting flow	Opposing flow
20	0.117500	-0.118311	5.623131	5.589598
40	0.087242	-0.087581	7.938306	7.924895
60	0.072842	-0.073041	9.738014	9.698182
80	0.063942	-0.064078	11.241741	11.221180
100	0.057728	-0.057828	12.571100	12.555150
Slp	-0.0007472	0.0007560	0.086850	0.087069

5.4 Results and Discussion

The system of governing equations is solved numerically for the specific ranges of the involved physical parameters such as thermal stratification parameter $(0 \leq S \leq 1.0)$, visco-elastic parameter $(0 \leq \beta \leq 0.6)$, thermal relaxation parameter $(0 \leq \Gamma_e \leq 0.6)$, mixed convection parameter $(-0.3 \leq \lambda_t \leq 1)$, thermal conductivity parameter $(0 \leq \delta \leq 0.3)$, Prandtl number $(0 \leq P_r \leq 100)$, stretching ratio parameter $(0 \leq A \leq 3.0)$, Schmidt number $(0 \leq S_c \leq 1.2)$, homogeneous reaction parameter $(0 \leq K \leq 0.7)$ and heterogeneous reaction parameter $(0 \leq Ks \leq 1.7)$ (see Ref. [146]). The present results are substantially useful in case of highly conducting fluid flows e.g., the flow of metals in the liquid form. The quantitative analysis of $-\theta'(0)$ for different values of δ and Γ_e for flow either assisting or opposing by the method of slope linear regression through the data points is shown in Table 5.6 (for details see [145]). A decrease in $Nu_x Re_x^{-1/2}$ with δ for assisting flow is estimated as -0.054355 whereas the rate of increase for the case of opposing flow is estimated as 0.432760. The increments in $Nu_x Re_x^{-1/2}$ with Γ_e for case weather assisting or opposing flow are 0.347215 and 0.254545 respectively. Table 5.9 shows the investigated numerical results of $Nu_x Re_x^{-1/2}$ for various values of β, P_r, M, δ, A and n for the case of Maxwell fluid $(\beta \neq 0)$ and in the presence of convection parameter $(\lambda_t = 1)$. It is clear that $Nu_x Re_x^{-1/2}$ rises for P_r, Γ_e and A conversely it reduces for β, M, δ, S, α_w and n for the assisting flow. On the other hand, $Nu_x Re_x^{-1/2}$ shall rise for the Prandtl number P_r, thermal relaxation parameter Γ_e, stretching ratio parameter A, variable wall thickness parameter α_w, thermal conductivity parameter δ whereas it decreases for Maxwell parameter β, magnetic parameter M, stratification parameter S and power index parameter n as depicted in Table 5.10.

The accuracy and convergence of the numerical results is assessed by computing the solution based error E_r at the extreme ends of the known boundary conditions which is defined as the maximum absolute error between the approximate solution at ξ_{max} and the actual conditions at the boundary. This error is subject to the tolerance $\xi_0 = 10^{-7}$ and is defined as:

Table 5.6: The quantitative analysis of $-\theta'(0)$ for different values of δ and Γ_e for both the cases either assisting or opposing flows by the method of slope linear regression through the data points [145].

| | $Nu_x Re_x^{-1/2}$ | |
δ	Assisting flow	Opposing flow
0.1	1.042613	0.785272
0.2	1.037241	0.815480
0.3	1.031742	0.871824
Slp	-0.054355	0.432760
Γ_e		
0.3	1.075623	0.836746
0.5	1.128415	0.881849
0.7	1.214509	0.938564
Slp	0.347215	0.254545

$$E_r = \max \left\{ |y_2 \left(\xi_{max} \right) - A| , |y_4 \left(\xi_{max} \right) - 0| , |y_6 \left(\xi_{max} \right) - 1| \right\} . \qquad (5.29)$$

The variation in E_r corresponds to number of iterations when $M = 0.2, A = 0.1, P_r = 1, \beta = 0.2, \delta = 0.3, n = 1.3$ $K = 0.5, S_c = 1.2,$ and $Ks = 1.0$ as depicted in Figs. 5.2-5.3 where J denotes the number of iterations.
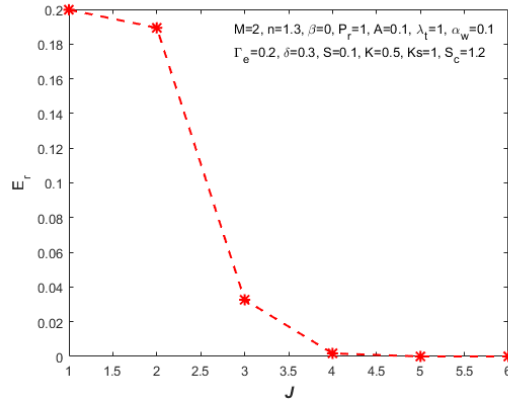
Fig. 5.2: Solution error against iterations for $\beta = 0$ (Newtonian case)
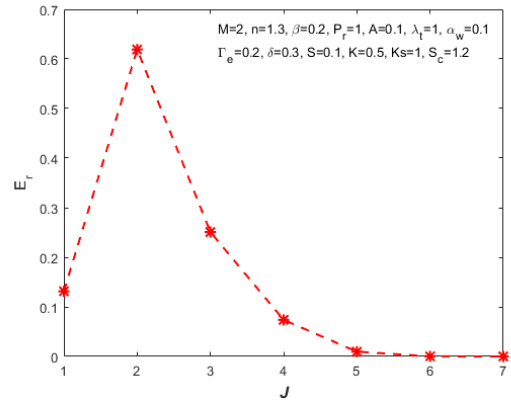
Fig. 5.3: Solution error against iterations for $\beta = 0.2$ (Maxwell model)

To inspect the influence of involved physical parameters on f' (velocity field), θ (temperature field) and ϕ (concentration field), the numerical results in graphical form are illustrated in Figs. 5.4-5.21. The parametric values are fixed as $M = 0.2, P_r = 0.8, \beta = 0.2, \alpha_w = 0.1, \delta = 0.3, n = 1.3, A = 0.1, K = 0.5, Ks =$

Table 5.7: Data comparing the numerical results of $-f''(0)$ for distinct values of $P_r, \beta, M, A, \delta, \alpha_w$ and n for assisting flow when $K = 0.5, Ks = 1, S_c = 1.2, \lambda_t = 1$.

M	P_r	A	n	α_w	β	Γ_e	δ	S	Assisting flow $-f''(0)$(bvp4c)	Assisting flow $-f''(0)$(shooting)
2.0	1.0	0.1	1.3	0.1	0.2	0.2	0.3	0.1	1.344933833367847	1.344933834361249
2.5									1.464822352691913	1.464822354089623
3.0									1.577578472732591	1.577578474626216
	1.0								1.344933833367847	1.344933834361249
	2.0								1.403081512378463	1.403081513350095
	3.0								1.437998066535871	1.437998067492622
		0.1							1.344933833367847	1.344933834361249
		0.2							1.224381820364593	1.224381821164717
		0.3							1.089778146777188	1.089778147413683
			1.3						1.344933833367847	1.344933834361249
			1.4						1.350227048412943	1.350227049444106
			1.5						1.355875675688296	1.355875678041932
				0.1					1.344933833367847	1.344933834361249
				0.3					1.324004161137572	1.324004162068257
				0.5					1.303611708986189	1.303611709857910
					0.2				1.344933833367847	1.344933834361249
					0.3				1.387174678699923	1.387174680195641
					0.4				1.428713097180999	1.428713099196934
						0.2			1.344933833367847	1.344933834361249
						0.3			1.349851972335295	1.349851973332640
						0.4			1.354703545470430	1.354703546473988
							0.1		1.354819857020148	1.354819858008785
							0.3		1.344933833367847	1.344933834361249
							0.5		1.336143488322098	1.336143489321317
								0.1	1.344933833367847	1.344933834361249
								0.2	1.386909774825476	1.386909775871208
								0.3	1.428812600999609	1.428812602098434

$1.0, \Gamma_e = 0.2, S = 0.1$ and $S_c = 1.2$ unless otherwise mentioned. Figs. 5.4-5.5, are sketched to highlight the effect of β on f' in the absence and presence of the convection parameter λ_t. Fig. 5.4 shows f' as a decreasing function of β implying that an increase in the values of β cuts down f' and hence the boundary-layer thickness, which is also conventionally true when the convection parameter is present. Physically, $\lambda_t \neq 0$ means mixed convection whereas $\lambda_t = 0$ is for no mixed convection. It is important to note that the increasing values of β contribute to the reduction in f' for flows either assisting or opposing as noted in Fig. 5.5. Figs. 5.6-5.7 reflect the impact of β on θ. The value of θ at the wall is

Table 5.8: Data comparing the numerical results of $-f''(0)$ for distinct values of $P_r, \beta, M, A, \delta, \alpha_w$ and n for opposing flow when $K = 0.5, Ks = 1, S_c = 1.2, \lambda_t = 1$.

M	P_r	A	n	α_w	β	Γ_e	δ	S	Opposing flow $-f''(0)$(bvp4c)	Opposing flow $-f''(0)$(shooting)
2.0	1.0	0.1	1.3	0.1	0.2	0.2	0.3	0.1	1.992457739650596	1.992457741917505
2.5									2.084575781612447	2.084575784409768
3.0									2.173854651027451	2.173854666908606
	1.0								1.992457739650596	1.992457741917505
	2.0								2.083046109108662	2.083046121487478
	3.0								2.061812071089239	2.061812073510933
		0.1							1.992457739650596	1.992457741917505
		0.2							1.814748622927784	1.814748624884158
		0.3							1.643444072284256	1.643444073987701
			1.3						1.992457739650596	1.992457741917505
			1.4						1.972354480052976	1.972354482293929
			1.5						1.954374460742803	1.954374463070022
				0.1					1.992457739650596	1.992457741917505
				0.3					1.971071536675758	1.971071538706785
				0.5					1.950216318889997	1.950216320808051
					0.2				1.992457739650596	1.992457741917505
					0.3				2.038220541903796	2.038220545339932
					0.4				2.083131537194593	2.083131541947168
						0.2			1.992457739650596	1.992457741917505
						0.3			1.987030315195248	1.987030317319197
						0.4			1.981559618924986	1.981559621019549
							0.1		1.974842014738829	1.974842016870703
							0.3		1.992457739650596	1.992457741917505
							0.5		2.009343969811091	2.009343971976457
								0.1	1.992457739650596	1.992457741917505
								0.2	1.932844696358433	1.932844698442282
								0.3	1.876313196709956	1.876313198718950

approximately one and away from this boundary becomes zero. This is, mainly, due to the change in the physical parameters. The, comparatively, higher values of β raise θ and this phenomenon occurs mainly due to a rise in the elasticity stress parameter but away from the boundary, θ tends to zero. Fig. 5.7, shows that the thermal boundary-layer thickens with a rise in β thus providing a raise to the surface rate of heat transfer. Furthermore, a similar situation occurs in the presence or absence of the mixed convection parameter i.e., $\lambda_t = 0$.

The effect of variable thermal conductivity δ on θ is presented in Figs. 5.8-5.9,

Table 5.9: Data comparing the numerical results of $-\theta'(0)$ for distinct values of $P_r, \beta, M, A, \delta, \alpha_w$ and n for assisting flow when $K = 0.5, Ks = 1, S_c = 1.2, \lambda_t = 1$.

M	P_r	A	n	α_w	β	Γ_e	δ	S	Assisting flow $Nu_x Re_x^{-1/2}$(bvp4c)	Assisting flow $Nu_x Re_x^{-1/2}$(shooting)
2.0	1.0	0.1	1.3	0.1	0.2	0.2	0.3	0.1	0.795685242443375	0.795685242213262
2.5									0.777863689785805	0.777863689545146
3.0									0.761800259718433	0.761800259464641
	1.0								0.795685242443375	0.795685242213262
	2.0								1.209089138600449	1.209089137900614
	3.0								1.539167293220001	1.539167291801142
		0.1							0.795685242443375	0.795685242213262
		0.2							0.837601494720709	0.837601494534534
		0.3							0.877122967919783	0.877122967745785
			1.3						0.795685242443375	0.795685242213262
			1.4						0.784871102510746	0.784871102322752
			1.5						0.774822295369534	0.774822297661127
				0.1					0.795685242443375	0.795685242213262
				0.3					0.784950650573613	0.784950650353843
				0.5					0.774479856350943	0.774479856136813
					0.2				0.795685242443375	0.795685242213262
					0.3				0.786142147000481	0.786142146758793
					0.4				0.777121147772825	0.777121147511526
						0.2			0.795685242443375	0.795685242213262
						0.3			0.829189939416099	0.829189939050014
						0.4			0.862199320769574	0.862199320244274
							0.1		0.887789857820678	0.887789857453383
							0.3		0.795685242443375	0.795685242213262
							0.5		0.724581021533058	0.724581021370532
								0.1	0.795685242443375	0.795685242213262
								0.2	0.769109848863160	0.769109848637892
								0.3	0.741780521827511	0.741780521608618

both with and without the Maxwell parameter β. These figures reflect that the increasing values of δ and β enhance θ. Because in the presumption $k(T) \geq k_\infty$ that is, the thermal conductivity is increased whenever $\delta > 0$, so for up-going values of δ, the thermal conductivity rises and hence θ increases. Figs. 5.10-5.11 are prepared for the analysis of the impact of P_r on θ both in the presence and absence of the Maxwell parameter β and in the assisting and opposing convection regions respectively. These graphical results show that θ reduces once the values of P_r are increased, therefore the thickness of the thermal boundary-layer declines in consequence to the higher values of P_r. This holds true for all values of the

Table 5.10: Data comparing the numerical results of $-\theta'(0)$ for distinct values of $P_r, \beta, M, A, \delta, \alpha_w$ and n for opposing flow when $K = 0.5, Ks = 1, S_c = 1.2, \lambda_t = 1$.

M	P_r	A	n	α_w	β	Γ_e	δ	S	Opposing flow $Nu_x Re_x^{-1/2}$(bvp4c)	Opposing flow $Nu_x Re_x^{-1/2}$(shooting)
2.0	1.0	0.1	1.3	0.1	0.2	0.2	0.3	0.1	0.621451310392101	0.621451310164980
2.5									0.616483523423893	0.616483523402749
3.0									0.610416645008779	0.610416645018083
	1.0								0.621451310392101	0.621451310164980
	2.0								0.617952194395247	0.617952191243758
	3.0								0.870608596371502	0.870608595019171
		0.1							0.621451310392101	0.621451310164980
		0.2							0.728240109728708	0.728240109528644
		0.3							0.795320118954000	0.795320118718450
			1.3						0.621451310392101	0.621451310164980
			1.4						0.617582509546634	0.617582509541626
			1.5						0.613841420498595	0.613841420479057
				0.1					0.621451310392101	0.621451310164980
				0.3					0.606041634389043	0.606041634397641
				0.5					0.590743829782126	0.590743829795341
					0.2				0.621451310392101	0.621451310164980
					0.3				0.607027356611328	0.607027356760770
					0.4				0.593010430440567	0.593010430749819
						0.2			0.621451310392101	0.621451310164980
						0.3			0.654392335028992	0.654392334841669
						0.4			0.687263082108660	0.687263081700653
							0.1		0.718379969716274	0.718379969537921
							0.3		0.621451310392101	0.621451310164980
							0.5		0.543804664086843	0.543804664186620
								0.1	0.621451310392101	0.621451310164980
								0.2	0.637937258094765	0.637937258015901
								0.3	0.649074562589486	0.649074562461125

convection parameter. The effect on f' and θ of A has been explored and displayed in Figs. 5.12 and 5.13. These figures clearly indicate that the thermal boundary-layer thickness falls when A rise. A similar trend is noted for f'. The impact on ϕ of K (strength of homogeneous reaction parameter) is researched in Fig. 5.14. It is worth noticing that to achieve the higher values of K, ϕ shall reduce but with an increase in K, the associated layer thickness rises. The characteristics of Ks (strength of heterogeneous reaction parameter) on ϕ is depicted in Fig. 5.15. The profile ϕ shows a decreasing behavior for the larger values of Ks. The concentration field against the Schmidt number S_c is presented in Fig. 5.16.

Table 5.11: Data comparing the numerical results of $-\phi'(0)$ for distinct values of $P_r, \beta, M, A, \delta, \alpha_w$ and n for assisting flow when $K = 0.5, Ks = 1, S_c = 1.2, \lambda_t = 1$.

M	P_r	A	n	α_w	β	Γ_e	δ	S	Assisting flow $Sh_x Re_x^{-1/2}$(bvp4c)	Assisting flow $Sh_x Re_x^{-1/2}$(shooting)
2.0	1.0	0.1	1.3	0.1	0.2	0.2	0.3	0.1	-0.331493511591765	-0.331493511530786
2.5									-0.324461736410449	-0.324461736353706
3.0									-0.317981648281040	-0.317981648239340
	1.0								-0.331493511591765	-0.331493511530786
	2.0								-0.320207215791463	-0.320207215749739
	3.0								-0.314588282599464	-0.314588282590207
		0.1							-0.331493511591765	-0.331493511530786
		0.2							-0.349042352590988	-0.349042352571037
		0.3							-0.364252486926798	-0.364252487128202
			1.3						-0.331493511591765	-0.331493511530786
			1.4						-0.329252776471584	-0.329252780542749
			1.5						-0.327030134764097	-0.327030134958497
				0.1					-0.331493511591765	-0.331493511530786
				0.3					-0.322848270746216	-0.322848302015735
				0.5					-0.314087031471762	-0.314087031410038
					0.2				-0.331493511591765	-0.331493511530786
					0.3				-0.327593901648241	-0.327593903109054
					0.4				-0.323880725012761	-0.323880744336981
						0.2			-0.331493511591765	-0.331493511530786
						0.3			-0.330436131591279	-0.330436131540341
						0.4			-0.329383408978007	-0.329383409062112
							0.1		-0.329912964268319	-0.329912964251495
							0.3		-0.331493511591765	-0.331493511530786
							0.5		-0.332974358209099	-0.332974358184884
								0.1	-0.331493511591765	-0.331493511530786
								0.2	-0.326836530581132	-0.326836533561167
								0.3	-0.321943794465317	-0.321943840251548

The larger Schmidt number enhances the concentration distribution. The Schmidt number is a term employed to describe the ratio between the momentum and mass diffusivity. The higher S_c corresponds to the small diffusivity and as a result, the concentration increases. Fig. 5.17 is presented to observe the impact of S on θ. The profile θ reduce for the rising values of S in both cases, weather assisting or opposing. This is because of the observation that once the values of S ascend, the difference between the surface and ambient temperatures, correspondingly, descend, thereby temperature decreases. Fig. 5.18 discloses the impact of Γ_e on θ. The temperature in both cases, either assisting or opposing lowers for the rising

Table 5.12: Data comparing the numerical results of $-\phi'(0)$ for distinct values of $P_r, \beta, M, A, \delta, \alpha_w$ and n for opposing flow when $K = 0.5, Ks = 1, S_c = 1.2, \lambda_t = 1$.

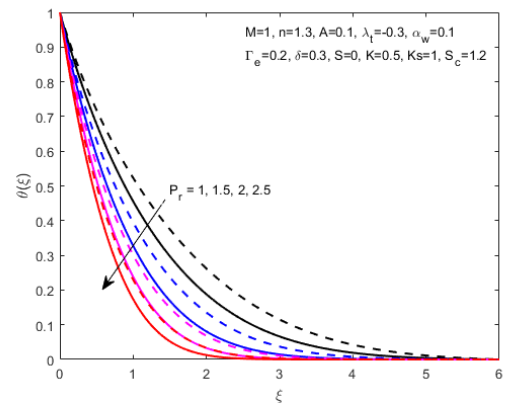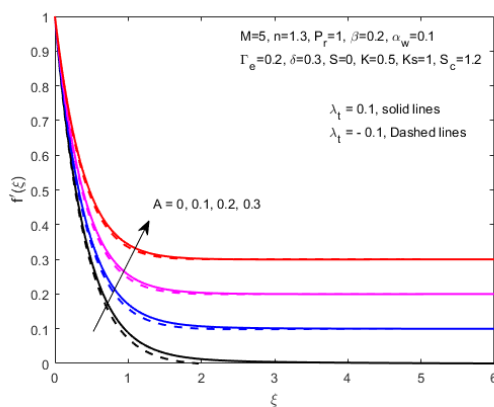| M	P_r	A	n	α_w	β	Γ_e	δ	S	Opposing flow $Sh_x Re_x^{-1/2}$(bvp4c)	Opposing flow $Sh_x Re_x^{-1/2}$(shooting)
2.0	1.0	0.1	1.3	0.1	0.2	0.2	0.3	0.1	-0.242525610129573	-0.242525610449071
2.5									-0.241074463600295	-0.241074463785822
3.0									-0.238734673652392	-0.238734674751676
	1.0								-0.242525610129573	-0.242525610449071
	2.0								-0.113782741616841	-0.113782741723205
	3.0								-0.127312848840723	-0.127312848812879
		0.1							-0.242525610129573	-0.242525610449071
		0.2							-0.304476290685308	-0.304476290725903
		0.3							-0.335609461732591	-0.335609461909846
			1.3						-0.242525610129573	-0.242525610449071
			1.4						-0.246653048534905	-0.246653066429389
			1.5						-0.250046241498275	-0.250046241623288
				0.1					-0.242525610129573	-0.242525610449071
				0.3					-0.227251016814343	-0.227251026154632
				0.5					-0.211573346520829	-0.211573374563131
					0.2				-0.242525610129573	-0.242525610449071
					0.3				-0.233749107867189	-0.233749111148911
					0.4				-0.225041015616277	-0.225041020242755
						0.2			-0.242525610129573	-0.242525610449071
						0.3			-0.245547011136372	-0.245547011573263
						0.4			-0.248523778501887	-0.248523781647725
							0.1		-0.252100323269710	-0.252100348777774
							0.3		-0.242525610129573	-0.242525610449071
							0.5		-0.231350411654402	-0.231350415972110
								0.1	-0.242525610129573	-0.242525610449071
								0.2	-0.262904404419716	-0.262904404515959
								0.3	-0.278199932175671	-0.278199933266695

values of Γ_e. This contributes to the eventual thermal boundary-layer thickness reduction. Physically, the parameter Γ_e appeared in the formulation of energy equation due to heat flux relaxation time. Corresponding to the ascending values of Γ_e, there is a larger heat flux relaxation time that is for larger Γ_e, particles of the fluid need more time to transfer heat to their adjacent particles and hence the temperature decays. Fourier's heat conduction model is a special case of CCHFM for $\Gamma_e = 0$. The temperature in case of CCHFM is less when compared with the classical Fourier's law. As the heat transfers instantly through the material for $\Gamma_e = 0$, so this fact strengthens the above argument. Fig. 5.19 reveals that

$Re^{1/2}{}_x C_f$ increases with β for higher values of the stratification parameter S in assisting flow but the reverse trend is observed for the case of opposing flow (see Ref. [147]). The variation in $Re^{-1/2}{}_x Nu_x$ for various Prandtl number P_r and buoyancy parameter λ_t is sketched in Fig. 5.20. $Re^{-1/2}{}_x Nu_x$ increases for the ascending values of P_r in both the assisting and the opposing flows whereas the increase in $Re^{-1/2}{}_x Nu_x$ is very small for the case of opposing flow as compared with the assisting flow. The variations in $Shu_x Re_x^{-1/2}$ are presented in Fig. 5.21 for various values of Schmidt number S_c and homogenous reaction parameter K in both the assisting and the opposing flows. Fig. 5.21 depicts that for a fixed value of Sc, $Re^{-1/2}{}_x Shu_x$ increases with homogeneous reaction parameter K and at a constant value of K, an unequal decrement in $Re^{-1/2}{}_x Shu_x$ with Sc is noticed for both the assisting and the opposing cases.
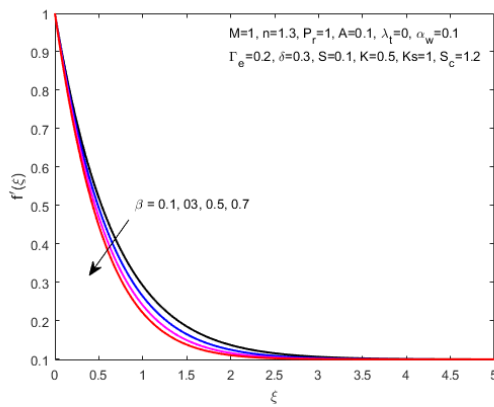
Fig. 5.4: Impact of β on f'
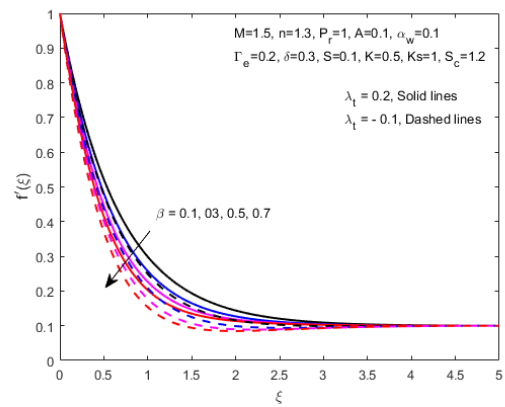
Fig. 5.5: Impact of β on f'
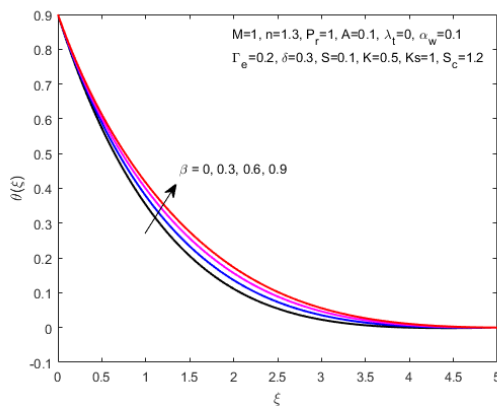
Fig. 5.6: Impact of β on θ
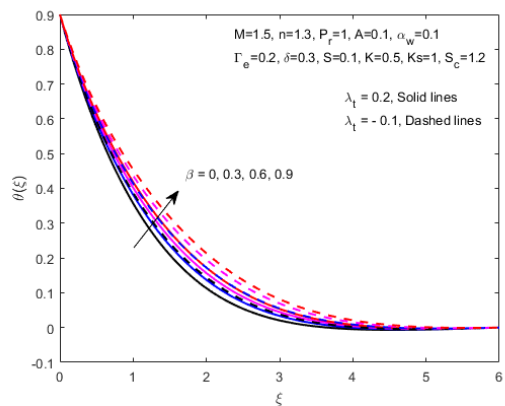
Fig. 5.7: Impact of β on θ
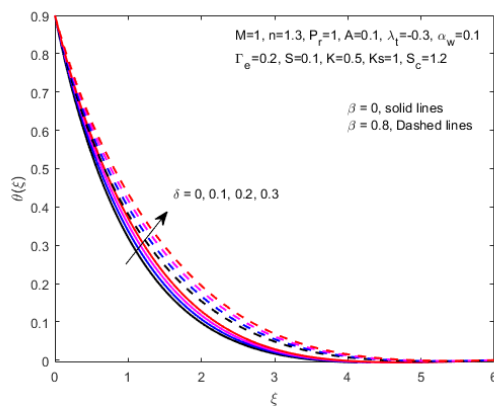
Fig. 5.8: Impact of δ on θ
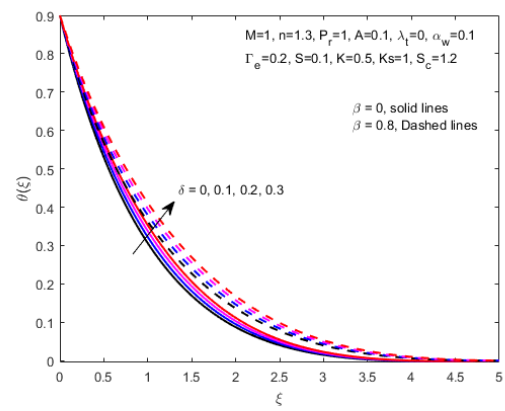
Fig. 5.9: Impact of δ on θ
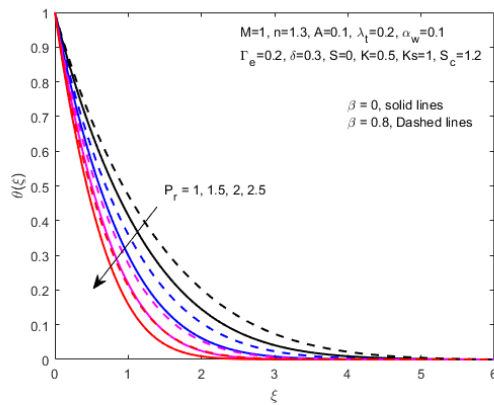
Fig. 5.10: Impact of P_r on θ (assisting case)

Fig. 5.11: Impacr of P_r on θ (opposing case)

Fig. 5.12: Impact of A on f'
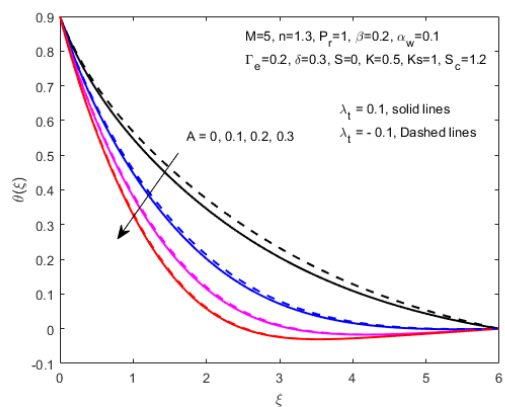
Fig. 5.13: Impact of A on θ
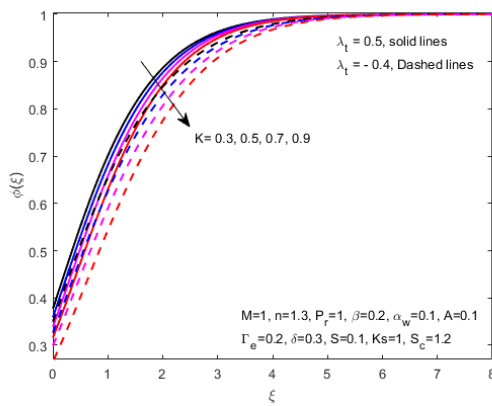
Fig. 5.14: Impact of K on f'
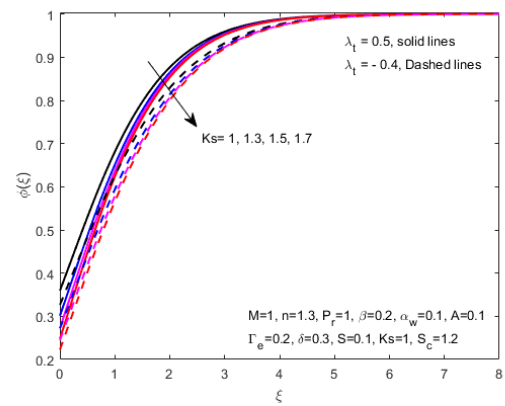
Fig. 5.15: Impact of Ks on f'
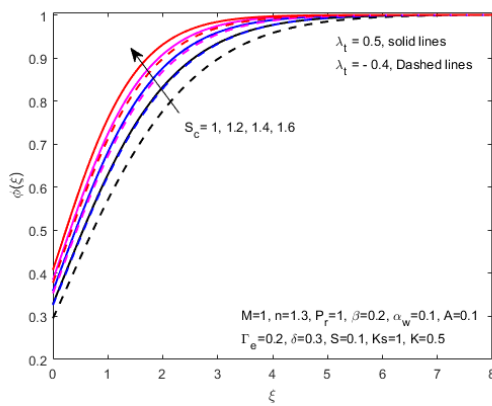
Fig. 5.16: Impact of S_c on ϕ
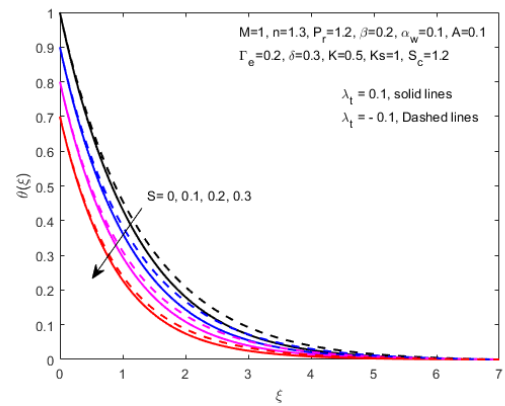
Fig. 5.17: Impact of S on θ.
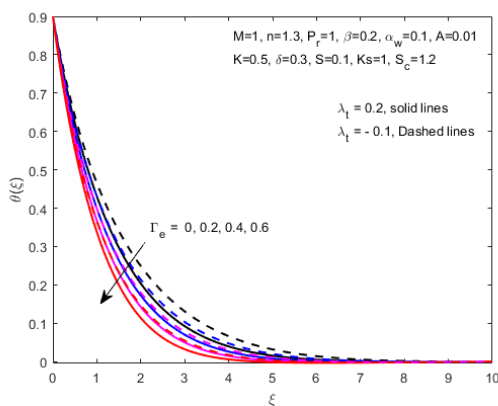
Fig. 5.18: Impact of Γ_e on θ
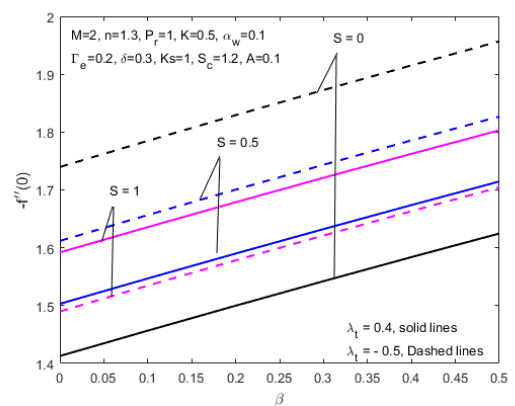
Fig. 5.19: Impact of S on $-f''(0)$
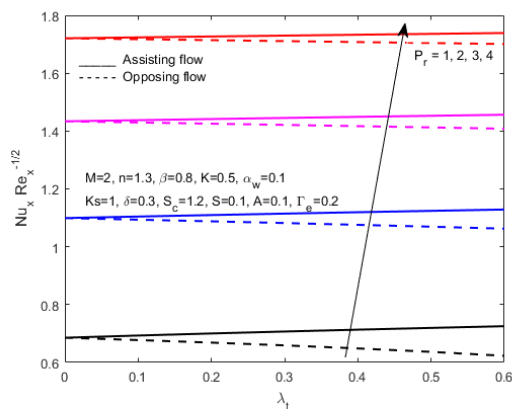
Fig. 5.20: Impact of P_r on $Nu_x Re_x^{-1/2}$
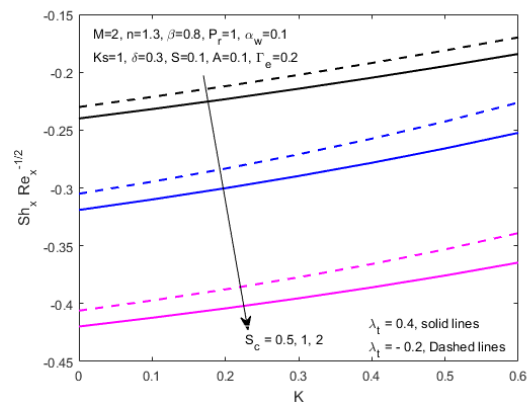
Fig. 5.21: Impact of S_c on $Sh_x Re_x^{-1/2}$

5.5 Final Remarks

In this chapter, MHD mixed convection UCM fluid flow over a stretching sheet with variable thickness close to a stagnation-point is explored numerically. Heat transfer characteristics are analyzed under the assumption of variable thermal conductivity. Furthermore, homogeneous-heterogeneous chemical reactions and thermal stratification have also been considered in the present study. Both the assisting and the opposing flows are discussed through tables and graphs. The ODEs are obtained via suitable similarity transformations. The numerical solutions of temperature, concentration and velocity profiles are obtained by employing the shooting technique and examined for different physical parameters. Some of the important findings of the present piece of research have been summarized as below:

- The velocity and momentum boundary-layer thickness reduces for the up-surged values of β in both the assisting and the opposing regimes.

- The impact of β on f' and θ is dissimilar. The velocity diminishes whereas the temperature upturns.

- The temperature in the case of CCHFM is less as compared with the classical Fourier's law.

- A higher augmentation in θ is witnessed for δ in case of the Maxwell fluid.

- The larger values of the thermal stratification parameter decays the temperature.

- An upturn in the strength of K enhances the concentration profile.

- The concentration profile for the higher values of S_c is found to rise.

Chapter 6

MHD UCM Nanofluid Flow in a Porous Medium Using CCHFM

6.1 Introduction

This chapter tries to determine, systematically, the phenomenon of a slip flow of a UCM nanofluid, once generated by an inclined surface through a porous medium and magnetic field. The diffusion model for mass and heat transfer introduced by Cattaneo-Christov is incorporated in the modeling process. The relaxation framework visco-elastic system is formulated for UCM nanofluid to determine both heat and mass transfer by CCHFM. Effects of the thermophoresis, Brownian motion and heat generation and chemical reaction are also considered. For a definitive confirmation of the boundary-layer approximations, it is assumed that the ratio between the forces of inertia and those of viscosity are high enough. Similarity transformations are put to use in order to acquire a dimensionless form of governing equations. These dimensionless equations have been cracked, numerically, with the shooting method. The present chapter focuses, primarily, on the research of important parameters appearing in the governing equations and their impacts on the local Nusselt number, skin-friction co-efficient, velocity, concentration and temperature distributions. A rise in heat transfer rate for an augmentation in the Prandtl number is identified whereas the heat transfer rate is subsided for the Maxwell parameter and thermal relaxation parameter. This study follows a

definite format. Section 6.2 deals with the problem pertaining to configuration. Section 6.3 concerns itself with the information regarding the formulation of governing equations, the numerical approach and validation of the code. The resultant numerical and graphical conclusions stand elaborated in section 6.4. Section 6.5 is the sum and product, annunciating the more significant findings of the entire research of the chapter.

6.2 Mathematical Formulation of the Problem
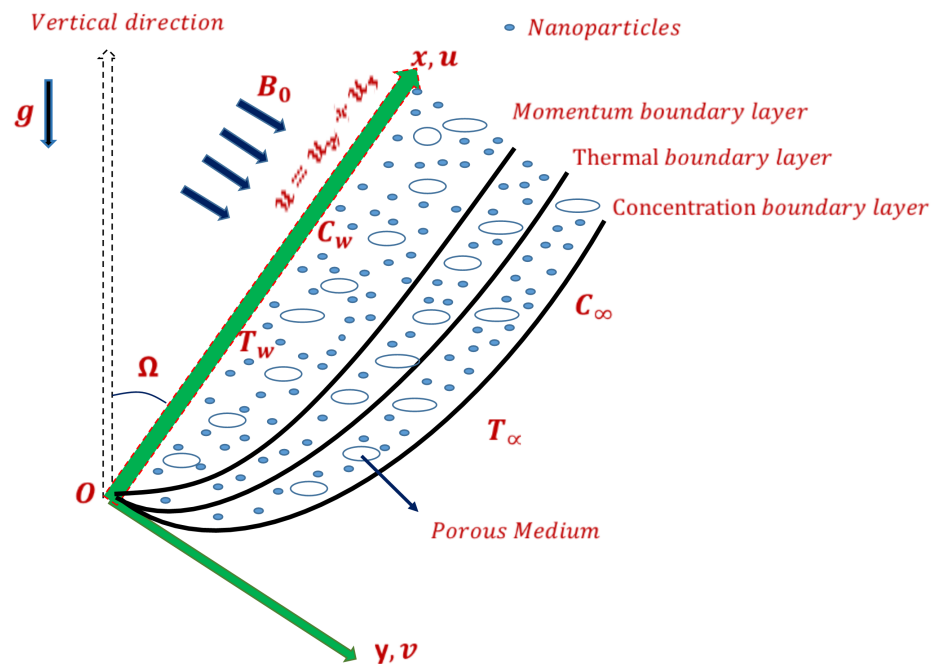
Fig. 6.1: Schematic of physical model.

A laminar, steady and incompressible UCM nanofluid flow through a porous medium has been considered. The stretching velocity of sheet which makes an angle Ω with the vertical direction, has been taken as $U_w(x) = s_0 x$. The energy equation is modified by incorporating radiation and heat generation effects. The flow direction is taken as $x-$axis direction perpendicular to it is taken as $y-$axis, as illustrated in Fig. 6.1. Moreover, the chemical reaction with the thermophoresis

and Brownian motion effects are also considered. The velocity slip condition is further assimilated in the present work. Represent the temperature as T_w and concentration as C_w at surface while far away the surface as T_∞ and C_∞. A uniform magnetic field B_0 in perpendicular direction is applied. As the magnetic Reynold's number is considered as small, so on the basis of this consideration, the induced magnet field is neglected (see [148]). Moreover, the above assumptions allow the Joule heating, viscous dissipation and body forces to be neglected (see [47]). The constitutive equations of UCM nanofluid model under the assumed circumstances are given as [149, 150]:

$$\frac{\partial v}{\partial y} + \frac{\partial u}{\partial x} = 0, \tag{6.1}$$

$$u\frac{\partial u}{\partial x} + v\frac{\partial u}{\partial y} = \nu\frac{\partial^2 u}{\partial y^2} - \Lambda\left(u^2\frac{\partial^2 u}{\partial x^2} + v^2\frac{\partial^2 u}{\partial y^2} + 2uv\frac{\partial^2 u}{\partial x\partial y}\right) - \frac{\sigma B_0^2}{\rho}\left(u + \Lambda v\frac{\partial u}{\partial y}\right)$$
$$- \frac{\nu}{\epsilon_0}u + \left[\beta_T\ (T - T_\infty) + \beta_C\ (C - C_\infty)\right]\ g\cos\Omega, \tag{6.2}$$

The thermal and concentration diffusion in modified Fourier and Fick's prospective have been investigated in this work. In the light of CCHFM, the generalized version of Fourier and Fick's models are

$$\mathbf{q} + \Lambda_h\left(\frac{\partial \mathbf{q}}{\partial t} + (\nabla \cdot \mathbf{v})\,\mathbf{q} + \mathbf{v}\cdot\nabla\mathbf{q} - \mathbf{q}\cdot\nabla\mathbf{v}\right) = -k\nabla T,$$

$$\tag{6.3}$$

$$\mathbf{J} + \Lambda_m\left(\frac{\partial \mathbf{J}}{\partial t} + (\nabla \cdot \mathbf{v})\,\mathbf{J} + \mathbf{v}\cdot\nabla\mathbf{J} - \mathbf{J}\cdot\nabla\mathbf{v}\right) = -D_B\nabla C,$$

$$\tag{6.4}$$

where $\mathbf{q}$ and $\mathbf{J}$ are heat and mass fluxes respectively. The Fourier and Fick's laws may be recovered for $\Lambda_h = 0$ and $\Lambda_m = 0$ as a special case. For the incompressible and steady laminar flow, Eqs. (6.3) and (6.4) are reduced to the following form:

$$\mathbf{q} + \Lambda_h\left(\mathbf{v}\cdot\nabla\mathbf{q} - \mathbf{q}\cdot\nabla\mathbf{v}\right) = -k\nabla T, \tag{6.5}$$

$$\mathbf{J} + \Lambda_m\left(\mathbf{v}\cdot\nabla\mathbf{J} - \mathbf{J}\cdot\nabla\mathbf{v}\right) = -D_B\nabla C, \tag{6.6}$$

Using the Rosseland approximation, the thermal radiation is simulated and in view of this, q_r (see [121]) is stated as:

$$q_r = -\frac{4\sigma^*}{3k^*}\frac{\partial T^4}{\partial y}, \tag{6.7}$$

The Taylor series in order to linearize the term T^4 about T_∞ is applied under the assumption of sufficiently small temperature differences within the mass. Approximating the expansion of T^4 and ignoring the smaller terms, we have

$$T^4 \cong 4T_\infty^3 T - 3T_\infty^4. \tag{6.8}$$

Using (6.7) and (6.8), we get

$$\frac{\partial q_r}{\partial y} = -\frac{16T_\infty^3 \sigma^*}{3k^*}\frac{\partial^2 T}{\partial y^2}. \tag{6.9}$$

The energy and concentration equations, utilizing Eqs. (6.5) and (6.6) with thermophoresis and Brownian forces effects along with BCs ([151]) are

$$u\frac{\partial T}{\partial x} + v\frac{\partial T}{\partial y} + \Lambda_h\Omega_h = \alpha\frac{\partial^2 T}{\partial y^2}$$
$$+ \frac{Q_0\,(T - T_\infty)}{(\rho C_p)_f} + \tau\left(D_B\frac{\partial T}{\partial y}\frac{\partial C}{\partial y} + \frac{D_T}{T_\infty}\left(\frac{\partial T}{\partial y}\right)^2\right) + \frac{16T_\infty^3\sigma^*}{3k^*(\rho C_p)_f}\frac{\partial^2 T}{\partial y^2}, \tag{6.10}$$

$$u\frac{\partial C}{\partial x} + v\frac{\partial C}{\partial y} + \Lambda_m\Omega_m = D_B\frac{\partial^2 C}{\partial y^2} + \frac{D_T}{T_\infty}\frac{\partial^2 T}{\partial y^2} - K_c\,(C - C_\infty). \tag{6.11}$$

where

$$\Omega_h = u^2\frac{\partial^2 T}{\partial x^2} + v^2\frac{\partial^2 T}{\partial y^2} + 2uv\frac{\partial^2 T}{\partial x\partial y} + \left(u\frac{\partial u}{\partial x} + v\frac{\partial u}{\partial y}\right)\frac{\partial T}{\partial x} + \left(u\frac{\partial v}{\partial x} + v\frac{\partial v}{\partial y}\right)\frac{\partial T}{\partial y},$$

$$\Omega_m = u^2\frac{\partial^2 C}{\partial x^2} + v^2\frac{\partial^2 C}{\partial y^2} + 2uv\frac{\partial^2 C}{\partial x\partial y} + \left(u\frac{\partial u}{\partial x} + v\frac{\partial u}{\partial y}\right)\frac{\partial C}{\partial x} + \left(u\frac{\partial v}{\partial x} + v\frac{\partial v}{\partial y}\right)\frac{\partial C}{\partial y}.$$

$$\left.\begin{array}{l} u = U_w(x) + U_s(x) = s_0 x + \Delta\dfrac{\partial u}{\partial y} - \Lambda\left(u\dfrac{\partial u}{\partial x} - s_0 u + v\dfrac{\partial u}{\partial y}\right), v = 0, \\[2mm] T = T_w, C = C_w \quad \text{at} \quad y = 0, \\[2mm] u \to 0, \ \dfrac{\partial u}{\partial y} \to 0, \ T \to T_\infty, \ C \to C_\infty \ \text{ as } \ y \to \infty. \end{array}\right\} \tag{6.12}$$

The similarity transformations given below are invoked [152] to obtain the dimensionless form of the mathematical model:

$$\eta = \sqrt{\frac{s_0}{\nu}}y, \ u = s_0 x f'(\eta), \ v = -\sqrt{s_0\nu}f(\eta), \ \phi = \frac{C - C_\infty}{C_w - C_\infty}, \ \theta = \frac{T - T_\infty}{T_w - T_\infty}.$$

(6.13)

Using the above transformations, the non-linear similarity equations are obtained as:

$$f''' + \beta(2ff'f'' - f^2 f''') - f'^2 + ff'' - M(f' - \beta ff'') + (\lambda_t\theta + \lambda_c\phi)\cos\Omega$$
$$- K_p f' = 0,$$

(6.14)

$$(1 + (4/3)R_d)\,\theta'' - P_r\Gamma_e(f^2\theta'' + ff'\theta') + P_r\left(N_b\theta'\phi' + N_t\theta'^2 + f\theta'\right) + \lambda_s\theta = 0,$$

(6.15)

$$\phi'' + \frac{N_t}{N_b}\theta'' + S_c f\phi' - S_c\Gamma_c(f^2\phi'' + ff'\phi') - S_c C_r\phi = 0,$$

(6.16)

with corresponding BCs are

$$\left.\begin{array}{l} f'(0) = 1 + Rf''(0) - \beta[f'^2(0) - f'(0)], \ f(0) = 0, \ \theta(0) = 1, \phi(0) = 1, \\ f'(\eta) \to 0, \quad \theta(\eta) \to 0, \quad \phi(\eta) \to 0 \quad \text{as} \quad \eta \to \infty. \end{array}\right\}$$

(6.17)

The dimensionless quantities used in Eqs. (6.14) − (6.17) are:

$$\left.\begin{array}{l} M = \dfrac{\sigma B_0^2}{\rho s_0}, \ \lambda_t = \dfrac{\beta_T(T_w - T_\infty)g}{s_0^2 x}, \ \lambda_c = \dfrac{\beta_C(C_w - C_\infty)g}{s_0^2 x}, \ \lambda_s = \dfrac{Q_0}{\rho C_p s_0}, \ R = \Delta\sqrt{\dfrac{s_0}{\nu}} \\[3mm] R_d = \dfrac{4\sigma^* T_\infty^3}{kk^*}, \quad \beta = \Lambda s_0, \quad \Gamma_e = \Lambda_h s_0, \quad \Gamma_c = \Lambda_m s_0, \quad N_t = \dfrac{\tau D_T(T_w - T_\infty)}{\nu T_\infty}, \\[3mm] N_b = \dfrac{\tau D_B(C_w - C_\infty)}{\nu}, \quad C_r = \dfrac{K_c}{s_0}, \quad P_r = \dfrac{\nu}{\alpha}, \quad S_c = \dfrac{\nu}{D_B}, \quad \tau = \dfrac{(\rho C_p)_p}{(\rho C_p)_f}. \end{array}\right\}$$

(6.18)

The important quantities of physical interest are:

$$C_f = \frac{\tau_w}{\rho U_w^2(x)}, \quad Nu_x = \frac{xq_w}{k(T_w - T_\infty)}, \quad Sh_x = \frac{xq_m}{D_B(C_w - C_\infty)},$$

(6.19)

where

$$\tau_w = \left[\mu \frac{\partial u}{\partial y} - \Lambda \left(v^2 \frac{\partial u}{\partial y} + 2uv \frac{\partial u}{\partial x} \right) \right]_{y=0}, \quad q_w = -k \left[\left(\frac{\partial T}{\partial y} \right) + q_r \right]_{y=0},$$

$$q_m = -D_B \left(\frac{\partial C}{\partial y} \right)_{y=0}, \tag{6.20}$$

and their non-dimensional form is

$$\mathrm{C}_f Re_x^{1/2} = f''(0), \quad Nu_x Re_x^{-1/2} \left[\frac{3}{3 + 4R_d} \right] = -\theta'(0),$$

$$\mathrm{Sh}_x Re_x^{-1/2} = -\phi'(0), \tag{6.21}$$

where the local Reynolds number is elucidated by $Re_x = \frac{U_w x}{\nu}$.

6.3   Solution Methodology

To obtain the numerical solutions of the system of non-dimensional ODEs $(6.14) - (6.16)$ with the boundary conditions (6.17), an iterative numerical technique known as the shooting technique [112] is invoked. The initial guesses are refined through the Newton method with respect to the tolerance $\varepsilon = 10^{-6}$. For numerical solutions, the domain $[0, \infty)$ has been replaced by $[0, \eta_{max}]$ for some suitable choice of η_{max}. For the ascending values of η_{max}, an asymptotic convergence of the numerical solutions has been witnessed. For code validation, bvp4c is the method against which the results are recomputed.

The MATLAB code validation has been done by reproducing the numerical results of $Nu_x Re_x^{-1/2}$ and $Sh_x Re_x^{-1/2}$ for the problems discussed by Khan and Pop [153], Makinde and Aziz [154], Wang [155] and Gorla and Sidawi [156] which have been presented in the Tables 6.1-6.2. The present results presented in Tables 6.1-6.2 are found in a very convincing agreement with the published results.

All the numerical outcomes, in this chapter, have been have acquired by using $\varepsilon = 10^{-6}$.

Table 6.1: Comparison of the present values of $-\theta'(0)$ and $-\phi'(0)$ with the already published values.

			$-\theta'(0)$			$-\phi'(0)$	
N_t	N_b	[153]	bvp4c	shooting	[153]	bvp4c	shooting
0.1	0.1	0.9524	0.95237159	0.95237164	2.1294	2.12935562	2.12935545
0.2		0.6932	0.69317319	0.69317327	2.2732	2.27395668	2.27395634
0.3		0.5201	0.52007925	0.52008070	2.5286	2.52862539	2.52854213
0.4		0.4026	0.40258122	0.40258427	2.7952	2.79515287	2.79504094
0.5		0.3211	0.32105496	0.32105915	3.0351	3.03512064	3.03497883
0.1	0.2	0.5056	0.50558106	0.50557898	2.3819	2.38186660	2.38184022
0.2		0.3654	0.36535806	0.36535800	2.5152	2.51521733	2.51517948
0.3		0.2731	0.27309597	0.27309721	2.6555	2.65545171	2.65540134
0.4		0.2110	0.21098391	0.21098601	2.7818	2.78176740	2.78170386
0.5		0.1681	0.16807698	0.16807969	2.8883	2.88832730	2.88825013
0.1	0.3	0.2522	0.25215593	0.25215504	2.4100	2.41001515	2.40999147
0.2		0.1816	0.18159768	0.18159787	2.5150	2.51499161	2.51496039
0.3		0.1355	0.13551430	0.13551515	2.6088	2.60881267	2.60877347
0.4		0.1046	0.10460907	0.10461035	2.6876	2.68760028	2.68755277
0.5		0.0833	0.08329883	0.08330041	2.7519	2.75186674	2.75181063
0.1	0.4	0.1194	0.11940588	0.11940554	2.3997	2.39964678	2.39962462
0.2		0.0859	0.08590208	0.08590226	2.4807	2.48073608	2.48070831
0.3		0.0641	0.06408156	0.06408207	2.5486	2.54860037	2.54856675
0.4		0.0495	0.04946498	0.04946570	2.6038	2.60383931	2.60379962
0.5		0.0394	0.03938919	0.03939005	2.6483	2.64825058	2.64820460
0.1	0.5	0.0543	0.05425343	0.05425332	2.3836	2.38356794	2.38354675
0.2		0.0390	0.03904044	0.03904057	2.4468	2.44680413	2.44677846
0.3		0.0291	0.02913593	0.02913621	2.4984	2.49836779	2.49833748
0.4		0.0225	0.02249955	0.02249993	2.5399	2.53986220	2.53982707
0.5		0.0179	0.01792228	0.01792271	2.5731	2.57309925	2.57305912

Table 6.2: Comparison of the values of $-\theta'(0)$ with the already published results.

Pr	Makinde and Aziz [154]	Wang [155]	Gorla and Sidawi [156]	Khan and Pop [153]	Present results
0.07	0.0656	0.0656	0.0656	0.0663	0.066828
0.20	0.1691	0.1691	0.1691	0.1691	0.169147
0.70	0.4539	0.4539	0.5349	0.4539	0.453916
2.00	0.9114	0.9114	0.9114	0.9113	0.911358
7.00	1.8954	1.8954	1.8905	1.8954	1.895403
20.0	3.3539	3.3539	3.3539	3.3539	3.353904
70.0	6.4622	6.4622	6.4622	6.4621	6.462200

Table 6.3: The quantitative analysis of $-\theta'(0)$ and $-\phi'(0)$ for different values of N_t and N_b by the method of slope linear regression through the data points [145].

N_t	$-\theta'(0)$	$-\phi'(0)$	N_b	$-\theta'(0)$	$-\phi'(0)$
0.1	0.952377	2.129394	0.1	0.952377	2.129394
0.2	0.693174	2.274022	0.2	0.505581	2.381871
0.3	0.520079	2.528638	0.3	0.252156	2.410019
0.4	0.402581	2.795170	0.4	0.119406	2.399650
0.5	0.321054	3.035143	0.5	0.054253	2.383571
Slp	-1.578308	2.264373	Slp	-2.245310	0.635443

6.4   Results and Discussion

Table 6.3 is presented for the quantitative analyses of $-\theta'(0)$ and $-\phi'(0)$ for different N_t when $N_b = 0.1$ and N_b when $N_t = 0.1$ with method of slope linear regression through the data points ([145]). It is observed that the estimated decline for N_t in $Nu_x Re_x^{-1/2}$ is -1.578308 and an upturn in $Sh_x Re_x^{-1/2}$ is 2.264373 whereas the rate of decrease in $Nu_x Re_x^{-1/2}$ and increase in $Sh_x Re_x^{-1/2}$ for N_b are estimated as -2.245310 and 0.635443 respectively. Tables 6.4-6.6 are presented to see the impacts of different physical parameters on the magnitude of $C_f Re_x^{1/2}$, $Nu_x Re_x^{-1/2}$ and $Sh_x Re_x^{-1/2}$. From Table 6.4, it is observed that the magnitude of $C_f Re_x^{1/2}$ is increased for $M, \beta, \Gamma_e, \Gamma_c$ and K_p whereas a decrement is noted for $\lambda_t, \lambda_c, \lambda_s$ and R. The rate of heat transfer is increased for P_r, R_d, λ_t and Γ_e while it is decreased for λ_s, R, N_b, N_t and K_p as depicted in Table 6.5. An increment in $Sh_x Re_x^{-1/2}$ is observed for the physical parameters $S_c, C_r, \lambda_c, \Gamma_c, N_b, N_t$ and λ_s. Moreover, it is examined from Table 6.6 that $Sh_x Re_x^{-1/2}$ for R, K_p and R_d is subsided. To inspect the influence of physical parameters on f' (velocity profile), θ (temperature profile) and ϕ (concentration profile), Figs. 6.2-6.21 have been portrayed. Figs. 6.2-6.4 are prepared to analyze the behavior of f', θ and ϕ for various values of β in the presence and absence of permeability of the medium. The influence of β on f' is highlighted in Fig. 6.2. This shows f' inside the boundary-layer is reduced for a rise in the parametric values of β. A reduction in f' is more prominent in the presence of porosity as compared to non-porous

Table 6.4: Numerical values of $-f''(0)$ for different values of $M, \beta, \lambda_t, \lambda_c, \Gamma_e, \Gamma_c,$ λ_s, R and K_p when $P_r = 6.2, R_d = 1.0, N_b = 0.5, N_t = 0.1, S_c = 1.2$ and $C_r = 1.0$ at $\eta_{max} = 6$.

M	β	λ_t	λ_c	Γ_e	Γ_c	λ_s	R	K_p	shooting	bvp4c
1.0	0.3	0.2	0.2	0.3	0.3	0.2	0.1	0.7	1.408981769359195	1.408981760799488
1.5									1.528827725890722	1.528827738193479
2.5									1.737719184629466	1.736401653993329
3.5									1.914104910166951	1.913344492473412
	0.1								1.346033449137126	1.346033446437884
	0.3								1.408981769359195	1.408981760799488
	0.5								1.468483663089692	1.468483650085422
		0.2							1.408981769359195	1.408981760799488
		0.4							1.371657977612344	1.371657969571944
		0.6							1.335159749100111	1.335159741579648
			0.2						1.408981769359195	1.408981760799488
			0.4						1.379963860007806	1.379963851990552
			0.6						1.351056501301065	1.351056493896277
				0.1					1.408343448007064	1.408343439486449
				0.3					1.408981769359195	1.408981760799488
				0.5					1.409656804591504	1.409656796058418
					0.1				1.408857819319769	1.408857810802922
					0.3				1.408981769359195	1.408981760799488
					0.5				1.409110093839360	1.409110085280229
						0.2			1.408981769359195	1.408981760799488
						0.4			1.408155334619385	1.408155326053278
						0.6			1.407217536507879	1.407217534831787
							0.1		1.408981769359195	1.408981760799488
							0.3		1.092996865753276	1.092996862302674
							0.5		0.891144801636828	0.891144799968380
								0.5	1.361588902073835	1.361588894504238
								0.7	1.408981769359195	1.408981760799488
								0.9	1.454457247654383	1.454457238080404

medium. Physically, the porous space is increased when the value of the porosity parameter is increased and consequently the more resistance in the flow path is occurred which reduces the fluid motion. The behavior of θ for distinct β is highlighted in Fig. 6.3. An increase in θ is examined against β and the increase in the presence of porosity is more significant as compared to the non-porous medium. In fact, heat is transfer due to the Darcian body force from the solid surface to the fluid layers. The increasing values of β leads to increase in ϕ as depicted in Fig. 6.4. The effects of M with and without porous medium on f', θ and ϕ are presented in Figs. 6.5-6.7. A reduction in f' while an upturn in θ and

Table 6.5: Numerical values of $-(1+\frac{4}{3}R_d)\theta'(0)$ for different values of $P_r, R_d, \lambda_t,$ $\Gamma_e, \lambda_s, R, N_b, N_t$ and K_p when $M = 1.0, \beta = 0.3, \lambda_c = 0.2, \Gamma_c = 0.3, S_c = 1.2$ and $C_r = 1.0$ at $\eta_{max} = 6$.

P_r	R_d	λ_t	Γ_e	λ_s	R	N_b	N_t	K_p	shooting	bvp4c
6.2	1.0	0.2	0.3	0.2	0.1	0.5	0.1	0.7	0.543731615939674	0.543731617978702
6.3									0.544253151771032	0.544253153876414
6.4									0.544647997561121	0.544647999717638
	0.5								0.396100058468638	0.396100051540705
	1.0								0.543731615939674	0.543731617978702
	1.5								0.658807577089189	0.658807581138090
		0.2							0.543731615939674	0.543731617978702
		0.4							0.559370381368134	0.559370382682745
		0.6							0.573701195808215	0.573701196124084
			0.1						0.538693035303599	0.538693040513521
			0.3						0.543731615939674	0.543731617978702
			0.5						0.548843121720950	0.548843118665118
				0.2					0.543731615939674	0.543731617978702
				0.4					0.461130562823355	0.461130562888754
				0.6					0.372250367085010	0.372250366259432
					0.1				0.543731615939674	0.543731617978702
					0.3				0.453397504228724	0.453397506469124
					0.5				0.388920024576455	0.388920025998827
						0.3			0.801512048237897	0.801512055527574
						0.5			0.543731615939674	0.543731617978702
						0.7			0.356396057773559	0.356396052935009
							0.1		0.543731615939674	0.543731617978702
							0.2		0.477231737262369	0.477231738260042
							0.3		0.423834904914378	0.418637720553488
								0.5	0.559591339816008	0.559591341955519
								0.7	0.543731615939674	0.543731617978702
								0.9	0.528557409500753	0.528557411159403

ϕ is witnessed for the ascending values of M.

The impact of R_d on θ is depicted in Fig. 6.8. A rise in the radiation parametric values leads to a rise in θ and the thermal boundary-layer thickness. Fig. 6.9 is prepared to examine the influence of Γ_e on θ. The up-going values of Γ_e escalate θ and the associated boundary-layer thickness near the surface but opposite trend is observed away from the sheet. The effect of λ_s on θ is presented in Fig. 6.10. An increase in θ is noted for against λ_s. Fig. 6.11 is presented to observe the variation in θ with respect to change in P_r. Decline in θ is significant when the fluid is Maxwell in comparison to Newtonian case.

Table 6.6: Numerical values of $-\phi'(0)$ for different values of $S_c, C_r, \lambda_c, \Gamma_c, N_t,$ N_b, R, λ_s, K_p and R_d when $M = 1.0, \beta = 0.3, \lambda_t = 0.2, \Gamma_e = 0.3$ and $P_r = 6.2$ at $\eta_{max} = 6$.

S_c	C_r	λ_c	Γ_c	N_t	N_b	R	λ_s	K_p	R_d	shooting	bvp4c
1.2	1.0	0.2	0.3	0.1	0.5	0.1	0.2	0.7	1.0	1.265021369739294	1.265021371939390
1.3										1.320605941498065	1.320605944856037
1.5										1.425577972819739	1.425577976621682
	1.0									1.265021369739294	1.265021371939390
	1.2									1.364844798673891	1.364844800985624
	1.4									1.457030320490569	1.457030323534983
		0.2								1.265021369739294	1.265021371939390
		0.4								1.266819447645340	1.266819450060388
		0.6								1.268599481625325	1.268599484586197
			0.1							1.262953121730714	1.262953120495422
			0.3							1.265021369739294	1.265021371939390
			0.5							1.267189818535676	1.267189826182688
				0.1						1.265021369739294	1.265021371939390
				0.2						1.291901594322014	1.291901596555589
				0.3						1.289963351310317	1.324304963207755
					0.3					1.242415515528244	1.242415516329919
					0.5					1.265021369739294	1.265021371939390
					0.7					1.269756723219835	1.269756725890805
						0.1				1.265021369739294	1.265021371939390
						0.3				1.243335538956715	1.243335540514373
						0.5				1.228079505128687	1.228079505532560
							0.2			1.265021369739294	1.265021371939390
							0.4			1.271145977705484	1.271145980344200
							0.6			1.277557622488675	1.277557623608687
								0.5		1.267752310595506	1.267752312633630
								0.7		1.265021369739294	1.265021371939390
								0.9		1.262448007404369	1.262448009842685
									1.0	1.265021369739294	1.265021371939390
									1.5	1.259360371637839	1.259360373923059

Figs. 6.12-6.13 are displayed to highlight the effect of S_c and C_r on ϕ when $\Gamma_c = 0$ (Fick's law) and $\Gamma_c = 0.5$ (CCHFM). The behavior of ϕ is decreasing for ascending values of both S_c and C_r. Fig. 6.14 is sketched to analyze the effect of β and K_p on $-f''(0)$. This figure shows that for the up-going values of β, $-f''(0)$ is increased whereas a decrement is noticed for K_p. The impact of velocity slip parameter R on $-f''(0)$ is presented in Fig. 6.15. The rise in $-f''(0)$ is witnessed for the escalating values of R. The variation in the rate of heat transfer rate against β, Γ_e and P_r is exhibited in Figs. 6.16-6.17. It is found that the rate of heat transfer is increased

for both ascending parametric values of Γ_e and P_r. Fig. 6.18-6.19 are dedicated to show the effect of N_t and N_b parameters on the heat transfer rate for two distinct values of K_p and Γ_e respectively. From Fig. 6.18, it is evident that $Nu_x Re_x^{-1/2}$ is reduced for the increment in N_b. It is also observed from the same figure that rate of heat transfer is subsided for the augmented values of N_t. Furthermore, it is witnessed that the heat transfer rate is increased for the augmentation in K_p. A decrement in the rate of heat transfer is seen against Γ_e. Figs. 6.20-6.21 are drawn to see the impact of S_c, Γ_c and C_r on the Sherwood number. An increasing trend for the concentration profile is seen for both the parameters S_c and C_r.
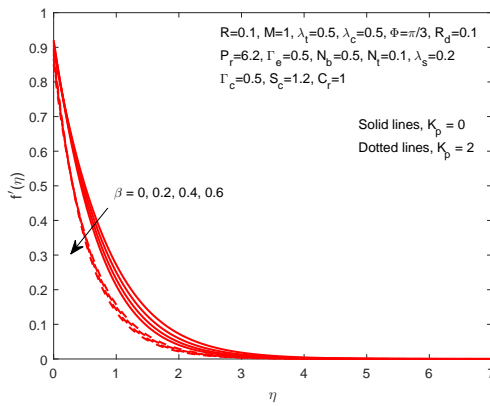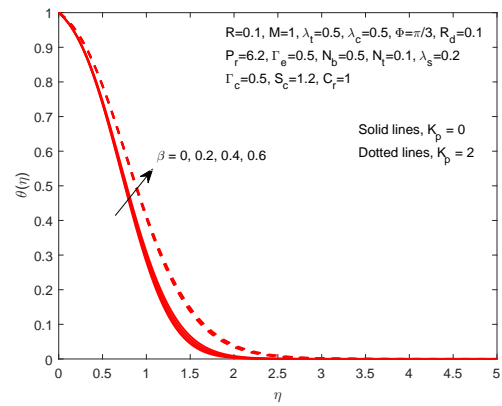

Fig. 6.2: Impact of β on f'

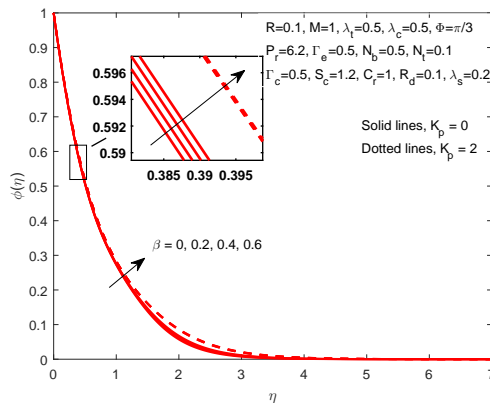Fig. 6.3: Impact of β on θ

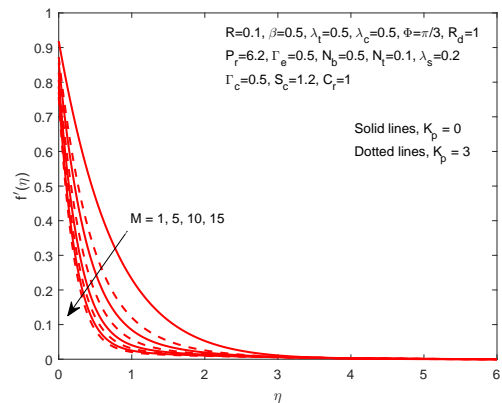Fig. 6.4: Impact of β on ϕ
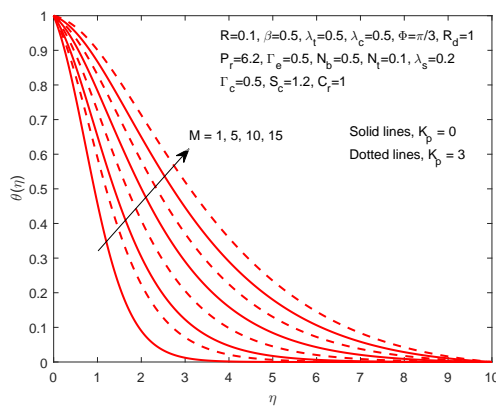

Fig. 6.5: Impact of M on f'
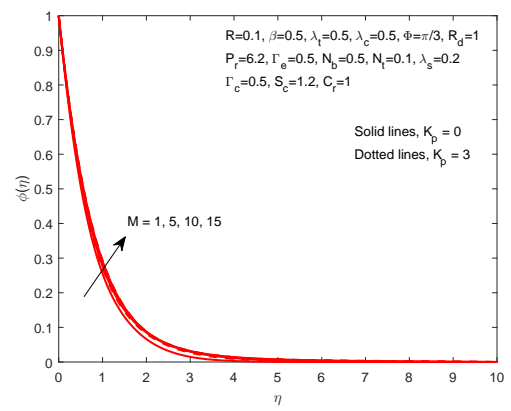
Fig. 6.6: Impact of M on θ

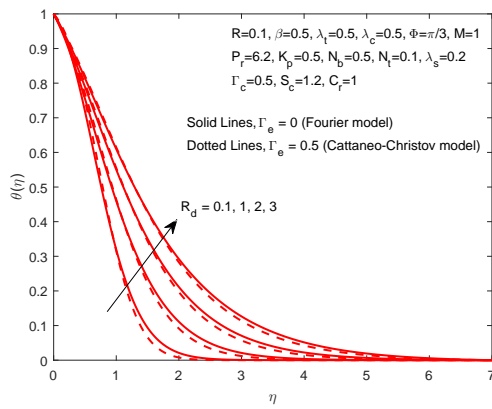Fig. 6.7: Impact of M on ϕ

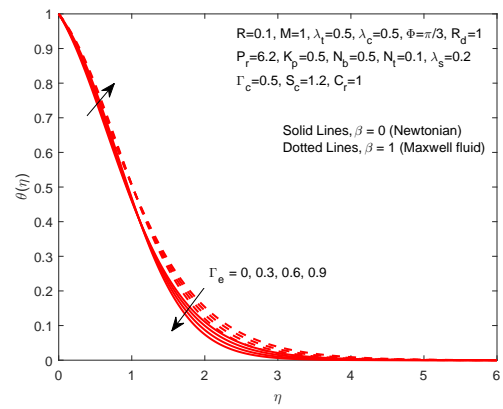Fig. 6.8: Impact of R_d on θ

Fig. 6.9: Impact of Γ_e on θ

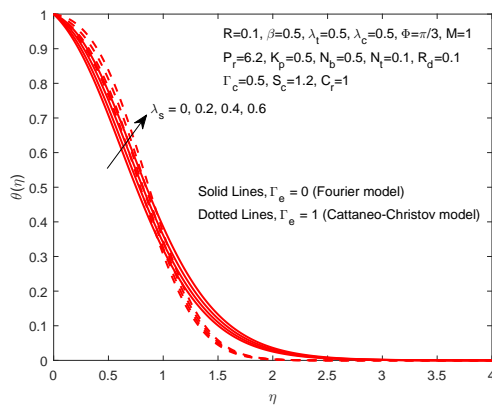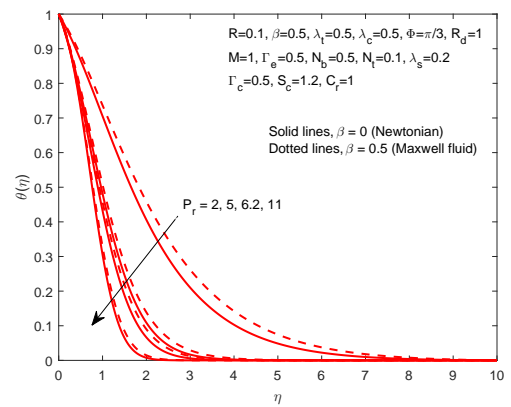Fig. 6.10: Impact of λ_t on θ
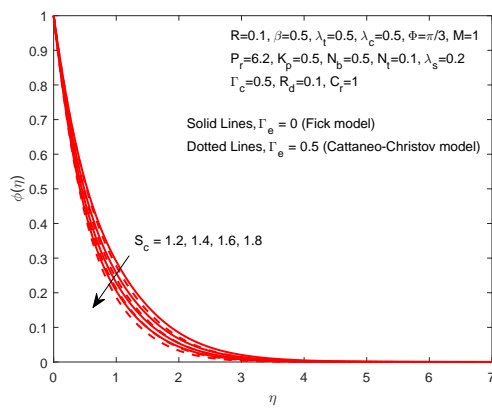

Fig. 6.11: Impact of P_r on θ

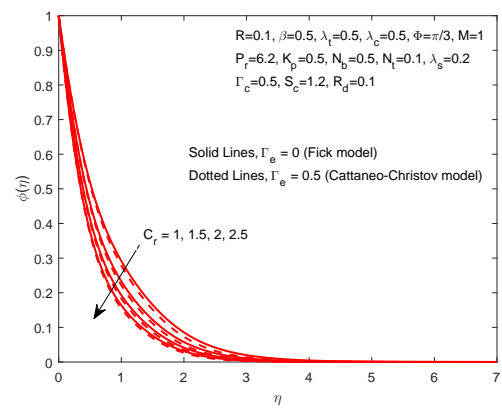Fig. 6.12: Impact of S_c on ϕ

Fig. 6.13: Impact of C_r on ϕ
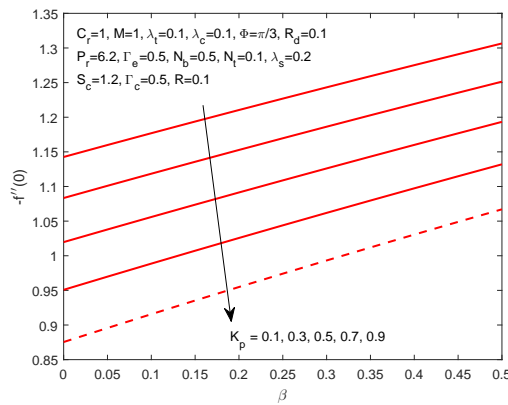
Fig. 6.14: Impact of β and K_p on $-f''(0)$
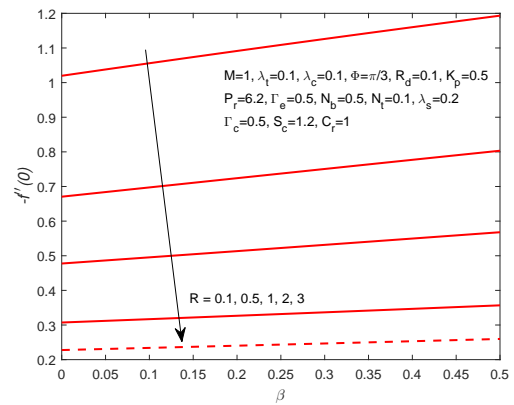
Fig. 6.15: Impact of β and R on $-f''(0)$
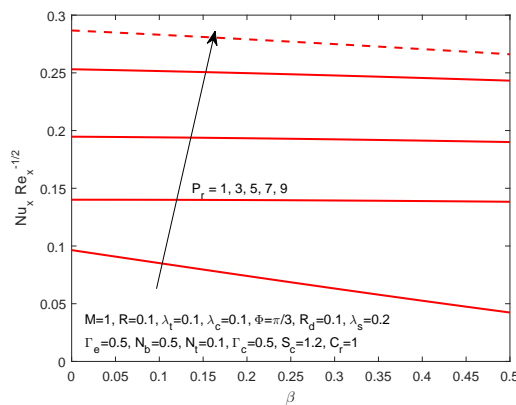
Fig. 6.16: Impact of β and P_r on $Nu_x Re_x^{-1/2}$
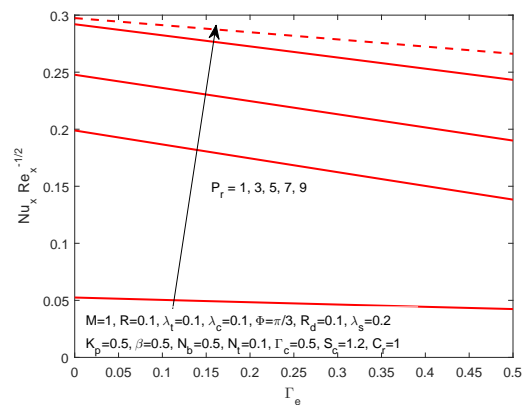
Fig. 6.17: Impact of Γ_e and P_r on $Nu_x Re_x^{-1/2}$
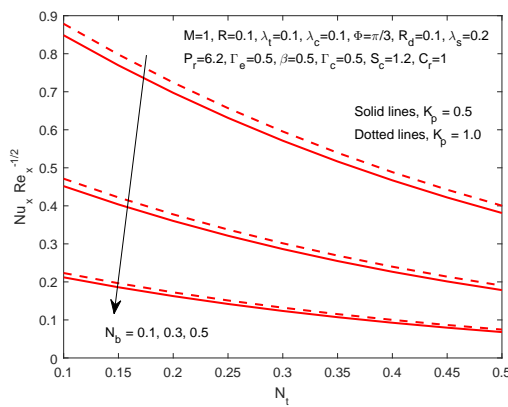
Fig. 6.18: Impact of N_t and K_p on $Nu_xRe_x^{-1/2}$
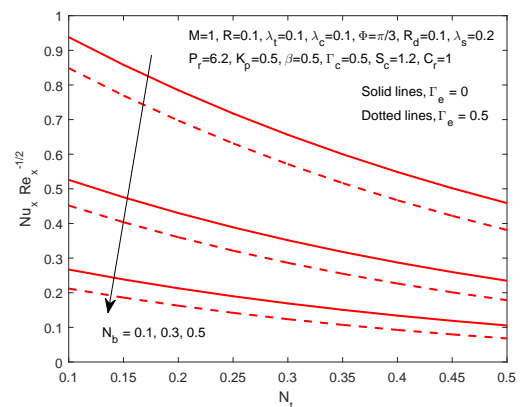
Fig. 6.19: Impact of N_t and Γ_e on $Nu_xRe_x^{-1/2}$
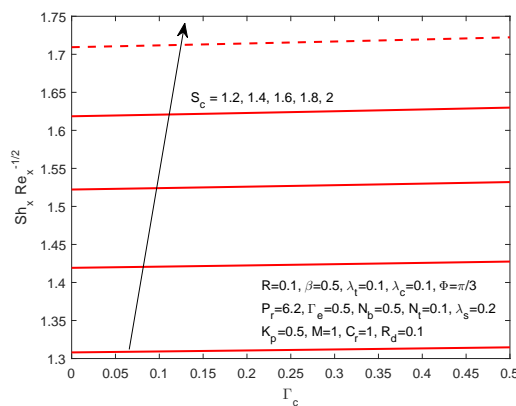
Fig. 6.20: Impact of Γ_c and S_c on $Sh_xRe_x^{-1/2}$
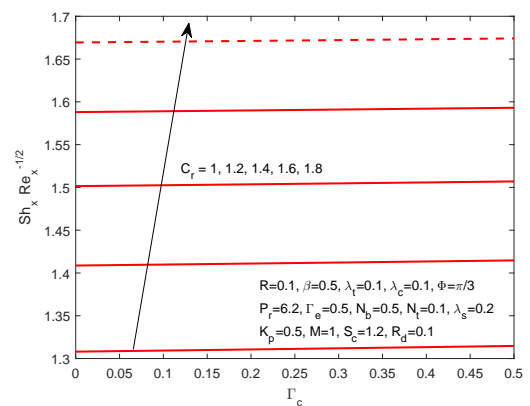
Fig. 6.21: Impact of Γ_c and C_r on $Sh_xRe_x^{-1/2}$

6.5 Final Remarks

This chapter tries to determine, systematically, the phenomenon of a slip flow of a UCM nanofluid, once generated by an inclined surface through a porous medium and magnetic field. The diffusion model for mass and heat transfer introduced by Cattaneo-Christov is incorporated in the modeling process. The relaxation framework visco-elastic system is formulated for UCM nanofluid to determine both heat and mass transfer by CCHFM. The effects of thermophoresis, Brownian motion and heat generation and chemical reaction are also considered. Suitable similarity

transformations, governing equations are stripped off, of their dimensionless existence. The converted system of equations is cracked numerically by the shooting technique. Using graphs and tables, the influence of physical parameters on the distributions of dimension free velocity, temperature and concentration are made conspicuous. The main findings of the analysis are as follow:

- The velocity is decreased for the augmented Maxwell parameter β while an increment in θ is witnessed.

- A decline in f' through a porous medium holds greater pronounce when brought in comparison to a non-porous medium.

- The temperature distribution for ascending magnetic parametric values is higher in the presence of porous medium than the temperature in the absence of non-porous medium.

- The magnitude of $-f''(0)$ is an increasing function of β but a fall down for an upturn in K_p and R is seen.

- The temperature is enhanced for R_d. Moreover, an increment in θ in case of CCHFM is less as compared with Fourier heat conduction model.

- The temperature is decreased for higher P_r and a decrement is more rapid in Newtonian fluid case than that of the Maxwell fluid.

- A rise in heat transfer rate for an augmentation in P_r is identified whereas the heat transfer rate is subsided for β and Γ_e.

- A decay in ϕ is witnessed by the ascending parametric values of S_c and C_r.

Chapter 7

MHD UCM Nanofluid Flow with Velocity Slip Effect and CCHFM

7.1 Introduction

This chapter explores the numerical solutions of UCM nanofluid flow in the presence of a magnetic field over an inclined stretching sheet. A special consideration has been given to the non-linear velocity slip, thermal radiation and heat generation effects. The modified Fourier and Fick's laws are incorporated in the modeling process. The mass transfer phenomenon is investigated under the Brownian motion, chemical reaction and thermophoresis effects. By making use of similarity transformations, the governing equations are converted into the non-dimensional form and then cracked numerically by the shooting technique. This chapter focuses, primarily, on the research of noticeable physical parameters and their impacts on the Nusselt number, skin-friction co-efficient, velocity, temperature and concentration profiles with the help of graphs and tables. The velocity close to the surface is reduced for the augmented slip parameter whereas away from the surface, an increment in the velocity profile is noticed. This study follows a definite format. Section 7.2 deals with the problem pertaining to configuration. Section 7.3 concerns itself with the information regarding the formulation of governing equations, the numerical approach and validation of the code. The resultant numerical and graphical conclusions stand elaborated in section 7.4. Section 7.5 is the sum

and product, annunciating the more significant findings of the entire research of the chapter.

7.2 Mathematical Formulation of the Problem

An electrically conducting, laminar, steady and incompressible UCM nanofluid flow towards an inclined surface has been considered. The surface makes an angle Ω with the vertical position. Thermal radiation effects have also been taken into account for modifying the energy equation. The coordinate axes are built up by taking the $x-$axis as flow direction and the direction perpendicular to it is $y-$ axis, as illustrated in Fig. 7.1. Furthermore, the thermophoresis and Brownian motion effects along with the chemical reaction have also been assumed. Moreover, non-linear velocity slip condition is also assimilated. The velocity of the stretching sheet has been taken as $u = U_w(x) = s_0 x$. The temperature at the surface and far away the surface are denoted as T_w and T_∞ respectively while C_w and C_∞ make the same sense for the concentration profile. The flow analysis has been carried out when the fluid passes through a magnetic field B_0, perpendicular to the flow. The induced magnetic field is to be ignored due to small Reynolds number [148, 157]. The viscous dissipation, Joule heating and body forces are neglected due to the above assumptions and the considered boundary-layer approximation. The constitutive equations of the UCM nanofluid model under the assumed circumstances are given as: [149, 150]

$$\frac{\partial v}{\partial y} + \frac{\partial u}{\partial x} = 0, \tag{7.1}$$

$$u\frac{\partial u}{\partial x} + v\frac{\partial u}{\partial y} = \nu\frac{\partial^2 u}{\partial y^2} - \Lambda\left(u^2\frac{\partial^2 u}{\partial x^2} + v^2\frac{\partial^2 u}{\partial y^2} + 2uv\frac{\partial^2 u}{\partial x\partial y}\right) - \frac{\sigma B_0^2}{\rho_f}\left(u + \Lambda v\frac{\partial u}{\partial y}\right)$$
$$+ \ [\beta_T \ (T - T_\infty) + \beta_C \ (C - C_\infty)] \ g\cos\Omega, \tag{7.2}$$

$$u\frac{\partial T}{\partial x} + v\frac{\partial T}{\partial y} = -\frac{1}{(\rho C_p)_f}\nabla \cdot \mathbf{q} + \frac{Q_0 (T - T_\infty)}{(\rho C_p)_f} - \frac{1}{(\rho C_p)_f}\frac{\partial q_r}{\partial y}$$
$$+ \ \tau\left(D_B\frac{\partial T}{\partial y}\frac{\partial C}{\partial y} + \frac{D_T}{T_\infty}\left(\frac{\partial T}{\partial y}\right)^2\right), \tag{7.3}$$

$$u\frac{\partial C}{\partial x} + v\frac{\partial C}{\partial y} = -\frac{1}{(\rho C_p)_f}\nabla \cdot \mathbf{J} + D_B\frac{\partial^2 C}{\partial y^2} + \frac{D_T}{T_\infty}\frac{\partial^2 T}{\partial y^2} - K_c (C - C_\infty). \tag{7.4}$$
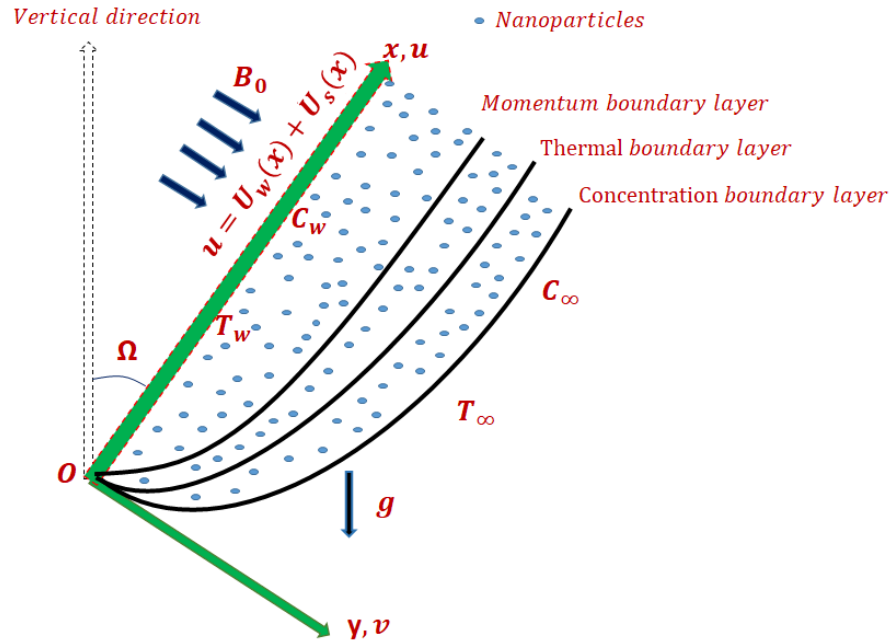
Fig. 7.1: Schematic of physical model

To investigate the thermal and concentration diffusion, the modified versions of the Fourier and Fick's laws have been utilized in the present study. In view of CCHFM, the Fourier and Fick's laws in the generalized form are stated as:

$$\mathbf{q} + \Lambda_h \left(\frac{\partial \mathbf{q}}{\partial t} + (\nabla.\mathbf{v}) \mathbf{q} + \mathbf{v}.\nabla \mathbf{q} - \mathbf{q}.\nabla \mathbf{v} \right) = -k\nabla T, \tag{7.5}$$

$$\mathbf{J} + \Lambda_m \left(\frac{\partial \mathbf{J}}{\partial t} + (\nabla.\mathbf{v}) \mathbf{J} + \mathbf{v}.\nabla \mathbf{J} - \mathbf{J}.\nabla \mathbf{v} \right) = -D_B \nabla C, \tag{7.6}$$

where $\mathbf{v}$ is the velocity field, $\mathbf{q}$ and $\mathbf{J}$ are used for the normal heat and mass fluxes respectively. The thermal conductivity is supposed to be linear in temperature. The Taylor series is used to linearize the term T^4 about T_∞. The model radiative heat flux q_r by Rosseland [121] with the help of the above linearization, is given as:

$$\frac{\partial q_r}{\partial y} = -\frac{16T_\infty^3 \sigma^*}{3k^*} \frac{\partial^2 T}{\partial y^2}. \tag{7.7}$$

The incompressibility $\nabla.\mathbf{v} = 0$ and steady flow conditions $\frac{\partial \mathbf{q}}{\partial t} = 0$ and $\frac{\partial \mathbf{J}}{\partial t} = 0$, simplify Eqs. $(7.3) - (7.4)$ to yield the following form:

$$u\frac{\partial T}{\partial x} + v\frac{\partial T}{\partial y}$$

$$+ \Lambda_h \left[u^2\frac{\partial^2 T}{\partial x^2} + v^2\frac{\partial^2 T}{\partial y^2} + 2uv\frac{\partial^2 T}{\partial x\partial y} + \left(u\frac{\partial u}{\partial x} + v\frac{\partial u}{\partial y}\right)\frac{\partial T}{\partial x} + \left(u\frac{\partial v}{\partial x} + v\frac{\partial v}{\partial y}\right)\frac{\partial T}{\partial y}\right]$$

$$= \left(\alpha + \frac{16T_\infty^3\sigma^*}{3k^*(\rho C_p)_f}\right)\frac{\partial^2 T}{\partial y^2} + \tau\left[D_B\frac{\partial T}{\partial y}\frac{\partial C}{\partial y} + \frac{D_T}{T_\infty}\left(\frac{\partial T}{\partial y}\right)^2\right] + \frac{Q_0\,(T - T_\infty)}{(\rho C_p)_f},$$

$$(7.8)$$

$$u\frac{\partial C}{\partial x} + v\frac{\partial C}{\partial y}$$

$$+ \Lambda_m \left[u^2\frac{\partial^2 C}{\partial x^2} + v^2\frac{\partial^2 C}{\partial y^2} + 2uv\frac{\partial^2 C}{\partial x\partial y} + \left(u\frac{\partial u}{\partial x} + v\frac{\partial u}{\partial y}\right)\frac{\partial C}{\partial x} + \left(u\frac{\partial v}{\partial x} + v\frac{\partial v}{\partial y}\right)\frac{\partial C}{\partial y}\right]$$

$$= D_B\frac{\partial^2 C}{\partial y^2} + \frac{D_T}{T_\infty}\frac{\partial^2 T}{\partial y^2} - K_c\,(C - C_\infty). \tag{7.9}$$

The associated conditions at the boundary surface together with the velocity slip effects [151, 158], are:

$$\left.\begin{aligned}
u &= U_w(x) + U_s(x) = s_0 x + \Delta\frac{\partial u}{\partial y} - \Lambda\left(u\frac{\partial u}{\partial x} - s_0 u + v\frac{\partial u}{\partial y}\right), \\
v &= 0, \quad T = T_w, \quad C = C_w, \quad \text{at} \quad y = 0, \\
u &\to 0, \quad \frac{\partial u}{\partial y} \to 0, \quad T \to T_\infty, \quad C \to C_\infty \quad \text{as} \quad y \to \infty.
\end{aligned}\right\} \tag{7.10}$$

To convert the mathematical model to the non-dimensional form, the following local similarity transformations are invoked [152]:

$$\eta = \sqrt{\frac{s_0}{\nu}}y, \ \psi = \sqrt{s_0\nu}xf\,(\eta), \ \phi = \frac{C - C_\infty}{C_w - C_\infty}, \ \theta = \frac{T - T_\infty}{T_w - T_\infty}, \tag{7.11}$$

where the stream function is demarcated as:

$$u = \frac{\partial\psi}{\partial y}, \ v = -\frac{\partial\psi}{\partial x}. \tag{7.12}$$

Employing the above transformations to Eqs. (7.2), (7.8) and (7.9), we get

$$f''' + \beta(2ff'f'' - f^2f''') - f'^2 - Mf' + (1 + M\beta)ff'' + (\lambda_t\theta + \lambda_c\phi) = 0, \tag{7.13}$$

$$(1 + (4/3)R_d)\,\theta'' - P_r\Gamma_e(f^2\theta'' + ff'\theta') + P_r\left(N_b\theta'\phi' + N_t\theta'^2 + f\theta'\right) + \lambda_s\theta = 0,$$

(7.14)

$$\phi'' + \frac{N_t}{N_b}\theta'' + S_cf\phi' - S_c\Gamma_c(f^2\phi'' + ff'\phi') - S_cC_r\phi = 0.$$

(7.15)

The corresponding BCs subject to (7.11), get the form:

$$\left.\begin{array}{l} f'(0) = 1 + Rf''(0) - \beta[f'^2(0) - f'(0)],\ f(0) = 0,\ \theta(0) = 1, \phi(0) = 1, \\[2mm] f'(\eta) \to 0, \quad \theta(\eta) \to 0, \quad \phi(\eta) \to 0 \quad \text{as} \quad \eta \to \infty. \end{array}\right\}$$

(7.16)

The dimensionless quantities used in Eqs. $(7.13) - (7.16)$ are

$$\left.\begin{array}{l} M = \dfrac{\sigma B_0^2}{\rho s_0}, \quad \lambda_t = \dfrac{\beta_T(T_w - T_\infty)g}{s_0^2 x}, \quad \lambda_c = \dfrac{\beta_C(C_w - C_\infty)g}{s_0^2 x}, \quad P_r = \dfrac{\nu}{\alpha}, \\[3mm] R_d = \dfrac{4\sigma^* T_\infty^3}{kk^*}, \quad \tau = \dfrac{(\rho C_p)_p}{(\rho C_p)_f}, \quad R = \Delta\sqrt{\dfrac{s_0}{\nu}}, \quad \lambda_s = \dfrac{Q_0}{\rho C_p s_0}, \quad \Gamma_c = \Lambda_m s_0, \\[3mm] N_b = \dfrac{\tau D_B(C_w - C_\infty)}{\nu}, \quad C_r = \dfrac{K_c}{s_0}, \quad S_c = \dfrac{\nu}{D_B}, \quad \Gamma_e = \Lambda_h s_0, \\[3mm] N_t = \dfrac{\tau D_T(T_w - T_\infty)}{\nu T_\infty}, \quad \beta = \Lambda s_0. \end{array}\right\}$$

(7.17)

The dimensional forms of important quantities of physical interests are

$$C_f = \dfrac{\tau_w}{\rho U_w^2(x)}, \quad Nu_x = \dfrac{xq_w}{k(T_w - T_\infty)}, \quad Sh_x = \dfrac{xq_m}{D_B(C_w - C_\infty)}. \ \Big\}$$

(7.18)

Here q_w and q_m are formulated as fellows:

$$\left.\begin{array}{l} \tau_w = \left[\mu\dfrac{\partial u}{\partial y} - \Lambda\left(v^2\dfrac{\partial u}{\partial y} + 2uv\dfrac{\partial u}{\partial x}\right)\right]_{y=0}, \quad q_w = -k\left[\left(\dfrac{\partial T}{\partial y}\right) + q_r\right]_{y=0}, \\[4mm] q_m = -D_B\left(\dfrac{\partial C}{\partial y}\right)_{y=0}. \end{array}\right\}$$

(7.19)

Similarity variables are used to acquire a dimension free form of above relations as:

$$\left.\begin{array}{l} C_f Re_x^{1/2} = f''(0), \quad Nu_x Re_x^{-1/2}\left[\dfrac{3}{3 + 4R_d}\right] = -\theta'(0), \\[4mm] Sh_x Re_x^{-1/2} = -\phi'(0), \end{array}\right\}$$

(7.20)

where the local Reynolds number is elucidated by $Re_x = \frac{U_w x}{\nu}$.

7.3   Solution Methodology

The system of non-dimensional ODEs $(7.13) - (7.15)$ with BCs (7.16) has been cracked iteratively by an efficient numerical technique named as the shooting method [112]. The refinement of the initial guesses s_1, s_2 and s_3 is carried out through the Newton method subject to the tolerance of $\varepsilon = 10^{-6}$. For numerical solution, the domain $[0, \infty)$ has been replaced by $[0, \eta_{max}]$ for some suitable choice of η_{max}. An asymptotic convergence of the numerical solutions has been observed by increasing the value of η_{max}. The variables f, θ and ϕ have been renamed as y_1, y_4 and y_6 respectively for converting the problem into the following IVP

$$
\left.
\begin{aligned}
y_1' &= y_2, \\
y_2' &= y_3, \\
y_3' &= \frac{1}{1 - \beta y_1^2} \left[y_2^2 + M y_2 - (1 + M\beta) y_1 y_3 - 2\beta y_1 y_2 y_3 - (\lambda_t\, y_4 + \lambda_c\, y_6) \cos \Omega \right], \\
y_4' &= y_5, \\
y_5' &= \frac{3 P_r}{3 + 4 R_d - 3 P_r \Gamma_e\, y_1^2} \left[\Gamma_e y_1 y_2 y_5 - y_1 y_5 - N_b\, y_7 y_5 - N_t\, y_5^2 - (1/P_r)\lambda_s y_4 \right], \\
y_6' &= y_7, \\
y_7' &= \frac{-1}{1 - S_c \Gamma_c\, y_1^2} \left[S_c y_1 y_7 - S_c \Gamma_c\, y_1 y_2 y_7 - S_c\, C_r\, y_6 + \frac{N_t}{N_b} y_5' \right],
\end{aligned}
\right\}
\tag{7.21}
$$

with

$$
\left.
\begin{aligned}
&y_1\,(0) = 0, \quad y_2\,(0) = s_1, \quad y_3\,(0) = (s_1 - \beta(s_1 - s_1^2) - 1)/R, \quad y_4\,(0) = 1, \\
&y_5\,(0) = s_2, \quad y_6\,(0) = 1, \quad y_7\,(0) = s_3.
\end{aligned}
\right\}
\tag{7.22}
$$

The halting standard for this iterative process is

$$
\max \left\{ |y_2\,(\eta_{max}) - 0|, |y_5\,(\eta_{max}) - 0|, |y_6\,(\eta_{max}) - 0| \right\} < \varepsilon.
$$

Table 7.1: Data comparing the numerical results of $-\theta'(0)$ and $-\phi'(0)$ with the already published values when $N_b = 0.1, P_r = 10, S_c = 10, \lambda_t = \lambda_c = \lambda_s = \beta = \Gamma_e = \Gamma_c = M = R_d = C_r = 0$ and $R = 0$

N_t	Khan and Pop [153]		Achariya *et al.* [159]		Hsiao *et al.* [160]		Present results	
	$-\theta'(0)$	$-\phi'(0)$	$-\theta'(0)$	$-\phi'(0)$	$-\theta'(0)$	$-\phi'(0)$	$-\theta'(0)$	$-\phi'(0)$
0.1	0.9524	2.1294	0.9524	2.1294	0.952432	2.129474	0.952377	2.129394
0.2	0.6932	2.2732	0.6932	2.2740	0.693211	2.273201	0.693174	2.274022
0.3	0.5201	2.5286	0.5201	2.5287	0.520147	2.528633	0.520079	2.528638
0.4	0.4026	2.7952	0.4026	2.7952	0.402631	2.795216	0.402581	2.795170
0.5	0.3211	3.0351	0.3211	3.0352	0.321149	3.035122	0.321054	3.035141

Table 7.2: Data comparing the numerical results of $-\theta'(0)$ and $-\phi'(0)$ with the already published results when $S_c = 10, P_r = 10, \lambda_t = \lambda_c = \lambda_s = \beta = \Gamma_e = \Gamma_c = M = R_d = C_r = 0$ and $R = 0$.

N_t	N_b	Khan and Pop [153]		Makinde and Aziz [154]		Present results	
		$-\theta'(0)$	$-\phi'(0)$	$-\theta'(0)$	$-\phi'(0)$	$-\theta'(0)$	$-\phi'(0)$
0.1	0.1	0.9524	2.1294	0.9524	2.1294	0.952377	2.129394
0.2	0.1	0.6932	2.2740	0.6932	2.2740	0.693174	2.274022
0.3	0.1	0.5201	2.5286	0.5201	2.5286	0.520079	2.528638
0.4	0.1	0.4026	2.7952	0.4026	2.7952	0.402581	2.795170
0.5	0.1	0.3211	3.0351	0.3211	3.0351	0.321054	3.035143
0.1	0.2	0.5056	2.3819	0.5056	2.3819	0.505581	2.381871
0.1	0.3	0.2522	2.4100	0.2522	2.4100	0.252156	2.410019
0.1	0.4	0.1194	2.3997	0.1194	2.3997	0.119406	2.399650
0.1	0.5	0.0543	2.3836	0.0543	2.3836	0.054253	2.383571

To validate the MATLAB code, the numerical values of $Nu_x Re_x^{-1/2}$ and $Sh_x Re_x^{-1/2}$ for the problems discussed by Khan and Pop [153], Achariya *et al.* [159], Hsiao [160], Makinde and Aziz [154], Wang [155] and Gorla and Sidawi [156] have been reproduced in Tables 7.1-7.3. The present results presented in Tables 7.1-7.3 are found in a very convincing agreement with the published results.

7.4 Results and Discussion

The specific ranges of the parameters involved in the system of governing equations namely the Maxwell parameter $(0 \leq \beta \leq 0.5)$, magnetic parameter $(0 \leq M \leq 0.5)$, thermal buoyancy parameter $(0 \leq \lambda_t \leq 0.5)$, concentration

Table 7.3: Data comparing the numerical results of $-\theta'(0)$ with the already published results when $\lambda_t = \lambda_c = \lambda_s = \beta = \Gamma_e = \Gamma_c = M = R_d = C_r = R = N_t = 0, S_c = 10$ and $N_b \to 0$.

P_r	Makinde and Aziz [154]	Wang [155]	Gorla and Sidawi [156]	Khan and Pop [153]	Present results
0.07	0.0656	0.0656	0.0656	0.0663	0.066828
0.20	0.1691	0.1691	0.1691	0.1691	0.169147
0.70	0.4539	0.4539	0.5349	0.4539	0.453916
2.00	0.9114	0.9114	0.9114	0.9113	0.911358
7.00	1.8954	1.8954	1.8905	1.8954	1.895403
20.0	3.3539	3.3539	3.3539	3.3539	3.353904
70.0	6.4622	6.4622	6.4622	6.4621	6.462200

Table 7.4: The quantitative analysis of $-\theta'(0)$ and $-\phi'(0)$ for different values of N_t when $N_b = 0.1$ and N_b when $N_t = 0.1$ by the method of slope linear regression through the data points [145].

N_t	$-\theta'(0)$	$-\phi'(0)$	N_b	$-\theta'(0)$	$-\phi'(0)$
0.1	0.952377	2.129394	0.1	0.952377	2.129394
0.2	0.693174	2.274022	0.2	0.505581	2.381871
0.3	0.520079	2.528638	0.3	0.252156	2.410019
0.4	0.402581	2.795170	0.4	0.119406	2.399650
0.5	0.321054	3.035143	0.5	0.054253	2.383571
Slp	-1.578308	2.264373	Slp	-2.245310	0.635443

buoyancy parameter $(0 \leq \lambda_c \leq 0.5)$, inclined stretching sheet angle $(0 \leq \Omega \leq 0.5)$, radiation parameter $(0 \leq R_d \leq 0.5)$, Prandtl number $(0 \leq P_r \leq 0.5)$, thermal relaxation parameter $(0 \leq \Gamma_e \leq 0.5)$, Brownian motion parameter $(0 \leq N_b \leq 0.5)$, thermophoresis parameter $(0 \leq N_t \leq 0.5)$, internal heat source parameter $(0 \leq \lambda_s \leq 0.5)$, Schmidt number $(0 \leq S_c \leq 0.5)$, concentration relaxation parameter $(0 \leq \Gamma_c \leq 0.5)$ and chemical reaction parameter $(0 \leq C_r \leq 0.5)$ are demarcated in order to solve the governing system (see detail in Ref. [146]). Table 7.4 is presented for the quantitative analyses of $-\theta'(0)$ and $-\phi'(0)$ for different N_t and N_b with method of slope linear regression through the data points (for details see [145]). A decrement in $Nu_x Re_x^{-1/2}$ and a rise in $Sh_x Re_x^{-1/2}$ for N_t are estimated as -1.578308 and 2.264373 respectively whereas the rate of decrease in $Nu_x Re_x^{-1/2}$ and increase in $Sh_x Re_x^{-1/2}$ for N_b are -2.245310 and 0.635443 respectively. This can also be observed through graphical results.

Table 7.5: The numerical values of $-f''(0)$ for different values of $M, \beta, \lambda_t, \lambda_c,$ $\Gamma_e, \Gamma_c, \lambda_s$ and R when $N_b = 0.5, N_t = 0.1, R_d = 0.5, C_r = 1.0, S_c = 1.2$ and $P_r = 6.2$.

M	β	λ_t	λ_c	Γ_e	Γ_c	λ_s	R	$-f''(0)$
0.5	0.3	0.1	0.1	0.5	0.5	0.2	0.1	1.111271
1.5								1.408484
2.5								1.639761
3.5								1.832086
	0.1							1.036174
	0.3							1.111271
	0.5							1.168169
		0.1						1.111271
		0.2						1.092835
		0.3						1.074613
			0.1					1.111271
			0.2					1.094462
			0.3					1.077733
				0.1				1.109795
				0.3				1.110535
				0.5				1.111271
					0.1			1.111012
					0.3			1.111139
					0.5			1.111271
						0.1		1.111403
						0.2		1.111271
						0.3		1.111134
							0.1	1.111271
							0.5	0.744287
							0.9	0.560814

To analyze the impact of different physical parameters involved in the dimensionless mathematical model (7.13)-(7.16) on the temperature, concentration and velocity profiles, Figs. 7.2-7.23 have been presented and analyzed. Figs. 7.2-7.7 are furnished to look into the impact of the Maxwell parameter β, magnetic field parameter M, concentration buoyancy parameter λ_c, thermal buoyancy parameter λ_t, velocity slip parameter R and inclined sheet angle Ω on the non-dimensional velocity f'. The impact of β on f' is disclosed in Fig. 7.2. A reduction in f' is witnessed for a rise in β. The fluid relaxation parameter known as visco-elastic parameter, plays a significant role in case of the visco-elastic

Table 7.6: The numerical values of $-(1+\frac{4}{3}R_d)\theta'(0)$ for different values of $P_r, R_d, \lambda_t, \Gamma_e,\ \lambda_s, R, N_b, N_t$ and M when $\beta = 0.3, \lambda_t = 0.1, \Gamma_c = 0.5, C_r = 1.0, S_c = 1.2$ and $P_r = 6.2$.

P_r	R_d	λ_t	Γ_e	λ_s	R	N_b	N_t	M	$-(1+\frac{4}{3}R_d)\theta'(0)$
6.2	0.5	0.1	0.5	0.2	0.1	0.5	0.1	0.5	0.564694
6.3									0.561706
6.4									0.558624
	0.5								0.564694
	1.0								0.752334
	1.5								1.126298
		0.1							0.564694
		0.2							0.569563
		0.3							0.574285
			0.1						0.562767
			0.3						0.563831
			0.5						0.564694
				0.1					0.599319
				0.2					0.564694
				0.3					0.529528
					0.1				0.564694
					0.5				0.441572
					0.9				0.366316
						0.3			0.953515
						0.5			0.564694
						0.7			0.307091
							0.1		0.564694
							0.2		0.467093
							0.3		0.384389
								1.5	0.472342
								2.5	0.400706
								3.5	0.342872

materials. The smaller values of β show the fluid behavior as the Newtonian and viscous while the larger values address the characteristics of the fluid as the non-Newtonian. Thus for the ascending values of β, the velocity as well as the velocity boundary-layer thickness reduces.

The impact of M on f' is depicted in Fig. 7.3. A rise in M leads to a fall in f'. Physically, the magnetic field exerts a damping effect on the flow by creating an opposing force known as the Lorentz force. This force resists the motion and as consequence, a reduction in f' takes place. Figs. 7.4 and 7.5 are prepared to

Table 7.7: The numerical values of $-\phi'(0)$ for different values of $S_c, C_r, \lambda_c, \Gamma_c, N_b, N_t, R, \lambda_s, M$ and R_d when $\beta = 0.3, \lambda_t = 0.1, \Gamma_e = 0.5$ and $P_r = 6.2$.

S_c	C_r	λ_c	Γ_c	N_t	N_b	R	λ_s	M	$-\phi'(0)$
1.2	1.0	0.1	0.5	0.1	0.5	0.1	0.2	0.5	1.301828
1.3									1.359947
1.5									1.469408
	1.0								1.301828
	1.2								1.401802
	1.4								1.494247
		0.1							1.301828
		0.2							1.303051
		0.3							1.304262
			0.1						1.296021
			0.3						1.298835
			0.5						1.301828
				0.1					1.301828
				0.2					1.347080
				0.3					1.401479
					0.3				1.263584
					0.5				1.301828
					0.7				1.307904
						0.1			1.301828
						0.5			1.266876
						0.9			1.246297
							0.1		1.298597
							0.2		1.301828
							0.3		1.305100
								1.5	1.280714
								2.5	1.266277
								3.5	1.255160

check the effect of concentration and thermal buoyancy parameters on f'. The up-going values of the concentration and thermal buoyancy parameters escalate f'. The surface slip effects on f' are presented in Fig. 7.6. The higher values of R reduce f' near the wall but far away the wall, an opposite trend is noticed. Fig. 7.7 is sketched to observe the variation in f' for various values of the inclined stretching sheet angle. An increasing trend is noted for the ascending values of the inclined sheet angle.

Figs. 7.8-7.13 are drawn to highlight the effect of M, Γ_e, N_b, P_r, R_d and N_t on

θ. Fig. 7.8 shows that θ is increased with an increment in M. The behavior of θ for various values of Γ_e is displayed in Fig. 7.9. It is found that an increment in Γ_e near the surface elevates θ and the thermal boundary-layer thickness while an opposite behavior of θ is noted far away the surface. The model is reduced to the Fourier's law when Γ_e diminishes (i.e., $\Gamma_e = 0$). The impact of N_t and N_b on θ is exhibited in Figs. 7.10 and 7.11. Fig. 7.10 is entirely devoted to the evaluation of N_t on θ. Once the thermophoretic effect is raised, the exodus of the nanoparticles from the hot to the colder ambient fluid occurs, that's why, an increment in the temperature is witnessed which augments the growth of the thermal boundary-layer thickness. A similar trend is seen in θ for N_b as displayed in Fig. 7.11. The effect of P_r is presented in Fig. 7.12. For increasing P_r, θ increases as observed. It is because of the fact that the greater values of P_r lead to a low thermal diffusion process in comparison with the viscous diffusion. So, the heat transfer coefficient is decreased in case of higher values of P_r and hence the thermal boundary-layer thickness diminishes. Fig. 7.13 is presented to observe the effect of R_d on θ. The ascending values of R_d enhance θ as observed. Physically, more heat energy is transmitted in the flow for an increment in R_d. This coincides with the general behavior of the thermal radiation parameter.

Figs. 7.14-7.18 are plotted in order to highlight the effects of C_r, Γ_c, N_b, S_c and N_t on ϕ. The impact of C_r is disclosed in Fig. 7.14. The growing values of C_r reduce ϕ as depicted in Fig. 7.14. An increment in Γ_c shows a decrement in the concentration field as seen in Fig. 7.15. The variation in the concentration distribution against the values of N_b is sketched in Fig. 7.16. A rise in N_b reduces the concentration distribution. Physically, the random motion and collision of the macroscopic particles is increased with an enhancement in N_b which depreciates the concentration of the fluid. An opposite effect of N_t on the concentration is presented in Fig. 7.17. The influence of S_c on the concentration profile is presented in Fig. 7.18. A depreciating trend in the concentration is witnessed for the increasing values of S_c. Physically, the increasing values of S_c reduce the molecular diffusivity and as a result ϕ and the aligned thickness of concentration

boundary-layer suffer a reduction.

Fig. 7.19 is portrayed to inspect the influence of R and β on $-f''(0)$. It is prominent from the figure that $-f''(0)$ is increased for the ascending values of β but the ascending values of R reduces it significantly. To investigate the influence of R and λ_s on $Nu_x Re_x^{-1/2}$, Fig. 7.20 is prepared. A slip parameter causes a decrement in $Nu_x Re_x^{-1/2}$ and a significant decrement in $Nu_x Re_x^{-1/2}$ for the heat source/sink parameter is also noticed. The impact of N_b against different values of P_r on $Nu_x Re_x^{-1/2}$ is disclosed in Fig. 7.21. The increasing values of N_b reduce $Nu_x Re_x^{-1/2}$ while a boost in P_r enhances $Nu_x Re_x^{-1/2}$. This is due to the fact that the boundary-layer viscosity is progressively increased for an upturn in P_r. The effects of β and Γ_e on $Nu_x Re_x^{-1/2}$ is shown in Fig. 7.22. The value of $Nu_x Re_x^{-1/2}$ is decreased for the increasing values of both β and Γ_e. Fig. 7.23 is drawn to see the impact of C_r and S_c on $Sh_x Re_x^{-1/2}$. Both of these are observed to upsurge $Sh_x Re_x^{-1/2}$ as observed in this figure.
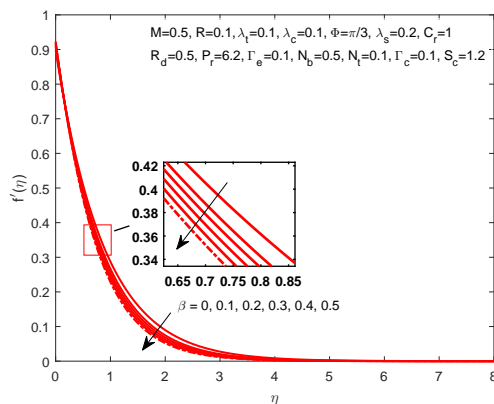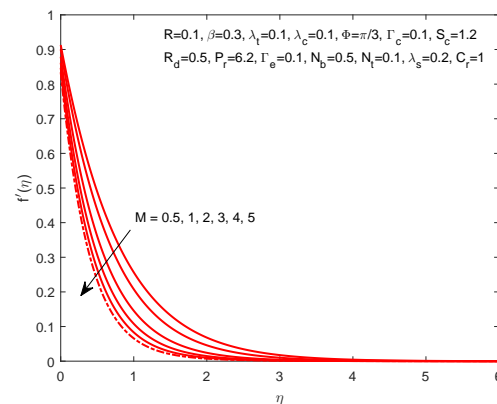

Fig. 7.2: Impact of β on f' Fig. 7.3: Impact of M on f'

7.5 Final Remarks

In this chapter, the numerical solution of UCM nanofluid flow in the presence of a magnetic field is investigated. A special consideration has been given to non-linear velocity slip, thermal radiation and heat generation effects. The modified
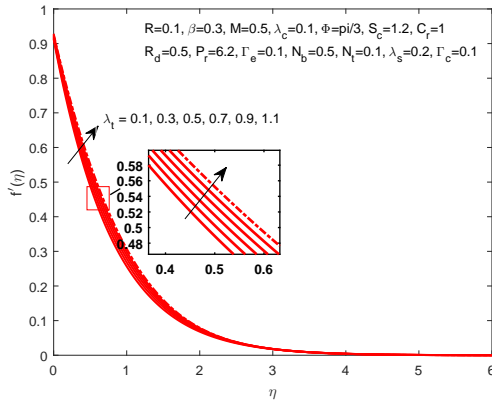
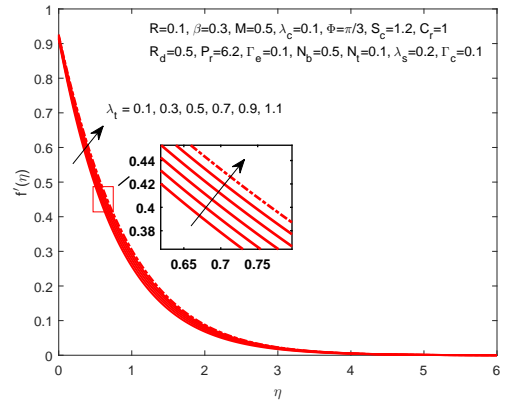Fig. 7.4: Impact of λ_c on f'
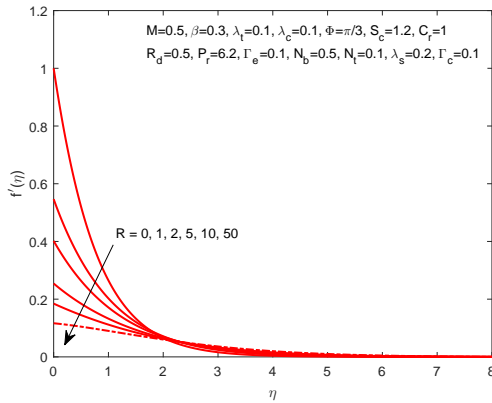

Fig. 7.5: Impact of λ_t on f'
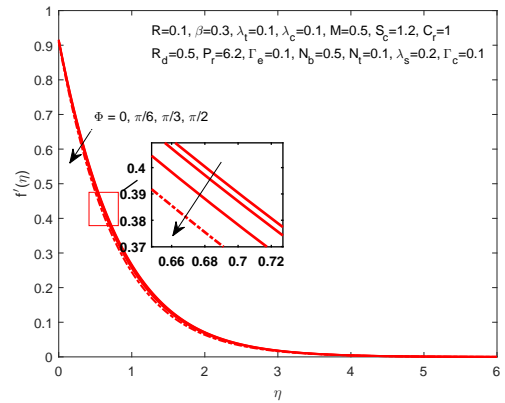

Fig. 7.6: Impact of R on f'
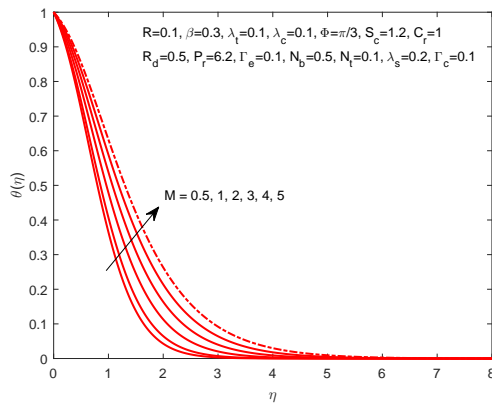

Fig. 7.7: Impact of Ω on f'
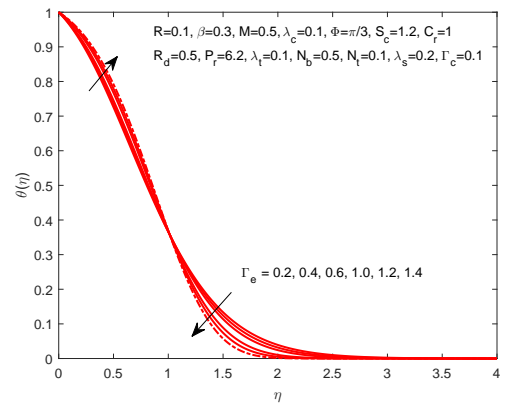

Fig. 7.8: Impact of M on θ

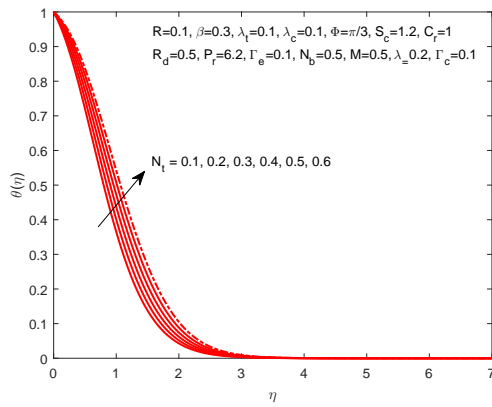Fig. 7.9: Impact of Γ_e on θ

Fig. 7.10: Impact of N_t on θ

Fig. 7.11: Impact of N_b on θ

Fig. 7.12: Impact of P_r on θ
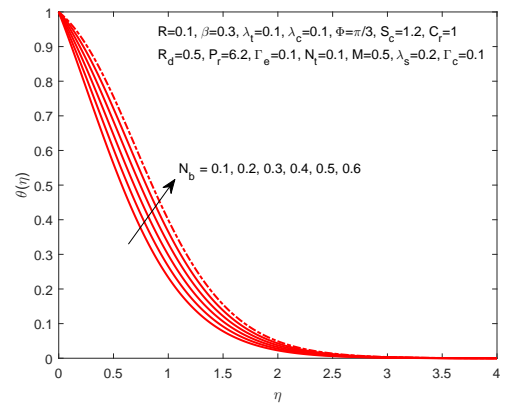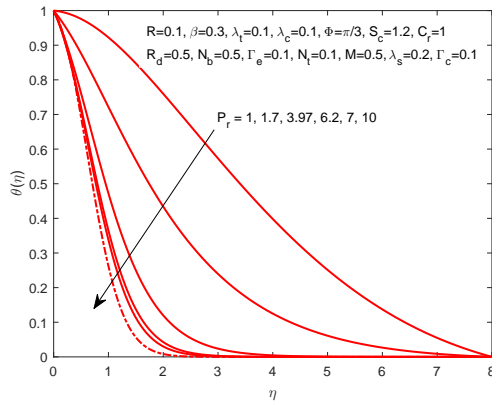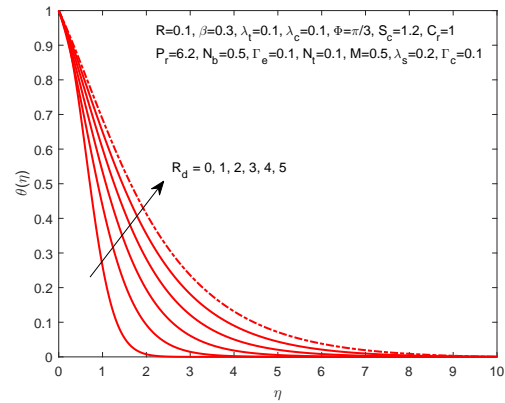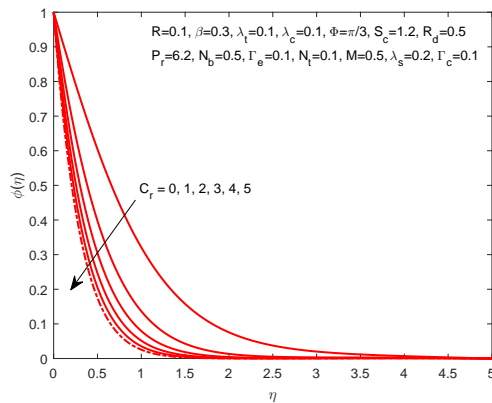

Fig. 7.13: Impact of R_d on θ

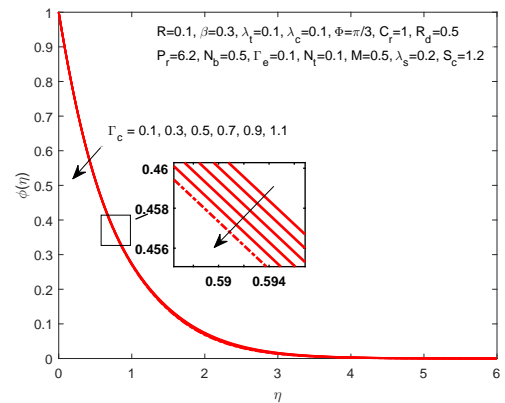Fig. 7.14: Impact of C_r on ϕ

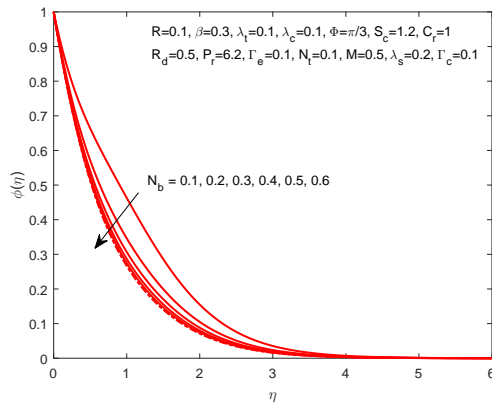
Fig. 7.15: Impact of Γ_c on ϕ

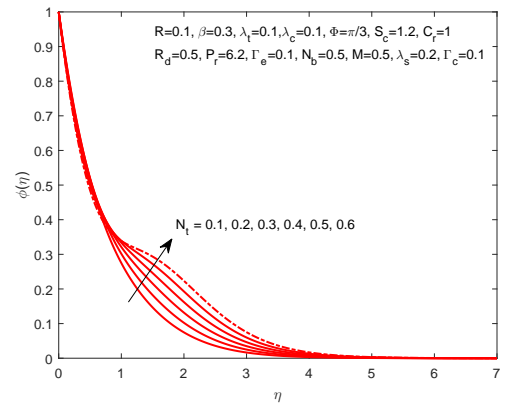Fig. 7.16: Impact of N_b on ϕ

Fig. 7.17: Impact of N_t on ϕ
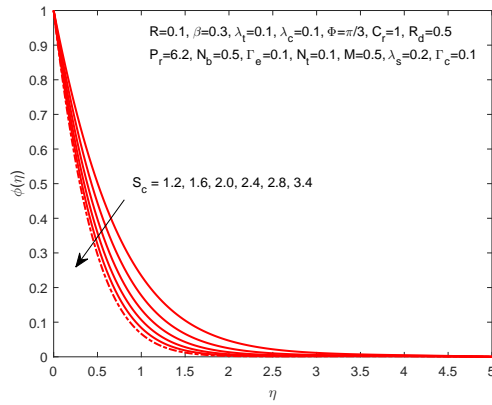
Fig. 7.18: Impact of S_c on ϕ
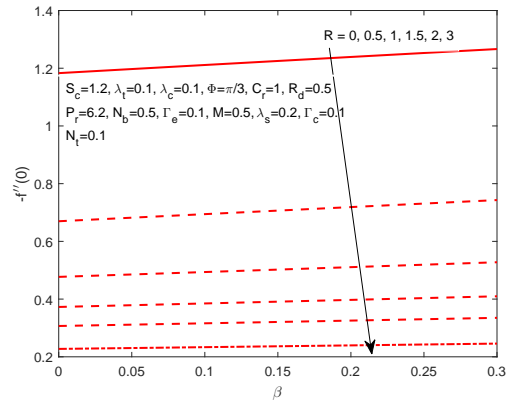
Fig. 7.19: Impact of β on $-f''(0)$
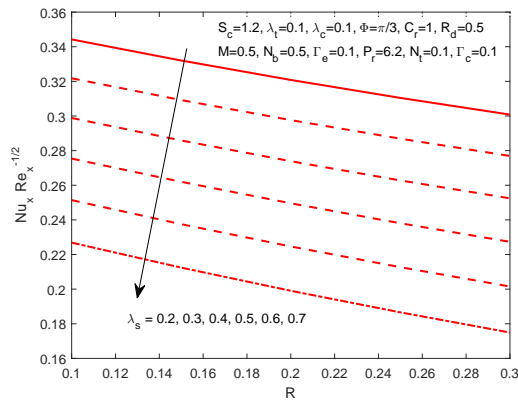
Fig. 7.20: Impact of R on $Nu_x Re_x^{-1/2}$
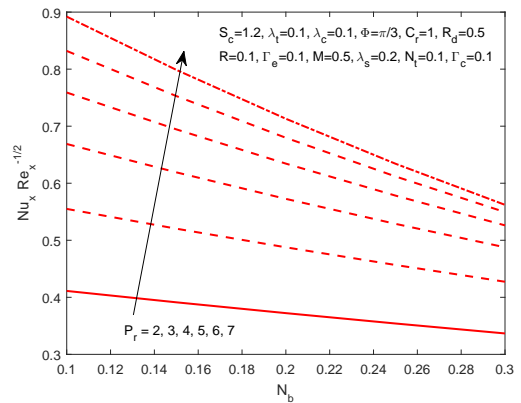
Fig. 7.21: Impact of N_b on $Nu_x Re_x^{-1/2}$
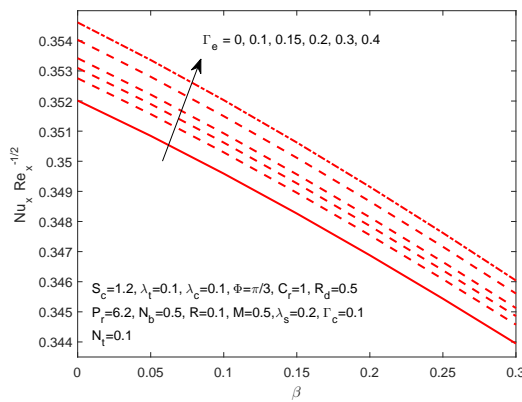
Fig. 7.22: Impact of β on $Nu_x Re_x^{-1/2}$
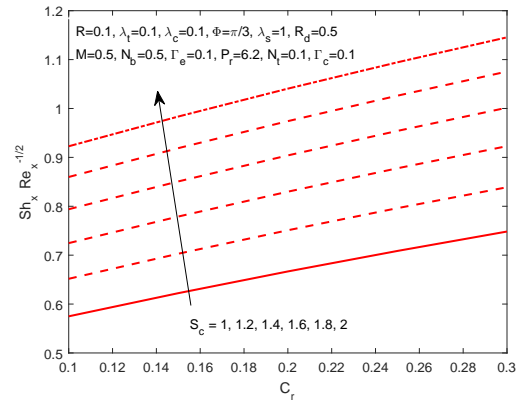
Fig. 7.23: Impact of S_c on $Sh_x Re_x^{-1/2}$

Fourier and Fick's laws are incorporated in the modeling process. The mass transfer phenomenon is investigated under the Brownian motion, chemical reaction and thermophoresis effects. By making use of some appropriate similarity transformations, the governing equations are converted into the non-dimensional form and then cracked numerically by the shooting technique. The impacts of noticeable physical parameters on the dimensionless velocity, temperature and concentration profiles are highlighted with the help of graphs and tables. The concluding point of the analysis are:

- The velocity close to the surface is reduced for the augmented slip parameter R whereas far away the surface, an increment in the velocity is noticed.

- The magnitude of $-f''(0)$ is increased for higher Maxwell parameter β but it is decreased for an upturn in the slip parameter R.

- The ascending values of M, the Maxwell parameter β and the angle of the inclined stretching sheet Ω cause a decay in the dimensionless velocity while an assisting behavior of the thermal and concentration buoyancy parameters is seen.

- An interesting effect of Γ_e on θ is examined near the wall, for the growing values of Γ_e, θ is observed to increase whereas a little bit away from the surface, a growth in θ is identified.

- The temperature distribution for the higher P_r falls down while R_d enhances θ and the thermal boundary-layer thickness.

- The heat transfer rate is noticed to improve for an augmentation in the Prandtl number P_r.

- A decay in ϕ is observed by increasing C_r.

Chapter 8

Conclusion

In this dissertation, the investigation focuses on the flow and heat transfer analysis of UCM fluid under the influence of generalized Fourier's heat conduction model and non-linear velocity slip effects due to stretching surfaces. Chapters 3 to 7 are arranged to discuss the main problems: the effects of MHD on flow and heat transfer of UCM fluid with Joule heating and thermal radiation under CCHFM are considered in chapter 3. The boundary-layer flow of UCM fluid over vertical stretching surface using CCHFM is discussed in chapter 4. In chapter 5, the mixed convective flow of UCM fluid in a thermally stratified medium along CCHFM is explored. MHD effects on the flow, heat and mass transfer for UCM fluid on an inclined porous and non-porous surfaces with CCHFM are investigated in chapters 6 and 7. The prime findings of the study presented in this thesis are listed below:

- A decrement in the velocity profile and the associated momentum boundary-layer thickness is observed for the ascending values of β whereas an accretion in the temperature distribution is witnessed.

- The value of $-f''(0)$ is an increasing function of β but it is decreased for an upturn in R and K_p.

- For the higher β, a more prominent increment in the values of $-f''(0)$ for the case of non-linear stretching sheet is noticed.

- The temperature field is observed to exhibit a decreasing behavior for the up-going Γ_e.

- An augmentation in P_r leads to a decrease in the temperature profile.

- The temperature is decreased for higher Prandtl number and this decrement is more rapid in the case of Newtonian fluid as compared to the Maxwell fluid.

- A rise in heat transfer rate for an augmentation in P_r is identified whereas the heat transfer rate is subsided for β and Γ_e.

- The heat transfers promptly within the material in case of Fourier's law (i.e. $\Gamma_e = 0$) as compared to the CCHFM.

- The temperature distribution for the ascending magnetic parametric values is higher in the presence of porous medium rather than the temperature in the absence of non-porous medium.

- The velocity close to the surface is reduced for the augmented R whereas far away from the surface, an increment in the velocity is noticed.

- The temperature in the boundary-layer is noticed to increase with the ascending values of R.

- The parameter M significantly reduces the fluid transport whereas an increment in M causes the temperature to rise.

- A rise in K_p reduces the velocity profile more promptly for the non-linear stretching case.

- A decrement in the non-dimensional velocity through a porous medium is more significant as compared to a non-porous medium.

- A decay in the concentration distribution is witnessed by the ascending parametric values of S_c and C_r.

8.1   Future Work

The utility of the research in this dissertation is invaluable especially when studying the heat transfer characteristics of non-Newtonian fluids (visco-elastic) due to

stretching surfaces under the most recent modified Fourier heat conduction model. Might I add that this thesis has certain limitations. It confines itself to the investigation of fluids that are steady in their flow. Advanced information in this regard can be gathered that can affect the heat transfer rate for unsteady cases i.e., the ones that include time effects when the flow is developed. Prospects, concerning the analysis of heat transfer effects caused by the stretching surfaces from various aspects, be they physical or geometrical are great.

Bibliography

[1] A. Mushtaq, M. Mustafa, T. Hayat, and A. Alsaedi, "Boundary layer flow over a moving plate in a flowing fluid considering non-linear radiations," *Int. J. Numer. Methods Heat Fluid Flow*, vol. 26(5), pp. 1617–1630, 2016.

[2] C. Liu, H. H. Wang, and Y. F. Peng, "Flow and heat transfer for three-dimensional flow over an exponentially stretching surface," *Chem. Eng. Comm.*, vol. 200, pp. 253–268, 2013.

[3] K. M. Abualnaja, "Numerical studies for MHD flow and gradient heat transport past a stretching sheet with radiation and heat production via DTM," *Appl. Appl. Math.*, vol. 13(2), pp. 915–924, 2018.

[4] T. Hayat, Z. Hussain, M. Farooq, and A. Alsaedi, "Magnetohydrodynamic flow of Powell-Eyring fluid by a stretching cylinder with Newtonian heating," *Therm. Sci.*, vol. 22(1B), pp. 371–382, 2018.

[5] H. Schlichting, *Boundary Layer Theory*, 6th ed. McGraw-Hill Series in Mechanical Engineering, New York, 1968.

[6] M. E. Ali and N. Sandeep, "Cattaneo-Christov model for radiative heat transfer of magnetohydrodynamic Casson-ferrofluid: A numerical study," *Results Phys.*, vol. 7, pp. 21–30, 2017.

[7] X. Xu and S. Chen, "Cattaneo-Christov heat flux model for heat transfer of Marangoni boundary layer flow in a copperwater nanofluid," *Heat Tran. -Asian Res.*, vol. 46, pp. 1281–1293, 2017.

[8] V. Nagendramma, C. S. K. Raju, and A. L. Ratnam, "Cattaneo-Christov heat flux model for Sakiadis flow of MHD Carreau fluid," *Int. J. Res. Sci. Eng.*, pp. 108–117, 2017.

[9] O. D. Makinde, N. Sandeep, I. L. Animasaun, and M. S. Tshehla, "Numerical exploration of Cattaneo-Christov heat flux and mass transfer in magneto-hydrodynamic flow over various geometries," *Defect Diffu. Forum*, vol. 374, pp. 67–82, 2017.

[10] L. Liu, L. Zheng, F. Liu, and X. Zhang, "Heat conduction with fractional Cattaneo-Christov upper-convective derivative flux model," *Int. J. Ther. Sci.*, vol. 112, pp. 421–426, 2017.

[11] R. V. M. S. S. K. Kumar and S. V. K. Varma, "MHD boundary layer flow of nanofluid through a porous medium over a stretching sheet with variable wall thickness: Using Cattaneo-Christov heat flux model," *J. Theor. Appl. Mech.*, vol. 48(2), pp. 72–92, 2018.

[12] K. Gangadhar, C. S. Kumar, S. M. Ibrahim, and G. Lorenzini, "Effect of viscous dissipation on Upper-Convected Maxwell fluid with Cattaneo-Christov heat flux model using spectral relaxation method," *Defect Diffu. Forum*, vol. 388, pp. 146–157, 2018.

[13] S. U. Rehman, A. Zeeshan, A. Majeed, and M. B. Arain, "Impact of Cattaneo-Christov heat flux model on the flow of Maxwell Ferromagnetic liquid along a cold flat plate embedded with two equal magnetic dipoles," *J. Mag.*, vol. 22(3), pp. 472–477, 2017.

[14] B. C. Sakiadis, "Boundary layer behavior on continuous solid surfaces: I. Boundary layer equation for two-dimensional and axisymmtric flow," *AICHE J.*, vol. 7, pp. 26–28, 1961.

[15] L. E. Erickson, L. C. Cha, and L. T. Fan, "The cooling of moving continuous flat sheet," *AICHE J.*, vol. 62, pp. 157–165, 1966.

[16] L. J. Crane, "Flow past a stretching plate," *J. Appl. Math. Phys. (ZAMP)*, vol. 21, pp. 645–647, 1970.

[17] J. E. Danberg and K. S. Fansler, "A nonsimilar moving-wall boundary-layer problem," *Quart. Appl. Math.*, vol. 34, pp. 305–309, 1976.

[18] C. Y. Wang, "The three-dimensional flow due to a stretching flat surface," *Phys. Fluids*, vol. 27, pp. 1915–1917, 1984.

[19] B. Siddappa and S. Abel, "Non-Newtonian flow past a stretching plate," *Z. Angew. Math. Physik*, vol. 36, pp. 890–892, 1985.

[20] M. K. Laha, P. S. Gupta, and A. S. Gupta, "Heat transfer characteristics of the flow of an incompressible viscous fluid over a stretching sheet," *Wrme- und Stoffbertragung*, vol. 24(3), pp. 151–153, 1989.

[21] R. Cortell, "Viscous flow and heat transfer over a nonlinear stretching sheet," *Appl. Math. Comput.*, vol. 184, pp. 864–873, 2007.

[22] M. M. Nandeppanavar, M. N. Siddalingappa, and H. Jyoti, "Heat transfer of viscoelastic fluid flow due to nonlinear stretching sheet with internal heat source," *Int. J. Appl. Mech. Eng.*, vol. 18, pp. 739–760, 2013.

[23] T. V. Laxmi and B. Shankar, "Effect of nonlinear thermal radiation on boundary layer flow of viscous fluid over nonlinear stretching sheet with injection/suction," *J. Appl. Math. Phys.*, vol. 4, pp. 307–319, 2016.

[24] M. I. Khan, T. Hayat, M. Waqas, M. I. Khan, and A. Alsaedi, "Impact of heat generation/absorption and homogeneous-heterogeneous reactions on flow of Maxwell fluid," *J. Mol. Liq.*, vol. 233, pp. 465–470, 2017.

[25] E. M. A. Elbashbeshy, H. G. Asker, K. M. Abdelgaberc, and E. A. S. EA, "Heat transfer over a stretching surface with variable thickness embedded in porous medium in the presence of Maxwell fluid." *J. Appl. Mech. Eng.*, vol. 7, p. 307, 2018.

[26] M. Hamid, M. Usman, Z. H. Khan, R. U. Haq, and W. Wang, "Numerical study of unsteady MHD flow of Williamson nanofluid in a permeable channel with heat source/sink and thermal radiation," *Eur. Phys. J. Plus*, vol. 133(12), p. 527, 2018.

[27] A. Gizachew and B. Shankar, "Analytical solutions of an MHD heat and mass transfer of a Jeffery fluid flow over a stretching sheet with the effect of slip velocity," *Advan. Appl. Sci.*, vol. 3(3), pp. 34–42, 2018.

[28] J. B. J., *Fourier, Theorie analytique De La chaleur*. Paris, 1822.

[29] C. Cattaneo, "Sulla conduzione del calore," *Atti Semin. Mat. Fis. Univ. Modena Reggio Emilia*, vol. 3, pp. 83–101, 1948.

[30] C. I. Christov, "On frame indifferent formulation of the Maxwell-Cattaneo model of finite speed heat conduction," *Mech. Res. Commun.*, vol. 36, pp. 481–486, 2009.

[31] F. Franchi and B. Straughan, "Thermal convection at low temperature," *J. NonEquilibr. Thermodyn.*, vol. 19, pp. 368–374, 1994.

[32] P. Puri and P. K. Kythe, "Discontinuities in velocity gradients and temperature in the Stokes first problem with nonclassical heat conduction," *Q. Appl. Math.*, vol. 55, pp. 167–176, 1997.

[33] K. Gangadhar, C. S. Kumar, S. M. Ibrahim, and G. Lorenzini, "Effect of viscous dissipation on upper-convected Maxwell fluid with Cattaneo-Christov heat flux model using Spectral relaxation method," *Defect and Diff. Forum*, vol. 388(11), pp. 146–157, 2018.

[34] S. Han, L. Zheng, C. Li, and Zhang, "Coupled flow and heat transfer in viscoelastic fluid with Cattaneo-Christov heat flux model," *Appl. Math. Lett.*, vol. 38, pp. 87–93, 2014.

[35] T. Hayat, T. Muhammad, A. Alsaedi, and M. Mustafa, "A comparative study for flow of viscoelastic fluids with Cattaneo-Christov heat flux," *PLoS ONE*, vol. 11, p. e0155185, 2016.

[36] A. Tanveer, S. Hina, T. Hayat, M. Mustafa, and B. Ahmad, "Effects of the Cattaneo-Christov heat flux model on peristalsis," *Eng. Appl. Compu. Fluid Mech.*, vol. 10(1), pp. 375–385, 2016.

[37] A. Shahid, M. M. Bhatti, O. A. Beg, and A. Kadir, "Numerical study of radiative Maxwell viscoelastic magnetized flow from a stretching permeable sheet with the CattaneoChristov heat flux model," *Neural Comput. Appl.*, vol. 30(11), pp. 3467–3478, 2018.

[38] A. Sarkar and P. K. Kundu, "Exploring the Cattaneo-Christov heat flux phenomenon on a Maxwell-type nanofluid coexisting with homogeneous/heterogeneous reactions," *Eur. Phys. J. Plus*, vol. 534, p. 132, 2017.

[39] T. Hayat, M. I. Khan, M. Farooq, A. Alsaedi, M. Waqas, and T. Yasmeen, "Impact of Cattaneo-Christov heat flux model in flow of variable thermal conductivity fluid over a variable thicked surface," *Int. J. Heat Mass Trans.*, vol. 99, pp. 702–710, 2016.

[40] M. A. Meraj, S. A. Shehzad, T. Hayat, F. M. Abbasi, and A. Alsaedi, "Darcy-Forchheimer flow of variable conductivity Jeffrey liquid with Cattaneo-Christov heat flux theory," *Appl. Math. Mech. -Engl. Ed.*, vol. 38, pp. 557–566, 2017.

[41] M. Mustafa, "Cattaneo-Christov heat flux model for rotating flow and heat transfer of upper convected Maxwell fluid," *AIP Adv.*, vol. 5, p. 047109, 2015.

[42] A. Mushtaq, S. Abbasbandy, M. Mustafa, T. Hayat, and A. Alsaedi, "Numerical solution for Sakiadis flow of upper-convected Maxwell fluid using Cattaneo-Christov heat flux model," *AIP Adv.*, vol. 6, p. 015208, 2016.

[43] T. Hayat, M. Zubair, M. Waqas, A. Alsaedi, and M. Ayub, "Application of non-Fourier heat flux theory in thermally stratified flow of second grade liquid with variable properties," *Chin. J. Phys.*, vol. 55, pp. 230–241, 2017.

[44] M. G. Reddy, "Influence of Lorentz force, Cattaneo-Christov heat flux and viscous dissipation on the flow of micropolar fluid past a nonlinear convective stretching vertical surface," *Non-linear Eng.*, vol. 6(4), pp. 317–326, 2017.

[45] M. Awais, S. E. Awan, K. Iqbal, Z. A. Khan, and M. A. Z. Raja, "Hydromagnetic mixed convective flow over a wall with variable thickness and Cattaneo-Christov heat flux model: OHAM analysis," *Results Phys.*, vol. 8, pp. 621–627, 2018.

[46] G. A. Faiz, M. S. A. Sami, P. Sibanda, and M. Khumalo, "The effect of thermophoresis on unsteady Oldroyd-B nanofluid flow over stretching surface," *PLoS One*, vol. 10(8), p. e0135914, 2015.

[47] M. S. Abel, J. V. Tawade, and M. M. Nandeppanavar, "MHD flow and heat transfer for the upper-convected Maxwell fluid over a stretching sheet," *Meccanica*, vol. 47, pp. 385–393, 2012.

[48] S. Abel, K. V. Prasad, and A. Mahaboob, "Buoyancy force and thermal radiation effects in MHD boundary layer viscoelastic fluid flow over continuously moving stretching surface," *Int. J. Thermal Sci.*, vol. 44, pp. 465–476, 2005.

[49] T. Sarpakaya, "Flow of non-Newtonian fluids in a magnetic field," *AIChE Journal*, vol. 07, pp. 324–328, 1961.

[50] C. H. Chen, "On the analytical solution of MHD flow and heat transfer for two types of viscoelastic fluid over a stretching sheet with energy dissipation, internal heat source and thermal radiation," *Int. J. Heat Mass Transfer*, vol. 19, pp. 4264–4273, 2010.

[51] N. S. Akbar, A. Ebaid, and Z. H. Khan, "Numerical analysis of magnetic field effects on Eyring-Powell fluid flow towards a stretching sheet," *J. Magn. Magn. Mater*, vol. 382, pp. 355–358, 2015.

[52] F. Mabood, W. A. Khan, and A. I. M. Ismail, "MHD boundary layer flow and heat transfer of nanofluids over a nonlinear stretching sheet," *J. Magn. Magn. Mater*, vol. 374, pp. 569–576, 2015.

[53] T. Hayat and M. Sajid, "Homotopy analysis of MHD boundary layer flow of an upper-convected Maxwell fluid," *Int. J. Eng. Sci.*, vol. 45, pp. 393–401, 2007.

[54] Y. Wang and T. Hayat, "Fluctuating flow of a Maxwell fluid past a porous plate with variable suction, Nonlinear Analysis," *Real World Applications*, vol. 9, pp. 1269–1282, 2008.

[55] S. Rashidi, M. Dehghan, R. Ellahi, M. Riaz, and M. T. Jamal-Abad, "Study of stream wise transverse magnetic fluid flow with heat transfer around an obstacle embedded in a porous medium," *J. Magn. Magn. Mater.*, vol. 378, pp. 128–137, 2015.

[56] R. Ellahi, S. U. Rahman, S. Nadeem, and K. Vafai, "The blood flow of Prandtl fluid through a tapered stenosed arteries in permeable walls with magnetic field," *Commun. Theor. Phys.*, vol. 63, pp. 353–358, 2015.

[57] M. S. Kandelousi and R. Ellahi, "Simulation of ferrofluid flow for magnetic drug targeting using the lattice Boltzmann method," *Z. N. A.*, vol. 70, pp. 115–124, 2015.

[58] K. Hiemenz, "Die Grenzschicht an einem in den gleichfrmigen Flssigkeitsstrom eingetauchten geraden Kreiszylinder," *Dingl. Polytech. J.*, vol. 32, pp. 321–410, 1911.

[59] M. M. Rashidi and N. Freidoonimehr, "Analysis of entropy generation in MHD stagnation-point flow in porous media with heat transfer," *Int. J. Comput. Methods Eng. Sci. Mech.*, vol. 15(4), pp. 345–355, 2014.

[60] K. Naganthran, R. Nazar, and I. Pop, "Unsteady stagnation-point flow and heat transfer of a special third grade fluid past a permeable stretching/shrinking sheet," *Scientific Reports*, vol. 6, p. 24632, 2016.

[61] T. Srinivasulu, S. Bandari, and C. Sumalatha, "MHD stagnation point flow of Casson nanofluid over a stretching sheet with effect of viscous dissipation," *Glo. J. Pure Appl. Math.*, vol. 13, pp. 4229–4244, 2017.

[62] R. Kandasamy, V. V. Balachandar, and S. B. Hasan, "Magnetohydrodynamic and heat transfer effects on the stagnation-point flow of an electrically conducting nanofluid past a porous vertical shrinking/stretching sheet in the presence of variable stream conditions," *Proc. Natl. Acad. Sci., India, Sect. A Phys. Sci.*, vol. 58, pp. 71–79, 2017.

[63] I. Tlili, W. A. Khan, and K. Ramadan, "Entropy generation due to MHD stagnation point flow of a nanofluid on a stretching surface in the presence of radiation," *J. Nanofluids*, vol. 7(5), pp. 879–890(12), 2018.

[64] M. Turkyilmazoglu, "Magnetic field and slip effects on the flow and heat transfer of stagnation point Jeffrey fluid over deformable surfaces," *Z. Naturforsch*, vol. 71(6)a, pp. 549–556, 2016.

[65] M. M. Nandeppanavar and S. Shakunthala, "Heat transfer analysis of stagnation point flow over a stretching cylinder in a suspension of carbon nanotube," *J. Nanofluids*, vol. 6(6), pp. 1173–1180(8), 2017.

[66] A. S. Butt, A. Ali, and A. Mehmood, "Hydromagnetic stagnation point flow and heat transfer of particle suspended fluid towards a radially stretching sheet with heat generation," *Proc. Natl. Acad. Sci., India, Sect. A Phys. Sci.*, vol. 87, pp. 385–394, 2017.

[67] P. Rana, M. J. Uddin, Y. Gupta, and A. I. M. Ismail, "Slip effects on MHD Hiemenz stagnation point nanofluid flow and heat transfer along a nonlinearly shrinking sheet with induced magnetic field: multiple solutions," *J. Braz. Soc. Mech. Sci. Eng.*, vol. 39(9), pp. 3363–3374, 2017.

[68] M. M. Nandeppanavar, M. C. Kemparaju, and M. S. Abel, "Thermal radiative MHD stagnation point slip flow and heat transfer due to a stretching sheet," *J. Nanofluids*, vol. 7(2), pp. 350–357(8), 2018.

[69] C. Neto, V. S. Craig, and D. R. Williams, "Evidence of shear-dependent boundary slip in Newtonian liquids," *Eur. Phys. J. E.*, vol. 12(1), pp. 71–74, 2003.

[70] G. C. Bhattacharyya, K. Mukhopadhyay, and S. Layek, "Slip effects on boundary layer stagnation-point flow and heat transfer towards a shrinking sheet," *Int. J. Heat Mass Transf.*, vol. 54(1-3), pp. 308–313, 2011.

[71] Y. X. Zhu and S. Granick, "Limits of the hydrodynamic no-slip boundary condition," *Phys. Rev. Lett.*, vol. 88, p. 054504, 2001.

[72] C. L. M. H. Navier, "Memoire Surles du Movement des," *Mem. Acad. Sci. Inst. Fr.*, vol. 1(6), pp. 414–416, 1823.

[73] R. B. Bird, R. C. Armstrong, and O. Hassager, *Dynamics of Polymeric Liquids, Fluid Mechanics*, 2nd ed. John Wiley and Sons, New York, 1987, vol. 1.

[74] O. D. Makinde, W. A. Khan, and Z. H. Khan, "Stagnation point flow of MHD chemically reacting nanofluid over a stretching convective surface with slip and radiative heat," *Proc. Inst. Mech. Eng., Part E: J. Process Mech. Eng.*, vol. 231(4), pp. 695–703, 2017.

[75] M. Turkyilmazoglu, "Multiple solutions of heat and mass transfer of MHD slip flow for the viscoelastic fluid over a stretching sheet," *Int. J. Ther. Sci.*, vol. 50, pp. 2264–2276, 2011.

[76] K. Kaladhar and O. D. Makinde, "Thermal radiation, Joule heating and Hall effects on mixed convective Navier slip flow in a channel with convective heating," *Diff. Foun.*, vol. 11, pp. 162–181, 2017.

[77] P. D. Ariel, T. Hayat, and S. Asghar, "The flow of an elasticoviscous fluid past a stretching sheet with partial slip," *Acta Mech.*, vol. 187(1-4), pp. 29–35, 2006.

[78] V. Anand, "Effect of slip on heat transfer and entropy generation charac-
teristics of simplified Phan-Thien-Tanner fluids with viscous dissipation un-
der uniform heat flux boundary conditions: exponential formulation," *Appl.
Therm. Eng.*, vol. 98, pp. 455–473, 2016.

[79] A. M. Megahed, "Slip flow and variable properties of viscoelastic fluid past
a stretching surface embedded in a porous medium with heat generation,"
J. Cent. South Univ., vol. 23(4), pp. 991–999, 2016.

[80] J. Li, L. Zheng, and L. Liu, "MHD viscoelastic flow and heat transfer over a
vertical stretching sheet with Cattaneo-Christov heat flux effects," *J. Mol.
Liq.*, vol. 221, p. 1925, 2016.

[81] O. A. Abegunrin and I. L. Animasaun, "Motion of Williamson fluid over
an upper horizontal surface of a paraboloid of revolution due to partial slip
and buoyancy: boundary layer analysis," *Defect Diff. Forum*, vol. 378, pp.
16–27, 2017.

[82] A. Haritha, Y. Devasena, and B. Vishali, "MHD heat and mass transfer of
the unsteady flow of a Maxwell fluid over a stretching surface with Navier
slip and convective boundary conditions," *Glob. J. Pure Appl. Math.*, vol.
13(6), pp. 2169–2179, 2017.

[83] S. Yu and T. A. Ameel, "Slip-flow heat transfer in rectangular microchan-
nels," *Int. J. Heat Mass Trans.*, vol. 44, pp. 4225–4234, 2002.

[84] M. Turkyilmazoglu, "Multiple analytic solutions of heat and mass transfer
of magnetohydrodynamic slip flow for two types of viscoelastic fluids over a
stretching surface," *J. Heat Transf.*, vol. 134, pp. 071 701–1–071 701–9, 2012.

[85] R. Kumar, S. Sood, S. A. Shehzad, and M. Sheikholeslami, "Numerical
modeling of time-dependent bio-convective stagnation flow of a nanofluid in
slip regime," *Results Phys.*, vol. 7, pp. 3325–3332, 2017.

[86] J. Zhu, S. Wang, L. Zheng, and X. Zhang, "Heat transfer of nanofluids considering nanoparticle migration and second-order slip velocity," *Appl. Math. Mech. -Engl. Ed.*, vol. 38(1), pp. 125–136, 2017.

[87] A. Mahdy and A. J. Chamkha, "Diffusion of chemically reactive species of a Maxwell fluid due to an unsteady stretching sheet with slip effect," *Ther. Sci.*, vol. 21(6A), pp. 2357–2367, 2017.

[88] B. Ramadevi, V. Sugunamma, K. A. Kumar, and J. V. R. Reddy, "MHD flow of Carreau fluid over a variable thickness melting surface subject to Cattaneo-Christov heat flux," *Multidisc. Mod. Mat. Struc.*, vol. 15(1), pp. 2–25, 2019.

[89] A. Chakrabarti and A. S. Gupta, "Hydromagnetic flow and heat transfer over a stretching sheet," *J. Appl. Fluid Math.*, vol. 37, pp. 73–78, 1979.

[90] P. R. Sharma and G. Singh, "Effects of variable thermal conductivity and heat source/sink on MHD flow near a stagnation point on a linearly stretching sheet," *J. Appl. Fluid Mech.*, vol. 2, pp. 13–21, 2009.

[91] S. Mukhopadhyay and I. C. Mandal, "Magnetohydrodynamic (MHD) mixed convection slip flow and heat transfer over a vertical porous plate," *Eng. Sci. Tech., an Int. J.*, vol. 18, pp. 98–105, 2015.

[92] K. Sharada and B. Shankar, "MHD mixed convection flow of a Casson fluid with convective boundary condition and effect of partial slip in the presence of Joule heating over a vertically stretching sheet," *Int. J. Innov. Res. Sci., Eng. Tech.*, vol. 6, 2017.

[93] K. Gangadhar, T. Kannan, and P. Jayalakshmi, "Magnetohydrodynamic micropolar nanofluid past a permeable stretching/shrinking sheet with Newtonian heating," *J. Braz. Soc. Mech. Sci. Eng.*, vol. 39(11), pp. 4379–4391, 2017.

[94] M. Abbaszadeh, A. Ababaei, A. A. A. Arani, and A. A. Sharifabadi, "MHD forced convection and entropy generation of CuO-water nanofluid in a microchannel considering slip velocity and temperature jump," *J. Braz. Soc. Mech. Sci. Eng.*, vol. 39(3), pp. 775–790, 2017.

[95] M. Sajid, Z. Abbas, N. Ali, T. Javed, and I. Ahmad, "Slip flow of a Maxwell fluid past a stretching sheet," *Walailak J. Sci. Technol.*, vol. 11, pp. 1093–1103, 2014.

[96] M. S. Tillack and N. B. Morley, *Magnetohydrodynamics. Standard handbook for electrical engineers*, 14th ed.   McGraw Hill, 1998.

[97] J. Harris, *Rheology and Non-Newtonian Flow.*   Longman, London, 1977, vol. 7.

[98] W. Tan and T. Masuoka, "Stoke's first problem for a second grade fluid in a porous half-space with heated boundary," *Int. J. Non-Linear Mech.*, vol. 40, pp. 515–522, 2005.

[99] J. N. Reddy, *An Introduction to Continuum Mechanics.*   Cambridge University Press, 2013, vol. 1.

[100] D. D. Joseph and L. Preziosi, "Addendum to the paper "heat waves"," *Rev. Mod. Phys.*, vol. 62, pp. 375–391, 1990.

[101] D. S. Chandrasekharaiah, "Hyperbolic thermoelasticity: a review of recent literature," *Appl. Mech. Rev.*, vol. 51, pp. 705–729, 1998.

[102] W. Dreyer and H. Struchtrup, "Heat pulse experiments revisited," *Continuum Mech. Thermodyn.*, vol. 5, pp. 3–50, 1993.

[103] W. M. Lai, D. Rubin, and E. Krempl, *Introduction to Continuum Mechanics.* Pergamon Press, New York, 1974.

[104] P. M. Jordan, W. Dai, and R. E. Mickens, "A note on the delayed heat equation: instability with respect to initial data," *Mech. Res. Commun.*, vol. 35, pp. 414–420, 2008.

[105] D. D. Joseph and L. Preziosi, "Heat waves," *Rev. Mod. Phys.*, vol. 61, pp. 41–73, 1989.

[106] D. Jou, J. Casas-Vzquez, and G. Lebon, "Extended irreversible thermodynamics revisited," *Rep. Prog. Phys.*, vol. 62, pp. 1035–1142, 1998.

[107] G. Caviglia, A. Morro, and B. Straughan, "Stability and wave motion in porous media," *Int. J. NonLinear Mech.*, vol. 27, pp. 251–263, 1992.

[108] P. J. Antaki, "Hotter than you think," *Machine Design*, vol. 13, pp. 116–118, 1995.

[109] R. E. Mickens and P. M. Jordan, "A positivity-preserving nonstandard finite difference scheme for the damped wave equation," *Numer. Methods Partial Differ. Equ.*, vol. 20(5), pp. 639–802, 2004.

[110] C. I. Christov and P. M. Jordan, "Heat conduction paradox involving second sound propagation in moving media," *Phys. Rev. Lett.*, vol. 94, p. 154301, 2005.

[111] C. I. Christov, "On the material invariant formulation of maxwell's displacement current," *Found. Phys.*, vol. 36, pp. 1701–1717, 2006.

[112] T. Y. Na, *Computational methods in engineering boundary value problems*, 1st ed.   Academic Press, 12 1979, vol. 145.

[113] J. Kunes, *Dimensionless Physical Quantities in Science and Engineering*, 1st ed.   Elsevier, 2 2012.

[114] R. S. Esfandiari, *Numerical Methods for Engineers and Scientists Using Matlab*.   Taylor and Francis Group, New York, 2013.

[115] J. Kierzenka, "Studies in the numerical solution of ordinary differential equations," Ph.D. dissertation, Southern Methodist University, Dallas, TX, 1998.

[116] L. F. Shampine, J. Kierzenka, and M. W. Reichelt, "Solving boundary value problems for ordinary differential equations in Matlab with bvp4c," *http : //www.mathworks.com/bvp$_t$utorial.*, 2000.

[117] Z. Abbas, M. Sajid, and T. Hayat, "MHD boundary-layer flow of an upper-convected Maxwell fluid in a porous channel," *Theor. Comput. Fluid Dyn.*, vol. 20, pp. 229–238, 2006.

[118] M. Renardy, "High Weissenberg number boundary layers for the upper-convected Maxwell fluid," *J. Non-Newtonian Fluid Mech.*, vol. 68, pp. 125–132, 1997.

[119] A. Mushtaq, M. Mustafa, T. Hayat, and A. Alsaedi, "Effects of thermal radiation on the stagnation-point flow of upper-convected Maxwell fluid over a stretching sheet," *J. Aerosp. Eng.*, vol. 27, 2014.

[120] D. H. Babu and P. V. S. Narayana, "Joule heating effects on MHD mixed convection of a Jeffrey fluid over a stretching sheet with power law heat flux: A Numerical Study," *J. Magnetism and Magnetic Materials*, vol. 412, pp. 185–193, 2016.

[121] M. Q. Brewster, *Thermal radiative transfer properties.* John Wiley and Sons, 1972.

[122] R. Cortell, "A numerical tackling on Sakiadis ow with thermal radiation," *Chin. Phys. Lett.*, vol. 25, 2008.

[123] M. Mustafa, J. A. Khan, T. Hayat, and A. Alsaedi, "Sakiadis flow of Maxwell fluid considering magnetic field and convective boundary conditions," *AIP Adv.*, vol. 5, p. 027106, 2015.

[124] M. I. Khan, M. Waqas, T. Hayat, M. I. Khan, and A. Alsaedi, "Chemically reactive flow of upper-convected Maxwell fluid with Cattaneo-Christov heat flux model," *J. Braz. Soc. Mech. Sci. Eng.*, vol. 39, pp. 4571–4578, 2017.

[125] N. C. Rosca, A. V. Roca, and I. Pop, "Stagnation point flow and heat transfer over a non-linearly moving flat plate in a parallel free stream with slip," *Commun. Nonlinear Sci. Numer. Simul.*, vol. 19, pp. 1822–1835, 2014.

[126] M. Shen, F. Wang, and H. Chen, "MHD mixed convection slip flow near a stagnation-point on a nonlinearly vertical stretching sheet," *Boundary Value Prob.*, vol. 2015, pp. 78–92, 2015.

[127] M. Hatami, M. Khazayinejad, and D. Jing, "Forced convection of Al_2O_3-water nanofluid flow over a porous plate under the variable magnetic field effect," *Int. J. Heat Mass Trans.*, vol. 102, pp. 622–630, 2016.

[128] S. A. M. Mehryan, F. M. Kashkooli, M. Soltani, and K. Raahemifar, "Fluid flow and heat transfer analysis of a nanofluid containing motile gyrotactic micro-organisms passing a nonlinear stretching vertical sheet in the presence of a non-uniform magnetic field; Numerical Approach," *PLoS ONE*, vol. 11(6), p. e0157598, 2016.

[129] A. Ishak, R. Nazar, and I. Pop, "Mixed convection on the stagnation point flow towards a vertical, continuously stretching sheet," *J. Heat Trans.*, vol. 129, p. 1087, 2007.

[130] L. G. Grubka and K. M. Bobba, "Heat transfer characteristics of a continuous stretching surface with variable temperature," *ASME J. Heat Trans.*, vol. 107, pp. 248–250, 1985.

[131] T. R. Mahapatra and A. S. Gupta, "Heat transfer in stagnation-point flow of a micropolar fluid towards a stretching sheet," *Heat Mass Transf.*, vol. 38, pp. 517–521, 2002.

[132] A. Ishak, R. Nazar, and I. Pop, "Mixed convection boundary layers in the stagnation-point flow towards a stretching vertical sheet," *Meccanica*, vol. 41, pp. 509–518, 2006.

[133] Z. Abbas, Y. Wanga, T. Hayat, and M. Oberlack, "Mixed convection in the stagnation-point flow of a Maxwell fluid towards a vertical stretching surface," *Nonlinear Anal.: Real World Appl.*, vol. 11, pp. 3218–3228, 2010.

[134] R. Nazar, N. Amin, D. Filip, and I. Pop, "Stagnation point flow of a micropolar fluid towards a stretching sheet," *Int. J. Non-Linear. Mech.*, vol. 39, pp. 1227–1235, 2004.

[135] M. Sajid, Z. Abbas, T. Javed, and N. Ali, "Boundary layer flow of an Oldroyd-B fluid in the region of stagnation point over a stretching sheet," *Can. J. Phys.*, vol. 88, pp. 635–640, 2010.

[136] T. Hayat, Z. Hussain, M. Farooq, A. Alsaedi, and M. Obaid, "Thermally stratified stagnation point flow of an Oldroyd-B fluid," *Int. J. Nonlinear. Sci. Numer. Simul.*, vol. 15, pp. 77–86, 2014.

[137] A. Mahdy, "Unsteady mixed convection boundary layer flow and heat transfer of nanofluids due to stretching sheet," *Nucl. Eng. Des.*, vol. 249, pp. 248–255, 2012.

[138] N. Bachok, A. Ishak, and I. Pop, "On the stagnation point flow towards a stretching sheet with homogeneous-heterogeneous reactions effects," *Commun. Nonlinear Sci. Numer. Simul.*, vol. 16, pp. 4296–4302, 2011.

[139] M. S. Abel, J. V. Tawade, and M. M. Nandeppanavar, "MHD flow and heat transfer for the upper-convected Maxwell fluid over a stretching sheet," *Meccanica*, vol. 47, pp. 385–393, 2012.

[140] W. M. Kays, *Convective heat and mass transfer*, 4th ed. New York:McGraw-Hill, 1966.

[141] M. Arunachalam and N. R. Rajappa, "Thermal boundary layer in liquid metals with variable thermal conductivity," *Appl. Sci. Res.*, vol. 34, pp. 179–187, 1978.

[142] M. M. Khader and A. M. Megahed, "Numerical solution for boundary layer flow due to a nonlinearly stretching sheet with variable thickness and slip velocity," *Eur. Phys. J. Plus*, vol. 128, p. 100, 2013.

[143] K. Sadeghy, A. H. Najafi, and M. Saffaripour, "Sakiadis flow of an upper-convected Maxwell fluid," *Int. J. Non-Linear Mech.*, vol. 40, pp. 1220–1228, 2005.

[144] K. Vajravelu, K. V. Prasad, and A. Sujatha, "Convection heat transfer in a Maxwell fluid at a non-isothermal surface," *Cent. Eur. J. Phys.*, vol. 9(3), pp. 807–815, 2011.

[145] N. A. Shah, I. L. Animasaun, R. O. Ibraheem, H. A. Babatunde, N. Sandeep, and I. Pop, "Scrutinization of the effects of Grashof number on the flow of different fluids driven by convection over various surfaces," *J. Mol. Liq.*, vol. 249, pp. 980–990, 2017.

[146] M. Turkyilmazoglu, "Determination of the correct range of physical parameters in the approximate analytical solutions of nonlinear equations using the Adomian decomposition method," *Mediterr. J. Math.*, vol. 13, pp. 4019–4037, 2016.

[147] T. M. Ajayi, A. J. Omowaye, and I. L. Animasaun, "Viscous dissipation effects on the motion of Casson fluid over an upper horizontal thermally stratified melting surface of a paraboloid of revolution: Boundary layer analysis," *J. Appl. Math.*, vol. 2017, 2017.

[148] M. Sheikholeslami and A. J. Chamkha, "Influence of Lorentz forces on nanofluid forced convection considering Marangoni convection," *J. Mol. Liq.*, vol. 225, pp. 750–757, 2017.

[149] A. J. Omowaye and I. L. Animasaun, "Upper-Convected Maxwell fluid flow with variable thermo-physical properties over a melting surface situated in hot environment subject to thermal stratification," *J. Appl. Fluid Mech.*, vol. 9(4), pp. 1777–1790, 2016.

[150] J. Sui, L. Zheng, and X. Zhang, "Boundary layer heat and mass transfer with Cattaneoe-Christov double-diffusion in upper-convected Maxwell nanofluid past a stretching sheet with slip velocity," *Int. J. Ther. Sci.*, vol. 104, pp. 461–468, 2016.

[151] M. Sajid, Z. Abbas, N. Ali, T. Javed, and I. Ahmad, "Slip flow of a Maxwell fluid past a stretching sheet," *Walailak J. Sci. Tech.*, vol. 11(12), pp. 1093–1103, 2014.

[152] A. S. Z. Sanatkar, "An approximate solution of the MHD flows of UCM fluids over porous stretching sheets by rational Legendre collocation method," *Int. J. Numer. Methods Heat Fluid Flow*, vol. 26(7), pp. 2218–2234, 2016.

[153] W. A. Khan and I. Pop, "Boundary-layer flow of a nanofluid past a stretching sheet," *Int. J. Heat Mass Transf.*, vol. 53, pp. 2477–2483, 2010.

[154] O. D. Makinde and A. Aziz, "Boundary layer flow of a nanofluid past a stretching sheet with a convective boundary condition," *Int. J. Therm. Sci.*, vol. 50, pp. 1326–1332, 2011.

[155] C. Y. Wang, "Free convection on a vertical stretching surface," *J. Appl. Math. Mech. (ZAMM)*, vol. 69, pp. 418–420, 1989.

[156] R. S. R. Gorla and I. Sidawi, "Free convection on a vertical stretching surface with suction and blowing," *Appl. Sci. Res.*, vol. 52, pp. 247–257, 1994.

[157] O. D. Makinde, N. Sandeep, I. L. Animasaun, and M. S. Tshehla, "Numerical exploration of Cattaneo-Christov heat flux and mass transfer in magneto-hydrodynamic flow over various geometries," *Defect Diffu. Forum*, vol. 374, pp. 67–82, 2017.

[158] M. I. Khan, M. Waqas, T. Hayat, M. I. Khan, and A. Alsaedi, "Chemically reactive flow of upper-convected Maxwell fluid with Cattaneo-Christov heat flux model," *J. Braz. Soc. Mech. Sci. Eng.*, vol. 39, pp. 4571–4578, 2017.

[159] N. Acharyaa, K. Das, and P. K. Kundua, "Cattaneo-Christov intensity of magnetised upper-convected Maxwell nanofluid flow over an inclined stretching sheet: A generalised Fourier and Ficks perspective," *Int. J. Mech. Sci.*, vol. 130, pp. 167–173, 2017.

[160] K. L. Hsiao, "Stagnation electrical MHD nanofluid mixed convection with slip boundary on a stretching sheet," *Appl. Therm. Eng.*, vol. 98, pp. 850–861, 2016.